รายงานวิจัยฉบับสมบูรณ์

โครงการ

การตรวจจับจุดยอดอาร์ในสัญญาณคลื่นไฟฟ้าหัวใจด้วยวิธีการประมวลผลสัญญาณขั้นสูง

R-peak detection in ECG signals based on advanced signal processing methods

โดย รองศาสตราจารย์ ดร. พรชัย พฤกษ์ภัทรานนต์

เดือน ปี ที่เสร็จโครงการ มิถุนายน 2558

สัญญาเลขที่ **RSA5680043**

รายงานวิจัยฉบับสมบูรณ์

โครงการ

การตรวจจับจุดยอดอาร์ในสัญญาณคลื่นไฟฟ้าหัวใจด้วยวิธีการประมวลผลสัญญาณขั้นสูง

R-peak detection in ECG signals based on advanced signal processing methods

โดย รองศาสตราจารย์ ดร. พรชัย พฤกษ์ภัทรานนต์

ภาควิชาวิศวกรรมไฟฟ้า คณะวิศวกรรมศาสตร์ มหาวิทยาลัยสงขลานครินทร์

สนับสนุนโดยสำนักงานกองทุนสนับสนุนการวิจัยและมหาวิทยาลัยสงขลานครินทร์
(ความเห็นในรายงานนี้เป็นของผู้วิจัย สกว. และมหาวิทยาลัยสงขลานครินทร์
ไม่จำเป็นต้องเห็นด้วยเสมอไป)

กิตติกรรมประกาศ

ทางคณะผู้วิจัยขอขอบคุณสำนักงานกองทุนสนับสนุนการวิจัย (สกว.) คณะวิศวกรรมศาสตร์ มหาวิทยาลัยสงขลานครินทร์ และมหาวิทยาลัยสงขลานครินทร์เป็นอย่างสูง ที่ร่วมกันให้ทุนสนับสนุนการวิจัยครั้งนี้

พรชัย พฤกษ์ภัทรานนต์

บทคัดย่อ

รหัสโครงการ: RSA5680043
ชื่อโครงการ: การตรวจจับจุดยอดอาร์ในสัญญาณคลื่นไฟฟ้าหัวใจด้วยวิธีการประมวลผลสัญญาณขั้นสูง
ชื่อนักวิจัย: รองศาสตราจารย์ ดร. พรชัย พฤกษ์ภัทรานนต์
E-mail Address: pornchai.p@psu.ac.th
ระยะเวลาโครงการ: 2 ปี

บทคัดย่อ :

การตรวจจับจุดยอดอาร์ในสัญญาณคลื่นไฟฟ้าหัวใจมีความสำคัญมากก่อนการวิเคราะห์ในลำดับถัดไปในการประยุกต์ใช้ทางการแพทย์ อัลกอริทึมการตรวจจับจุดยอดอาร์ประกอบด้วย 2 ขั้นตอนหลัก คือ ขั้นตอนการประมวลผลเบื้องต้นและขั้นตอนการตรวจจับบีต วัตถุประสงค์ของโครงการวิจัยนี้ คือ การพัฒนาอัลกอริทึมสำหรับการตรวจจับจุดยอดอาร์ในสัญญาณคลื่นไฟฟ้าหัวใจแบบอัตโนมัติ โดยเน้นที่การประยุกต์ใช้การประมวลผลขั้นสูง ได้แก่ ตัวกรองควอดราติกและการแปลงเวฟเล็ต ผลการศึกษาแสดงให้เห็นว่าตัวกรองควอดราติกสามารถเพิ่มอัตราส่วนสัญญาณคิวอาร์เอสต่อสัญญาณรบกวนในกรณีท้าทายบางกรณีได้ เช่น สัญญาณคิวอาร์เอสที่มีแอมปลิจูดขนาดเล็กและปะปนอยู่กับสัญญาณรบกวนแบบดริฟต์และสัญญาณคลื่นไฟฟ้าหัวใจที่มีรูปร่างผิดปกติ ด้วยการใช้ค่าขีดแบ่งแบบคงที่ค่าเดียวโดยไม่มีการประมวลผลใดเพิ่มเติมในขั้นตอนการตรวจจับบีต อัลกอริทึมสามารถให้ค่าอัตราการตรวจจับความผิดพลาดที่ 0.38% เมื่อประเมินจากสัญญาณคลื่นไฟฟ้าหัวใจ 48 ชุด ในฐานข้อมูล MIT-BIH arrhythmia database เพื่อการปรับปรุงความแม่นยำในการตรวจจับคิวอาร์เอส ผู้วิจัยได้เสนอการใช้ฟังก์ชันเวฟเล็ตแบบเม็กซิกันแฮ็ตร่วมกับตัวกรองสูงสุด ผลการศึกษาพบว่าฟังก์ชันเวฟเล็ตแบบเม็กซิกันที่สเกล 3 สามารถเพิ่มอัตราส่วนสัญญาณคิวอาร์เอสต่อสัญญาณรบกวนได้ดีในขั้นตอนการประมวลผลเบื้องต้น ส่วนตัวกรองสูงสุดที่มีความยาว 195 มิลลิวินาที สามารถลดความผิดพลาดแบบบวกได้อย่างมีนัยสำคัญ ด้วยการใช้ค่าขีดแบ่งแบบคงที่ค่าเดียวโดยไม่มีการประมวลผลใดเพิ่มเติมในขั้นตอนการตรวจจับบีต อัลกอริทึมสามารถให้ค่าอัตราการตรวจจับความผิดพลาดที่ 0.27% แนวทางการปรับปรุงค่าความถูกต้องในการตรวจจับให้ดียิ่งขึ้น ได้แก่ การใช้ฟังก์ชันเวฟเล็ตแบบแบนด์แยกและการใช้ฟังก์ชันเวฟเล็ตแบบแบนด์คู่ในขั้นตอนการประมวลผลเบื้องต้น และ/หรือ การใช้เทคนิคค่าขีดแบ่งแบบปรับตัวได้ในขั้นตอนการตรวจจับบีต

คำหลัก : สัญญาณคลื่นไฟฟ้าหัวใจ (อีซีจี) การตรวจจับบีตอีซีจี การประมวลผลสัญญาณ การตรวจจับคิวอาร์เอส ตัวกรองควอดราติก การแปลงเวฟเล็ต

Abstract

Project Code: RSA5680043

Project Title: R-peak detection in ECG signals based on advanced signal processing methods

Investigator: Associate Professor Dr. Pornchai Phukpattaranont

E-mail Address: pornchai.p@psu.ac.th

Project Period: 2 years

Abstract:

The R-peak detection in the ECG signal is very crucial as a preliminary step before subsequent analysis for inexpensive and noninvasive medical applications. The R-peak detection algorithm is composed of two main steps: preprocessing and beat detection. The objective of this research project is to develop a computer-based algorithm for automatically detecting R peaks in the ECG signal. The main focus of this work is the noise removal in preprocessing operation based on advanced signal processing methods, i.e. the quadratic filter and the wavelet transform. Results show that the quadratic filter is successful in improving QRS signal to noise ratio for some challenging situations such as low amplitude QRS complex corrupted by baseline drift and a variety of abnormal morphologies. Using a single fixed threshold without additional post-processing techniques in beat detection step, the QRS detection algorithm can achieve the detection error rate of 0.38% validated with 48 records of ECG signals from the MIT-BIH arrhythmia database. To improve QRS detection accuracy, we develop the QRS detection algorithm employing the efficient cascade of two combination steps, i.e., the Mexican hat wavelet function and the maximal filter. Results show that the Mexican hat wavelet function at scale 3 can significantly enhance QRS signal to noise ratio in preprocessing step. The subsequent beat detection step based on the maximal filter at the length of 195 ms is able to significantly reduce FP detections. Using a single threshold without any additional post-processing techniques, the proposed algorithm can achieve detection error rate of 0.27%. To obtain better detection accuracy, the use of separable band and the dual-band wavelet transforms in preprocessing step and/or adaptive thresholding techniques in beat detection step may allow us for better detection accuracy in the QRS detection algorithm.

Keywords: Electromyography (ECG), ECG beat detection, Signal processing, QRS detection, Quadratic filter, Wavelet transform

Table of Contents

List of Tables

List of Figures

Chapter 1

Introduction

1.1 Research Problem and its Significance

The electrocardiogram (ECG) provides very important information on the state of the heart, which can be used for medical monitoring and diagnosis. Figure 1.1 shows an example of three beats of ECG signal. Each beat consists of P wave, QRS complex, and T wave. The objective of this research is to develop an automatic algorithm for detecting R peaks, which is very crucial as a preliminary step for obtaining QRS complex, beat segmentation, and beat-to-beat intervals.

Further processing of these preliminary steps can be employed for a variety of medical applications. QRS complex can be used for monitoring the electrical activity of the heart during the ventricular contraction. After beat segmentation, each individual

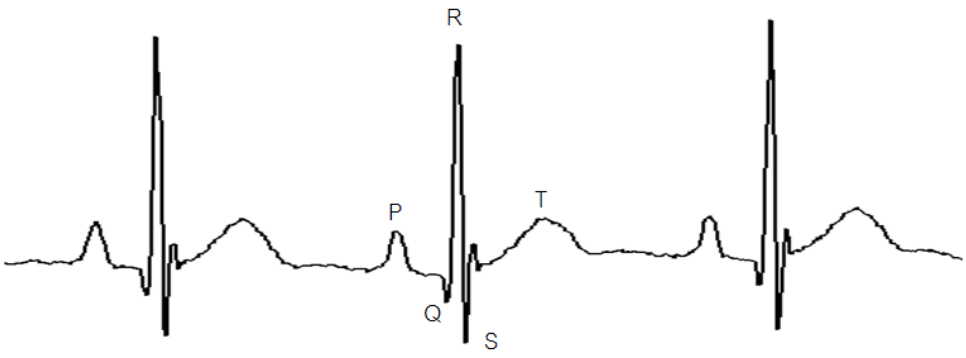

Figure 1.1: Three beats of ECG signal.

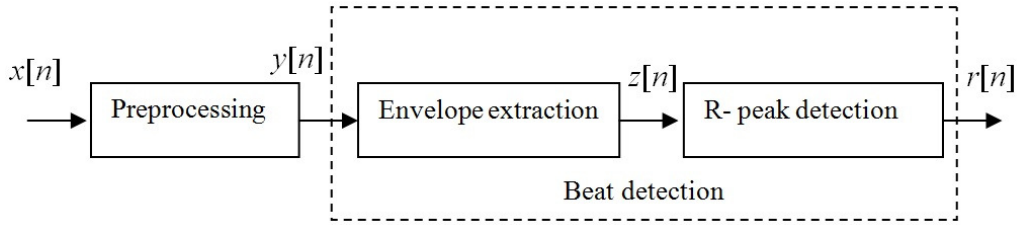

Figure 1.2: Schematic diagram of R-peak detection algorithm.

beat can be further categorized into different types of arrhythmia, such as normal beats, premature ventricular contraction beats, atrial premature beats, and other beats [1–3]. Series of beat-to-beat intervals is a basis used in analyzing heart rate variability. Heart rate variability analysis is an inexpensive and noninvasive tool for a variety of medical diagnoses such as obstructive sleep apnea syndrome [4, 5] and congestive heart failure [6,7]. In addition, the automatic QRS detection algorithm can be applied for discovering an abnormal ECG activity in a mobile ECG monitoring and alert system for elderly patients [8].

Figure 1.2 shows a schematic diagram of R-peak detection algorithm. The noises in the ECG signal $x[n]$ are removed in the preprocessing operation. Figure 1.3 shows an example of 9-beat ECG signals before ($x[n]$) and after ($y[n]$) noise removal in the top and bottom panels, respectively. Subsequently, to obtain the envelope signal $z[n], y[n]$ is processed with the envelope extraction algorithm. Figure 1.4 shows an example of signals in beat detection algorithm. The signals $y[n]$ and $z[n]$ are shown using thin and dotted lines, respectively. Then, the threshold value is defined as shown in Figure 1.4 with a thick line to determine the time interval $[t_1 \;\; t_2]$ where the R peak locates. Finally, the R peak is detected from the determination of the time t_R where the signal amplitude is maximum.

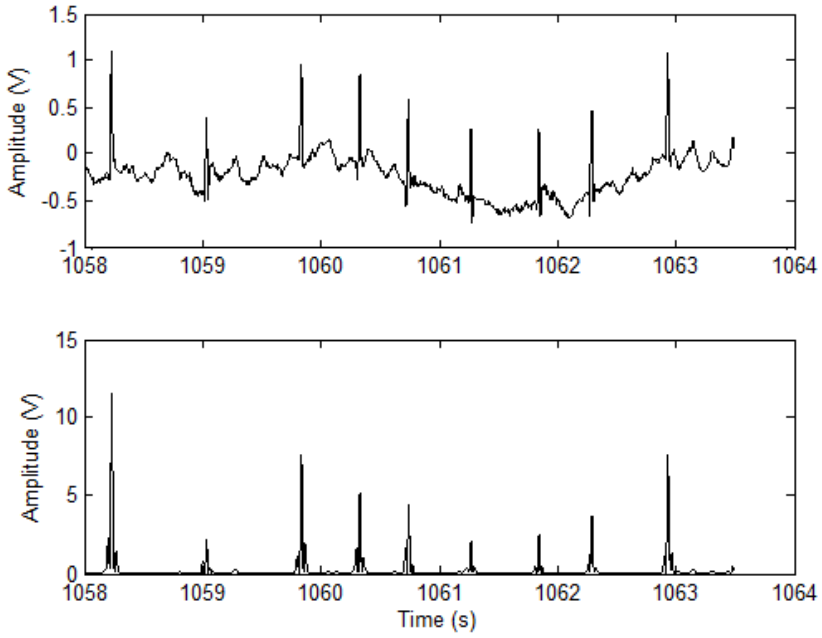

Figure 1.3: Noise removal in preprocessing operation. Top panel: ECG signal before noise removal ($x[n]$). Bottom panel: ECG signal after noise removal ($y[n]$).

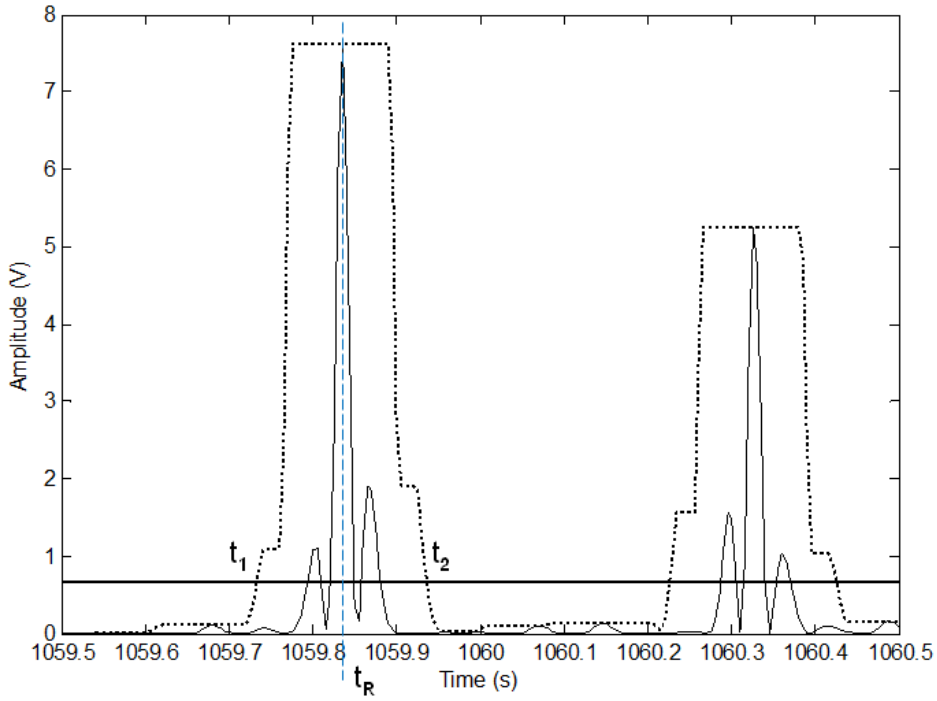

Figure 1.4: ECG beat detection algorithm. Thin line: ECG signal after noise removal ($y[n]$). Dotted line: Envelope signal ($z[n]$). Thick line: Threshold line.

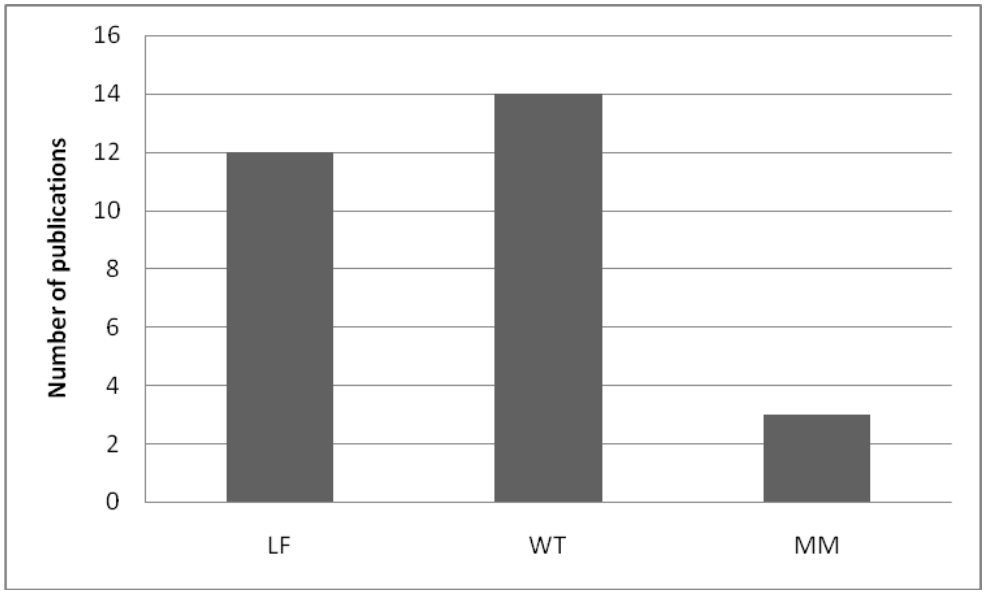

Figure 1.5: The number of publications categorized by preprocessing algorithms: linear filtering (LF), wavelet transform (WT), and mathematical morphology (MM).

1.2 Literature Reviews

Based on literature reviews, the contents of R peak detection in ECG papers can be presented in the following 4 sections: ECG preprocessing, ECG beat detection, performance evaluation, and performance comparison.

1.2.1 ECG Preprocessing

The aim of ECG preprocessing is to remove noises in ECG signals. Subsequently, further processing algorithms are performed for extracting signal envelope. The main noises in ECG signal can be divided into two types: low frequency noises and high frequency noises. While the low frequency noises are T-wave noise and baseline wander noise, the high frequency noises are muscle noise and power line noise. Based on literature reviews of 29 papers, ECG preprocessing algorithms can be classified into 3 categories: linear filtering (LF), wavelet transform (WT), and mathematical morphology (MM) as shown in Figure 1.5.

Firstly, the preprocessing operation in many previous publications employs LF techniques for noise removal in ECG signals [9–20]. Its main processing is based on a bandpass filter with a cutoff frequency 5-36 Hz, which is corresponding to the bandwidth of QRS interval in the ECG signal. In addition, signals after filtering are further processed with a variety of methods for calculating the envelope signal, for example, moving average filter [9, 10, 18], differential equation [9, 10, 12, 16, 17], squaring function [9, 10, 16, 17], genetic algorithm [11], Hilbert transform [12], and zero crossing [14].

Secondly, preprocessing algorithms based on WT are popularly used for removing noises in ECG signals [21–31]. After the output from wavelet transform is obtained, further processing methods used for determining the envelope signal include differential equation [22, 27], moving average filter [26, 29], filter bank [25], and zero crossing [24]. Thirdly, three papers of noise removal in ECG signals based on MM were published [32–34]. The examples of further processing after MM are differential equation [32] and wavelet transform [33]. Moreover, other noise removal techniques include artificial neural network [35] and S-transform [36].

Figure 1.6 shows the number of publications regarding noise removal in ECG signals categorized by 3 preprocessing algorithms covering the period 1985-2012. While LF and WT have gained popularity since 1985, the publication based on MM has begun since 2009. During the period 1985-2000, there are 3 publications from LF and WT. During the period 2001-2005, while the number of publication from LF is 3, the number of publication from WT decreases to 1. However, during the period 2006-2012, the number of publications based on LF and WT increases to 6 and 10, respectively. Since 2009, ECG noise removal based on MM has been of interest leading to 3 publications during the period 2009-2012.

1.2.2 ECG Beat Detection

After the noises in the ECG signal are removed in the preprocessing operation, the signal envelope is extracted, and the R peak is detected in ECG beat detection process. As

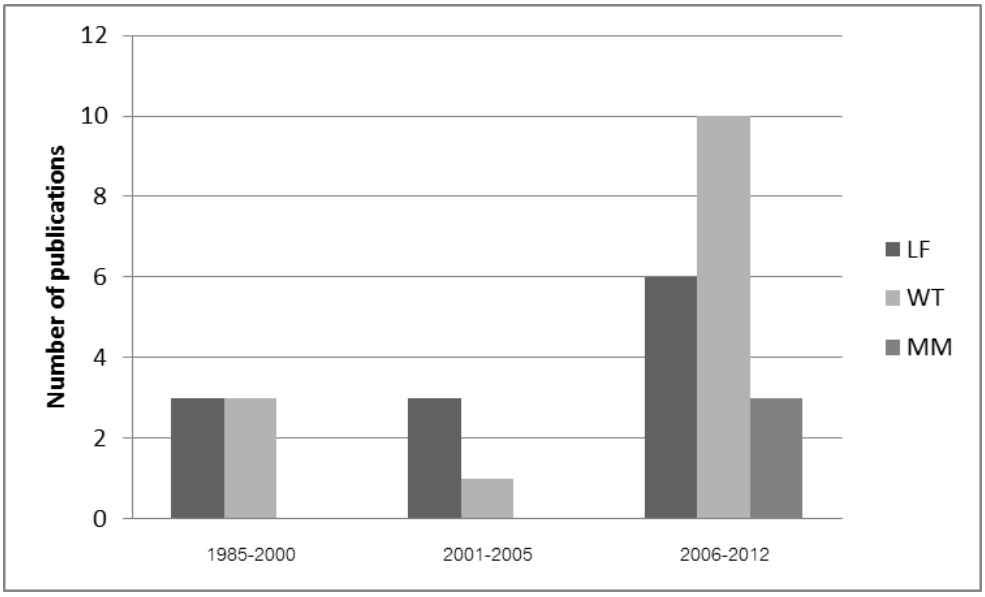

Figure 1.6: The number of publications categorized by preprocessing algorithms and publication years.

described in Figure 1.4, one can see that the threshold is a very important parameter. The threshold can be classified into two types: fixed threshold and adaptive threshold. The fixed threshold has an advantage of low computational complexity at an expense of detection accuracy. There are two categories of fixed threshold, i.e., single level [21, 28] and multiple levels [15, 25, 29]. While an example of single fixed threshold is given by [28]

$$\lambda = 0.3 \times \max(h), \tag{1.1}$$

where λ is a threshold and h is an envelope signal resulting from the absolute of product of wavelet coefficients, an example of multiple fixed thresholds can be expressed as [15]

$$\hat{X}_{df} = \begin{cases} 0 & \text{if} \quad 0 < X_{df} < T_1, \text{or } T_2 < X_{df} < 0 \\ X_{df} & \text{if} \quad X_{df} \geq T_1, \text{or } X_{df} \leq T_2 \end{cases} . \tag{1.2}$$

To achieve better detection accuracy, the adaptive threshold is used. Similar to the fixed threshold, the adaptive threshold can be categorized into single level [12, 14, 22, 26, 27, 32–34] and multiple levels [9–11, 13, 17]. Examples of single and multiple

adaptive thresholds are given by [12]

$$thr(i) = \begin{cases} 0.39\max(i), & RMS(i) > 0.18\max(i) \\ & \& \max(i) \leq 2\max(i-1) \\ 0.39\max(i-1), & RMS(i) > 0.18\max(i) \\ & \& \max(i) > 2\max(i-1) \\ 1.6RMS(i), & RMS(i) < 0.18\max(i) \end{cases}, \tag{1.3}$$

and [13]

$$LLV_n = V(n) + V(n-1),\ RLV_n = V(n) + V(n+1), \tag{1.4}$$

respectively.

In addition, some post-processing algorithms are used to achieve better detection rate. These post-processing algorithms include the checkup for irregular beat-to-beat interval information [9, 17, 27].

1.2.3 Performance Evaluation

The performance of QRS detection algorithm is evaluated with sensitivity (SEN), positive predictive rate (PPR), and detection error rate (DER). SEN is given by

$$\text{SEN} = \frac{\text{TP}}{\text{TP} + \text{FN}} \times 100, \tag{1.5}$$

where true positive (TP) is the number of correct QRS complex predictions. FN is the false negative prediction. In other words, the algorithm predicts that there is no QRS complex in the location where there is a real QRS complex. PPR can be expressed as

$$\text{PPR} = \frac{\text{TP}}{\text{TP} + \text{FP}} \times 100, \tag{1.6}$$

where FP is the false positive prediction. In other words, the algorithm predicts that there is a QRS complex in the location where there is no QRS complex. DER is used for evaluating the accuracy of algorithm including both FN and FP values, which can be given by

$$\text{DER} = \frac{\text{FN} + \text{FP}}{\text{TP} + \text{FN}} \times 100. \tag{1.7}$$

Table 1.1: The 8 most-cited papers that are popularly used as a comparison with the new proposed R-peak detection algorithm.

Paper	Type	Thresholding (THV)	Cited	SEN(%)	PPR(%)	DER(%)
Pan [9]	LF	Four levels adaptive THV	12	99.75	99.54	0.71
Hamilton [10]	LF	Three levels adaptive THV	11	99.69	99.77	0.54
Poli [11]	LF	Three levels adaptive THV	7	99.60	99.50	0.90
Lee [13]	LF	Two levels adaptive THV	2	99.69	99.87	0.43
Li [23]	WT	Four levels adaptive THV	6	99.89	99.94	0.17
Afonso [25]	WT	Two levels fixed THV	10	99.55	99.59	0.86
Choi [27]	WT	Single level adaptive THV	1	99.66	99.80	0.54
Zhang [32]	MM	Single level adaptive THV	2	99.81	99.80	0.39

1.2.4 Performance Comparison

Based on the considerations of 29 papers, Table 1.1 shows 8 most-cited papers that are popularly used as a comparison with the new proposed R peak detection algorithm in terms of accuracy. The first four papers use LF in preprocessing step ([9–11, 13]). Papers [9] and [10] are used in performance comparisons by other 12 and 11 papers, respectively. Both papers remove noises using a bandpass filter with a cutoff frequency 5-15 Hz. Subsequently, the signal envelope is detected by the following operations: differential equation, square function, and moving average filtering. The main difference in both papers is the number of levels in adaptive thresholding. That is, while paper [9] uses four levels of adaptive thresholding, paper [10] uses three levels of adaptive thresholding. Results show that DER of [9] and [10] are 0.71% and 0.54%, respectively. Paper [11] used in comparison with other 7 papers provides the DER value of 0.9%. Paper [13] giving the DER value of 0.43% is used in comparison with other 2 papers. Both papers employ multiple adaptive thresholding in beat detection algorithm.

The next three papers [23], [25], and [27] comprising WT in their preprocessing step provide the DER values of 0.17%, 0.86%, and 0.54%, respectively. They are used in performance comparisons by other 6, 10 and 1 papers, respectively. While discrete wavelet transform for noise removal and single fixed thresholding for beat detection are exploited in [23], filter bank and multiple fixed thresholding are used in [25]. Paper [27] employs db 10 WT and Butterworth lowpass filter with a cutoff frequency 20 Hz for noise

removal. Moreover, single adaptive thresholding is used for ECG beat detection. The last paper [32] utilizes the MM based on multiscale mathematical morphology filtering for removing noise. The single adaptive thresholding is used in beat detection step. Its DER value is 0.39%. This paper was used in performance comparison by other 2 papers.

Table 1.2: ECG records that provide top five highest DER values.

Paper	Type	1st	2nd	3rd	4th	5th
Pan [9]	LF	108(12.38%)	222(7.10%)	105(3.43%)	203(2.76%)	228(1.46%)
Hamilton [10]	LF	108(5.38%)	222(3.04%)	105(2.90%)	203(2.47%)	210(1.60%)
Poli [11]	LF	207	108	105	104	203
Lee [13]	LF	222(3.73%)	203(2.38%)	114(2.09%)	105(1.75%)	201(1.36%)
Li [23]	WT	108(1.57%)	105(1.08%)	203(0.86%)	201(0.66%)	228(0.49%)
Afonso [25]	WT	108(11.89%)	203(4.03%)	105(3.20%)	210(2.36%)	208(2.09%)
Choi [27]	WT	108(4.71%)	228(3.56%)	201(2.39%)	203(2.05%)	105(2.02%)
Zhang [32]	MM	106(2.00%)	116(1.27%)	113(1.16%)	105(1.00%)	223(0.99%)

Table 1.2 shows the ECG records that provide the top five highest DER values in the papers from Table 1.1. Results show that the DER of ECG record 108 is highest in 5 of 8 papers. In addition, ECG record 108 and 203 are found in all papers that use LF and WT as a preprocessing step for noise removal (7 from 8 papers). However, the ECG record 105 is found in all 8 papers. It is interesting to note that the ECG records 108 and 203 are not found in the paper that employs MM for noise removal. Other ECG data found in 3 papers are 222, 228, and 201.

1.3 Objective

The objective of this research is to develop a computer-based algorithm for automatically detecting R peaks in an ECG signal. The main focus of this work is to remove noise and enhance QRS signal to noise ratio in preprocessing operation based on advanced signal processing methods, i.e. quadratic filter (QF) and wavelet transform. If the R peak can be emphasized by the preprocessing operation, the detection accuracy can be obtained with minimal computational complexity because adaptive thresholding and post-processing operations may not be required.

1.4 Methodology

Quadratic Filter

To develop the R-peak detection algorithm based on the quadratic filter, the study procedures are as follows.

- Maximize QRS signal to noise ratio in preprocessing step for noise removal by investigating the most appropriate center frequency and bandwidth of the QF.
- Study computational complexity reduction of the QF using singular value decomposition (SVD).
- Investigate the appropriate thresholding technique and post-processing methods for the R-peak detection algorithm based on the QF to increase detection accuracy. In addition, the trade-off between detection accuracy and computational complexity will be carefully studied.

Wavelet Transform

To develop the R-peak detection algorithm based on the wavelet transform, the study procedures are as follows.

- Maximize QRS signal to noise ratio in preprocessing step for noise removal by investigating the most appropriate wavelet function, wavelet scale, and combination of wavelet coefficients at various scales to maximize QRS signal to noise ratio.
- Investigate the most appropriate thresholding technique and post-processing methods for the R-peak detection algorithm based on the wavelet function to increase detection accuracy. In addition, the trade-off between detection accuracy and computational complexity will be carefully studied.

1.5 Scope of Research

ECG data used in performance evaluation for the proposed algorithm are from MIT-BIH arrhythmia database [37, 38]. There are 48 records of ECG data. Each record consists of slightly over 30 minutes from two-channel of ECG data. Each channel was acquired at a sampling rate of 360 Hz. This database is considered as a class 1 database, which has been carefully scrutinized, thoroughly annotated, and used in many well-known publications. The ECG data from MIT-BIH have a variety of types including both normal and abnormal ECG data. In addition, there is a marker for each beat given by the expert demonstrating the QRS complex location and beat type. In this research project, the QRS complex is detected using the ECG signal from channel 1 or lead II only. In other words, the ECG signal from channel 1 was represented by $x[n]$.

1.6 Expected Benefits

The knowledge resulting from this research can be integrated to be a part of computer assisted system for ECG signal analysis. Their examples of applications include ECG signal prescreening and ECG monitoring in the elderly. As the ECG signal prescreening, it can help in the diagnosis of ECG abnormalities such as arrhythmia, obstructive sleep apnea syndrome, and congestive heart failure. Moreover, the decrease in the number of newborn babies and human longevity due to the development of science and public health have brought Thailand to be a country of aging society since 2005. As a result, the lack of a care taker for the elderly is a serious problem that is inevitable. To alleviate the problems, the health monitoring systems and smart home research for the elderly has been developed so that they can live independently on their own as much as possible. A small device that can send signals from multiple sensors such as acceleration and ECG electrodes used to check the movement of the elderly including the fall event notifications has been developed. The care taker can monitor the status of the user closely and can timely assist when situations are serious and in emergency. The knowledge resulting

from this research is a very important part for detecting abnormalities in ECG signals.

The rest of this report is organized as follows. Chapter 2 presents the QRS detection algorithm based on the QF. Subsequently, the QRS detection algorithm based on the wavelet function is given in chapter 3. Then, chapter 4 demonstrate the possibility in improving QRS signal to noise ratio using combination of the wavelet functions at various scales. Finally, the conclusions of this research project and recommendations for future work are stated in chapter 5.

Chapter 2

QRS Detection Based on Quadratic Filter

2.1 Introduction

The main focus of this chapter is to propose the R-peak detection algorithm, which is popularly known as the QRS detection algorithm in most previous publications, consisting of the quadratic filter (QF) capable of enhancing QRS signal to noise ratio in preprocessing operation. Results show that the QRS complex can be emphasized by the preprocessing operation based on the QF because of the significant increase in the QRS signal to noise ratio. As a result, the detection accuracy can be obtained without the need for adaptive thresholding and post-processing operations.

The rest of this chapter is organized as follows. Section 2.2 presents the design method for the QF. Section 2.3 describes the proposed QRS detection algorithm based on the QF. Results are given in section 2.4. Finally, discussion is provided in section 2.5.

2.2 Quadratic Filter Design

The application of the QF, which is derived from the second-order Volterra filter, in the ECG noise removal application has not been carefully studied. Unlike the linear filtering, the important advantage of the QF is that it has various degrees of freedom for optimization in removing noises contaminated in the ECG signal. Details of the QF

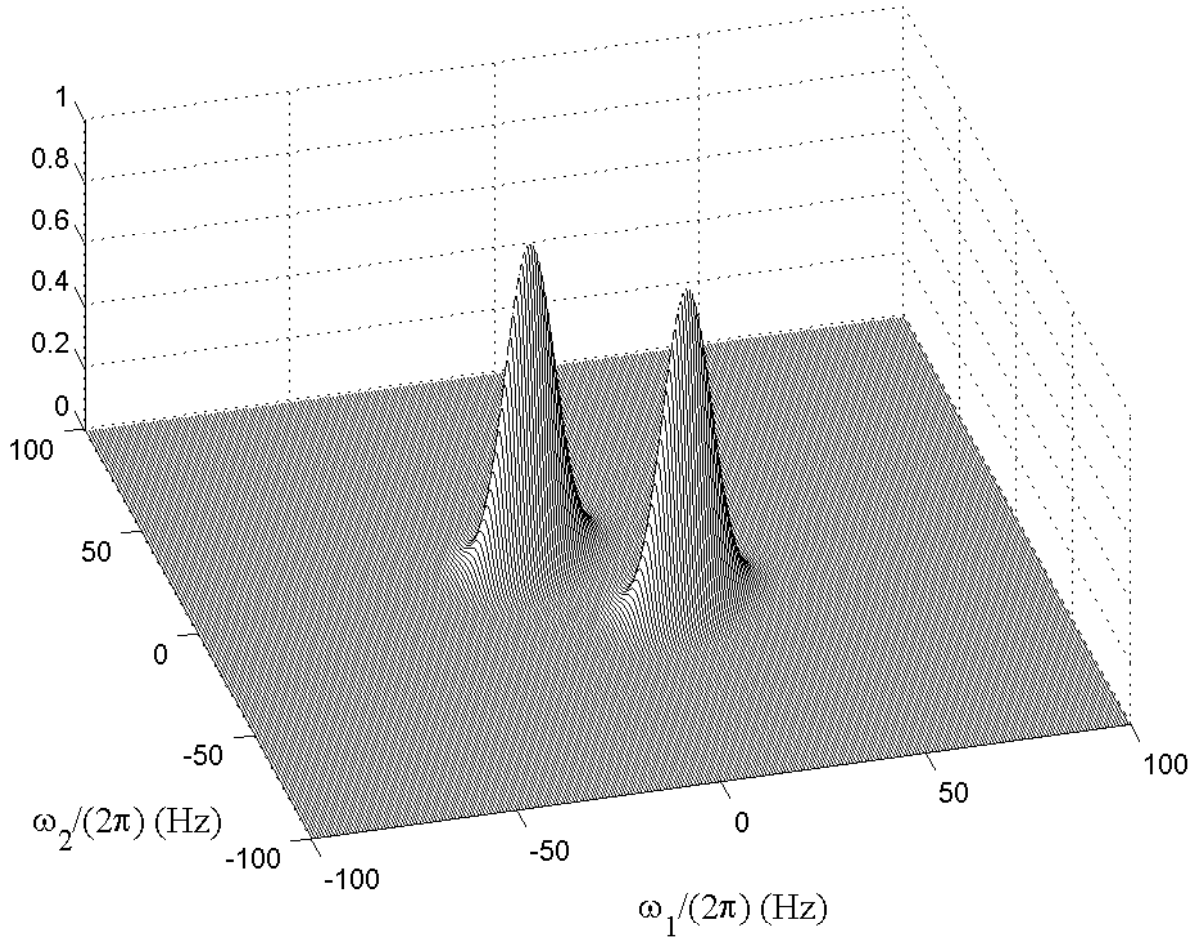

Figure 2.1: The modified 2D Gaussian function in the frequency domain.

derivation are given as follows.

The design of QF for removing noises in ECG signals is performed in frequency domain. Figure 2.1 shows an example of 2D magnitude frequency response of the QF. The linear-phased QF is designed based on the sum of two 2D Gaussian filters, which is given by

$$G(\omega_{1k}, \omega_{2l}) = \frac{G_1(\omega_{1k}, \omega_{2l}) + G_2(\omega_{1k}, \omega_{2l})}{\max\{G_1 + G_2\}}, \tag{2.1}$$

where

$$G_i(\omega_{1k}, \omega_{2l}) =$$

$$\exp\{-[A(\omega_{1k} - \omega_{ai})^2 + B(\omega_{1k} - \omega_{ai})(\omega_{2l} - \omega_{bi}) + C(\omega_{2l} - \omega_{bi})^2]\}, \tag{2.2}$$

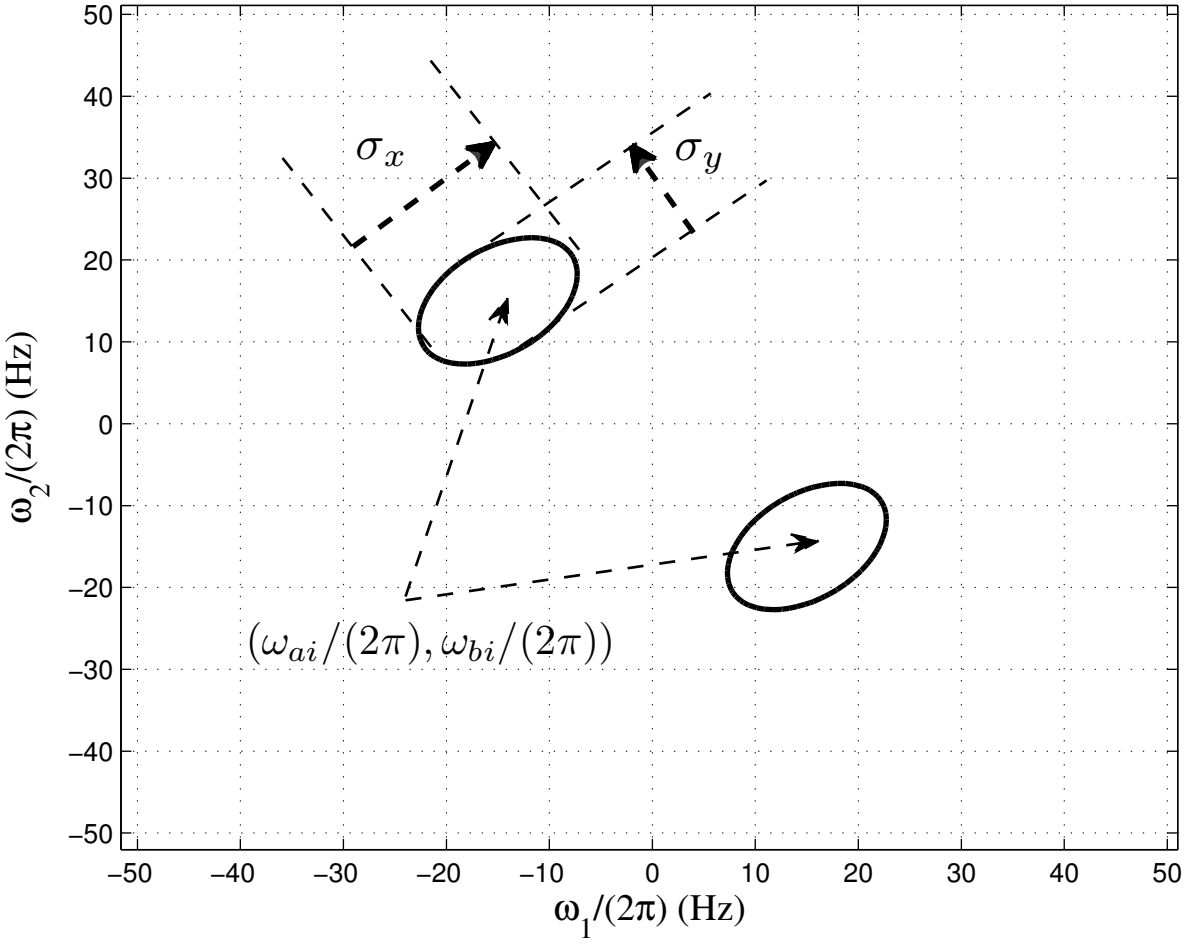

Figure 2.2: The contour plot at -6 dB showing parameters in the design of the QF: Passband width and center points.

for $i = 1, 2$ with:

$$A = (\frac{\cos\theta}{\sigma_x})^2 + (\frac{\sin\theta}{\sigma_y})^2 \tag{2.3}$$

$$B = -\frac{\sin 2\theta}{\sigma_x^2} + \frac{\sin 2\theta}{\sigma_y^2} \tag{2.4}$$

$$C = (\frac{\sin\theta}{\sigma_x})^2 + (\frac{\cos\theta}{\sigma_y})^2. \tag{2.5}$$

The coefficient $(\omega_{ai}, \omega_{bi})$ is the center of Gaussian filter, σ_x is a constant that defines the passband width along the cross-diagonal direction, σ_y is a constant that defines the passband width along the diagonal direction, and θ is the rotation angle.

Note that the passband frequencies should be approximately placed at the passband frequencies of the QRS response. To achieve the best filter for removing noise, parameters should be adjusted to maximize QRS signal to noise ratio. Figure 2.2 shows a contour plot at -6 dB of the magnitude of 2D frequency responses of the QF from Figure 2.1. The centers of Gaussian function are at $(\omega_{1k}, \omega_{2l})$ of (-15, 15) and (15, -15) Hz. Other parameters, i.e., $(\sigma_x, \sigma_y, \theta)$ for the QF are (1.1, 0.55, -π/4).

After the 2D magnitude frequency of the QF is formed, the frequency response can be given by

$$H(e^{j\omega_{1k}}, e^{j\omega_{2l}}) = G(\omega_{1k}, \omega_{2l}) e^{j\phi(\omega_{1k}, \omega_{2l})}, \tag{2.6}$$

where $G(\omega_{1k}, \omega_{2l})$ represents the desired magnitude response based on the 2D Gaussian filters given in (2.1) and $\phi(\omega_{1k}, \omega_{2l})$ is the phase response, which can be expressed as

$$\phi(\omega_{1k}, \omega_{2l}) = -\frac{N_1 - 1}{2}\omega_{1k} - \frac{N_2 - 1}{2}\omega_{2l}, \tag{2.7}$$

where $\omega_{1k} = (2\pi k/M_1) - \pi, k = 0, 1, ..., M_1 - 1$ and $\omega_{2l} = (2\pi l/M_2) - \pi, l = 0, 1, ..., M_2 - 1$. We use the QF size $N_1 = N_2 = N$. As a result, the phase delay of the signal output is $(N - 1)/2$.

Subsequently, the filter coefficients $h[n_1, n_2]$ can be obtained by the inverse DFT of $H(e^{j\omega_{1k}}, e^{j\omega_{2l}})$. Please see [39] for more details. Figure 2.3 shows the coefficients of the QF corresponding the design parameters shown in Figure 2.2. The ECG signal after noise removal $y[n]$ is produced by applying the QF coefficients to the ECG signal $x[n]$, which can be expressed as

$$y[n] = \sum_{k_1=0}^{P-1} \sum_{k_2=0}^{P-1} h[k_1, k_2] x[n - k_1] x[n - k_2], \tag{2.8}$$

Once a quadratic kernel $\mathbf{H}_0$ is obtained, equation (2.8) can be rewritten in the vector form as

$$y(n) = \mathbf{x}^T(n) \mathbf{H}_0 \mathbf{x}(n). \tag{2.9}$$

Then, an eignenvalue decomposition (EVD) is performed to determine its dominant modes (based on eigenvalue distribution). This has two possible advantages:

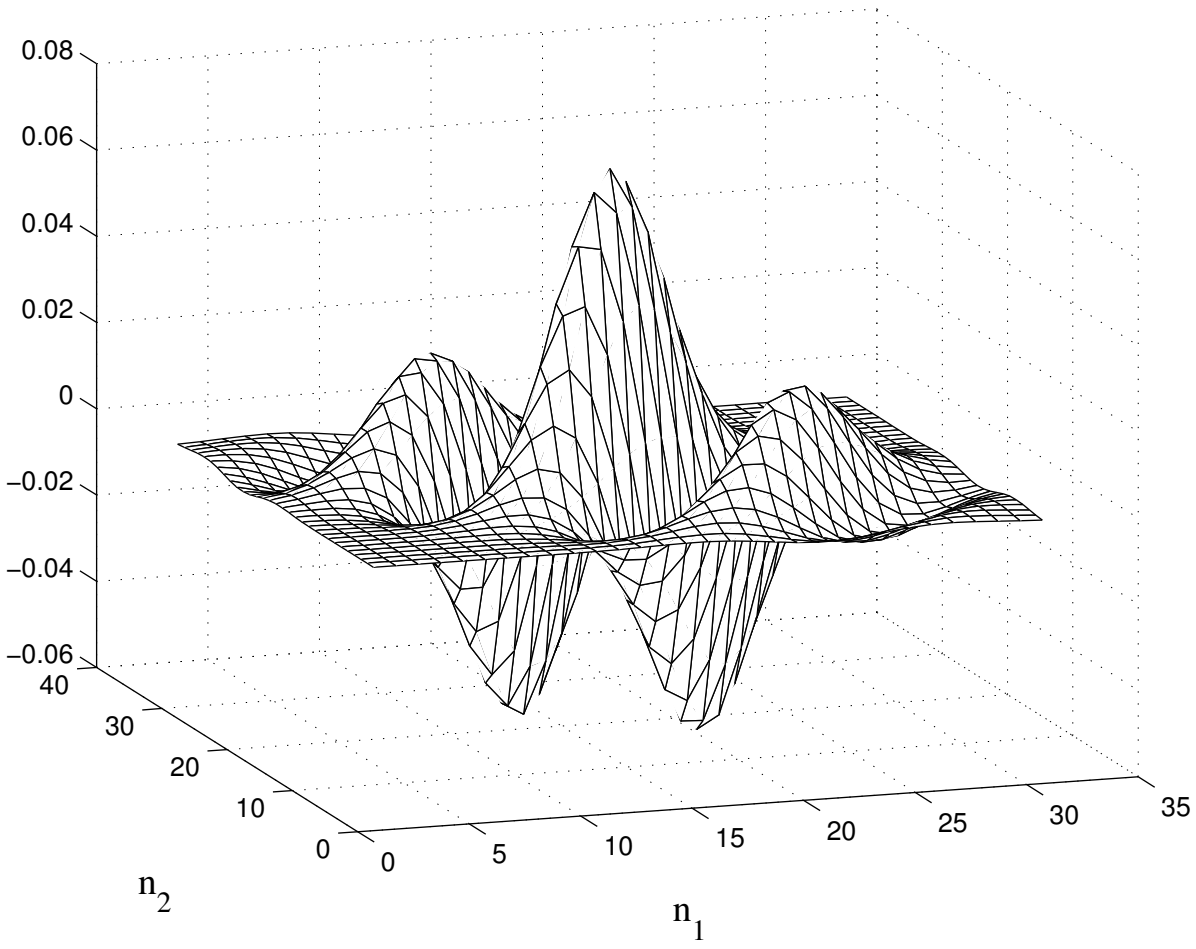

Figure 2.3: Coefficients of the QF shown in time domain.

- Under EVD, it is easy to identify and remove those modes that do not lead to an improvement in noise removal capability.

- In cases when only one or two dominant eigenmodes of $\mathbf{H}_0$ produce most of the energy, it is possible to implement the quadratic operator more efficiently. Specifically, a separable implementation of a low-order quadratic filter can be used.

The EVD of the quadratic kernel $\mathbf{H}_0$ is given by,

$$\mathbf{H}_0 = \mathbf{W}^T \mathbf{\Lambda} \mathbf{W}, \tag{2.10}$$

where $\mathbf{W}$ is a matrix composed of the eigenvectors $\mathbf{w}_1, \ldots, \mathbf{w}_P$ and Λ is the diagonal matrix constructed from the corresponding eigenvalues, $\lambda_1, \ldots, \lambda_P$, and P is the size of QF. Then, based on the EVD of $\mathbf{H}_0$, the estimation of quadratic components in equation (2.9) can be expressed as

$$\begin{aligned} y(n) &= \mathbf{x}^T(n)(\mathbf{W}^T \mathbf{\Lambda} \mathbf{W})\mathbf{x}(n) \\ &= (\mathbf{W}\mathbf{x}(n))^T \mathbf{\Lambda} (\mathbf{W}\mathbf{x}(n)) \\ &= \sum_{j=1}^{P} \lambda_j \left[\sum_{i=0}^{P-1} w_j(i) x(n-i) \right]^2 . \end{aligned} \tag{2.11}$$

2.3 Proposed Algorithm

Based on a schematic diagram of the QRS detection algorithm shown in Figure 1.2, the noises in the ECG signal $x[n]$ are removed in the preprocessing operation based on the QF designed using the method described in Section 2.2. Figure 2.4(a) and (b) shows an example of 10-beat ECG signals before and after noise removal in the top and bottom panels, respectively.

Subsequently, to obtain the envelope signal $z[n]$, $y[n]$ is processed with the envelope extraction algorithm. Figure 2.5(a) shows an example of signals in beat detection algorithm. The signals $y[n]$ and $z[n]$ are shown with the thin and dotted lines, respectively. Then, the threshold value is defined as shown in Figure 2.5(a) with a thick line to determine the time interval $[t_1 \;\; t_2]$ where the QRS complex locates. Finally, the R

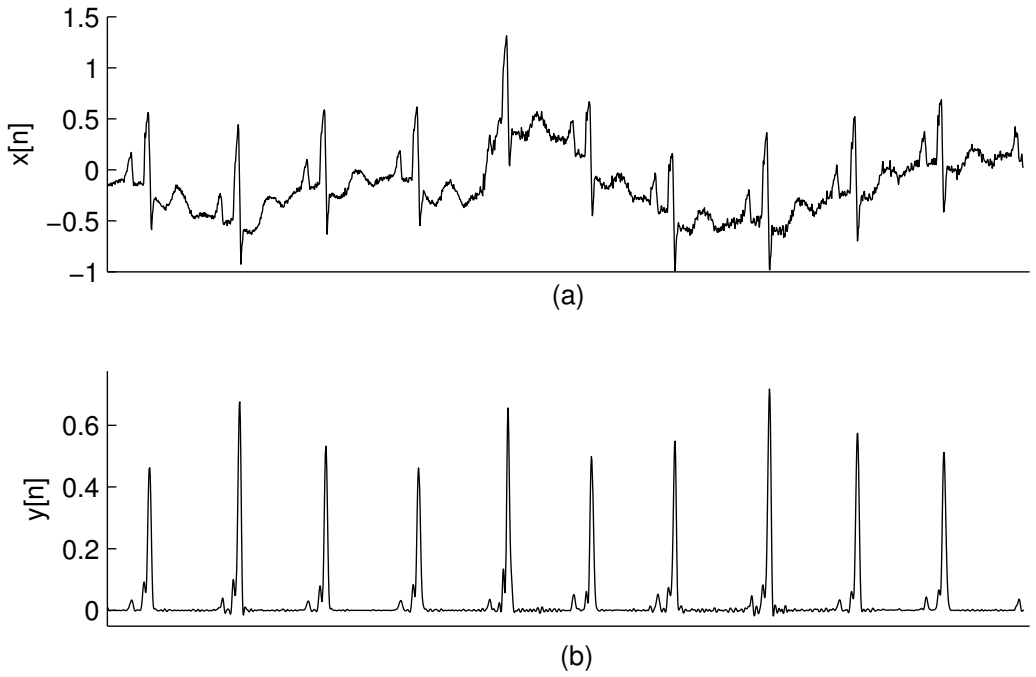

Figure 2.4: Noise removal in preprocessing operation. (a) ECG signal before noise removal $x[n]$. (b) ECG signal after noise removal $y[n]$.

peak in QRS complex is detected from the determination of the time t_R where the signal amplitude is maximum. Figure 2.5(b) shows the ECG signal overlaid by the markers from the proposed algorithm (square) and the expert (asterisk). The details of proposed algorithm can be summarized as follows.

1. Determine the signal $y[n]$ from the ECG signal $x[n]$ by processing with the QF.

2. Determine the envelope signal $z[n]$ from $y[n]$ using the maximal filter with the length $L = 120$ ms as given by

$$z[n] = \max_{k \in [n-L+1,n]} y[k]. \tag{2.12}$$

3. Detect the R peak in QRS complex using the following steps.

   (a) Calculate a threshold value thv from $thv = \lambda y_m[n]$, where $y_m[n]$ is the maximum value of $y[n]$ and λ is a constant in the range of 0.10 to 0.17.

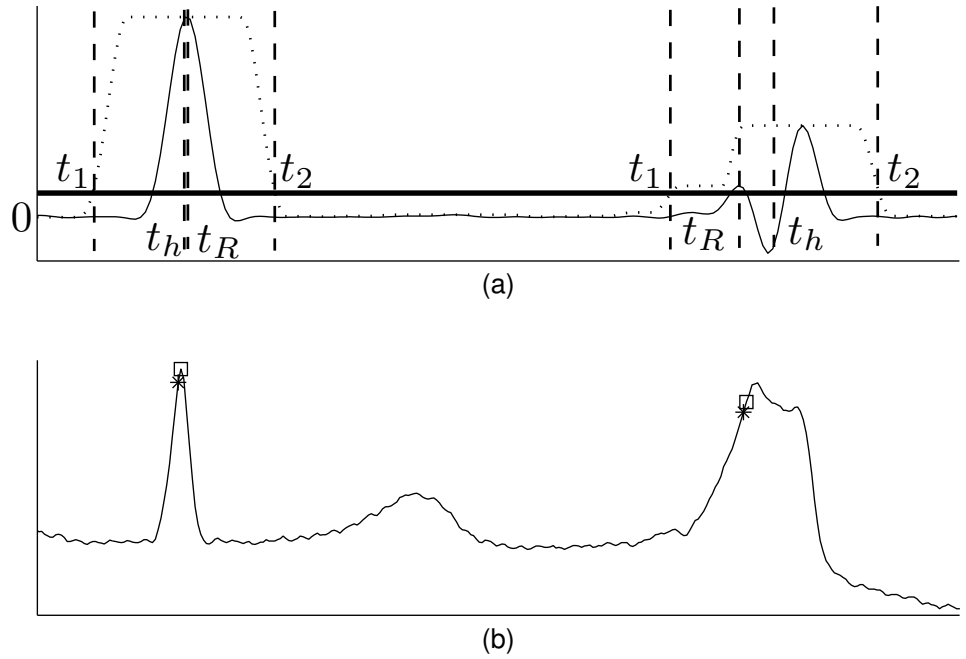

Figure 2.5: ECG beat detection algorithm. (a) Thin line: ECG signal after noise removal $y[n]$. Dotted line: Envelope signal $z[n]$. Thick line: Threshold value line. (b) ECG signal overlaid by the markers from the proposed algorithm (square) and the expert (asterisk). While the signal on the left hand side is a normal ECG beat, the signal on the right hand side is a premature ventricular contraction beat.

(b) Find the time duration where $z[n]$ is greater than thv and determine the beginning time t_1, the half-duration time t_h, and the ending time t_2.

(c) Determine the amplitude of $y[n]$ at t_h. If the amplitude is greater than zero, which indicates that it is not a premature ventricular contraction beat, go to step (d), else go to step (e).

(d) Determine R peak location t_R from the time between $[t_1 \;\; t_2]$ in $y[n]$ that gives the maximum amplitude.

(e) Determine R peak location t_R from the time between $[t_1 \;\; t_h]$ in $y[n]$ that gives the maximum amplitude.

2.4 Results

2.4.1 Parameter Adjustment

To achieve the optimum QF filter for noise removal in ECG signals, parameters under investigation are $(\omega_{1k}, \omega_{2l})$, σ_x, σ_y, and θ. However, the most important parameter is σ_y, which defines the cutoff frequency in the diagonal direction capable of enhancing the QRS signal to noise ratio. Figure 2.6 shows a comparison of 2D magnitude frequency response of the QF when the values of σ_y in the filter design are 0.4, 0.55, 0.7, and 0.85. We can clearly see that the higher in σ_y value, the wider in the passband width of the QF along the major diagonal direction.

Figure 2.7 shows an average DER value from 48 records of ECG data as a function of a σ_y value. Four values of σ_y are varied, i.e., 0.40, 0.55, 0.70, and 0.85 when $(\omega_{1k}, \omega_{2l})$, σ_x, and θ are fixed at (-15, 15), (15, -15) Hz, 1.1, and -π/4, respectively. Results show that the maximum average DER value of 0.38% can be obtained at the σ_y of 0.70.

Figure 2.8 shows the DER value as a function of threshold value thv determined using the increment step size of $\lambda = 0.1$ from records 100, 108, 207, and 222. The result from record 100 represents ECG data with low noise contamination. A wide range of

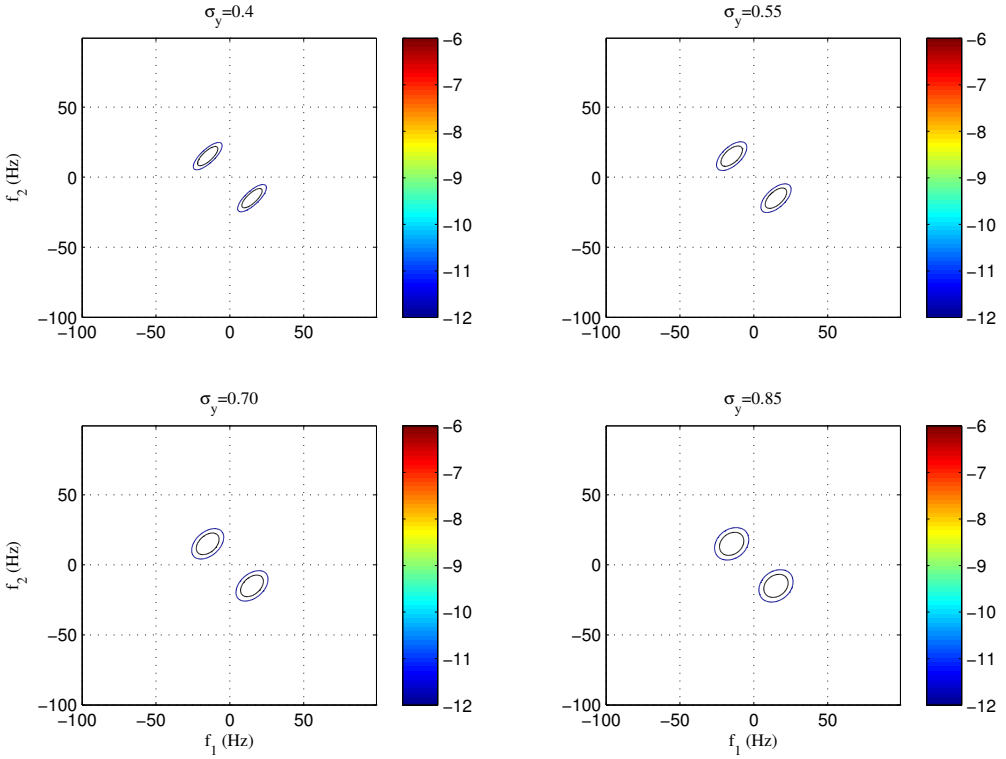

Figure 2.6: Comparison of contour plot of 2D magnitude frequency response of the QF when the values of σ_y are 0.4, 0.55, 0.7, and 0.85.

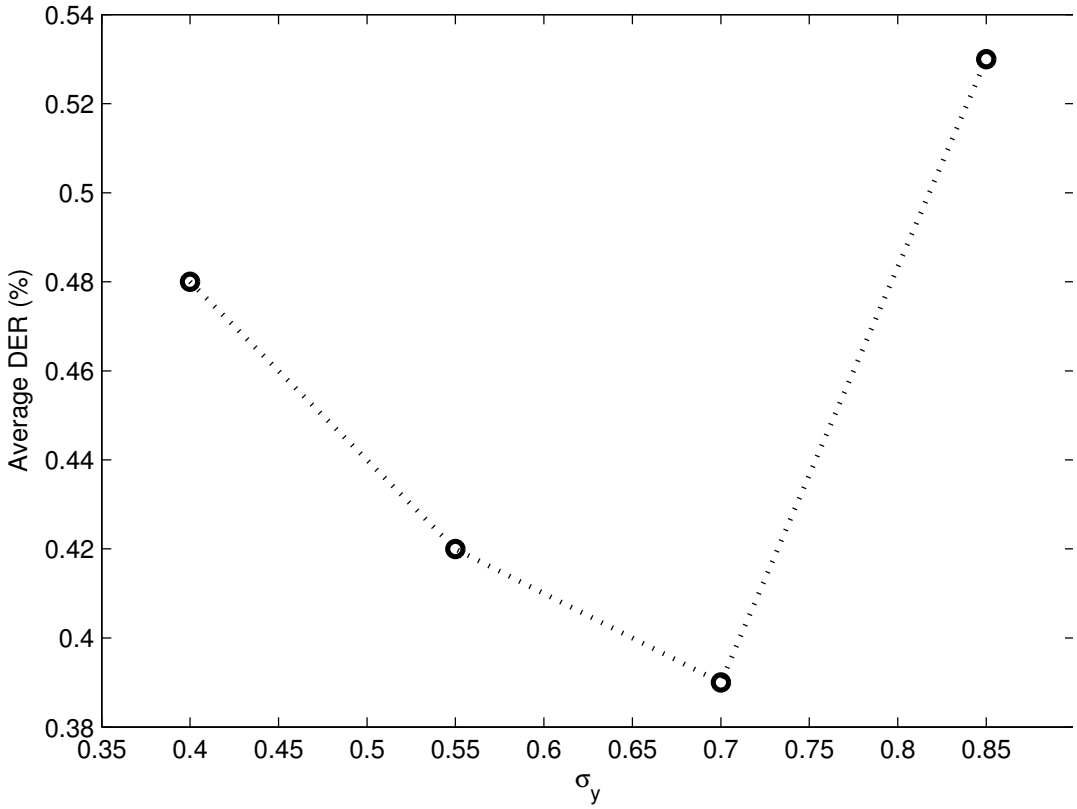

Figure 2.7: An average DER value from 48 records of ECG data as a function of a σ_y value.

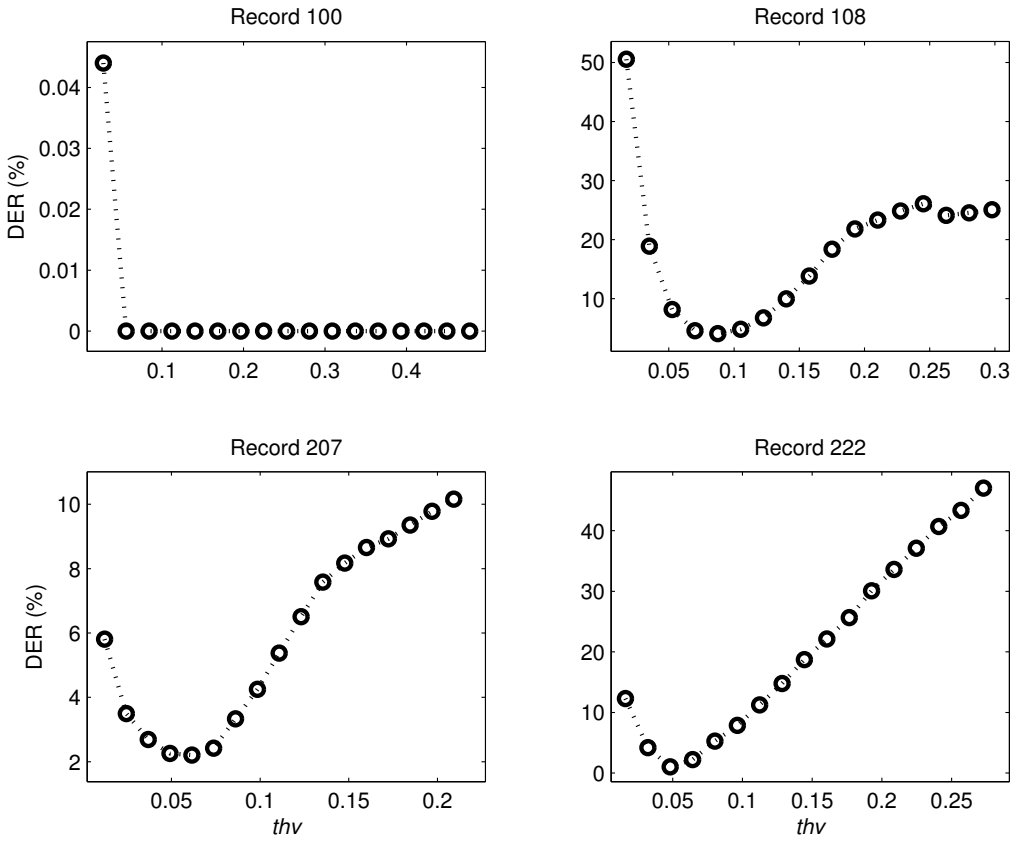

Figure 2.8: A DER value as a function of threshold value thv.

the λ values from 0.2 to 0.17, which are corresponding to the thv values from 0.056 to 0.478, can give the DER value of 0%. The results from record 108, 207, and 222 represent the ECG data consisting of various contaminated noises and irregular ECG beats. Only a single value of thv value can give the minimum DER. For example, the minimum DER of 4.08% for the record 108 can be obtained from the λ value of 0.05, which is corresponding to the thv value of 0.0876. Similar results also can be seen in the record 207 and 222.

2.4.2 Enhancement of QRS Signal to Noise Ratio

To illustrate the capability of the QF in enhancing QRS signal to noise ratio, example results from ECG data of record 121, 202, 200, 217, 105, and 108 are demonstrated.

Figure 2.9(a) shows the ECG data of record 121 from time 1650 s to time 1660 s. Although ECG data in this record are corrupted by baseline drift and some QRS complexes have very low amplitude, significant improvement in QRS signal to noise ratio of the ECG signal after noise removal $y[n]$ resulting from the QF can be obtained as shown in Figure 2.9(b). Figure 2.9(c) shows the envelope signal $z[n]$ and the threshold value thv, which allow us to correctly detect all QRS signals.

Figure 2.10(a) shows the ECG data of record 202 from time 760 s to time 770 s. ECG data in this record consist of 6 normal beats, an atrial premature beat, two aberrated atrial premature beats, and a premature ventricular contraction beat. Figure 2.10(b) shows that the QRS signal to noise ratio of $y[n]$ from the QF is good enough for all beats to be correctly detected using the envelope signal $z[n]$ and the threshold level thv shown in Figure 2.10(c).

Figure 2.11(a) shows the ECG data of record 200 from time 600 s to time 610 s. ECG data in this record consist of a fusion of ventricular and normal beat ("F"). In addition, we can see muscle noise in the segments [600-601 s] and [603-603.5 s]. Figure 2.11(b) shows that the QF can efficiently remove noise and enhance QRS signal to noise ratio. There is an FN detection shown in Figure 2.11(c) at time 602 s because the

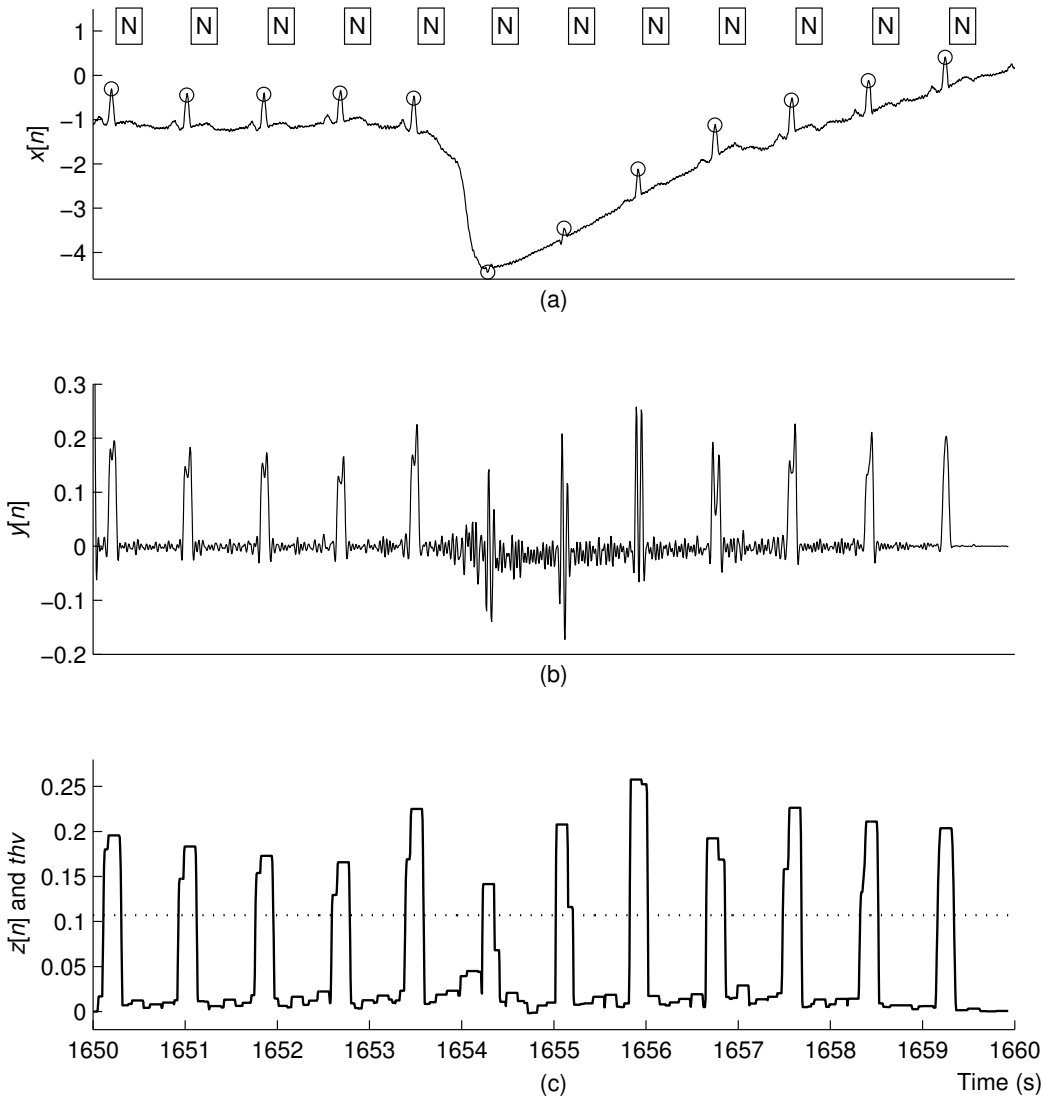

Figure 2.9: Results of the proposed algorithm applied on the ECG signal record 121. (a) The ECG signal before noise removal $x[n]$ overlaid by the circle markers from the expert. "N" stands for a normal beat. (b) The ECG signal after noise removal $y[n]$. (c) The envelope signal $z[n]$ (solid line) and the threshold level thv (dotted line).

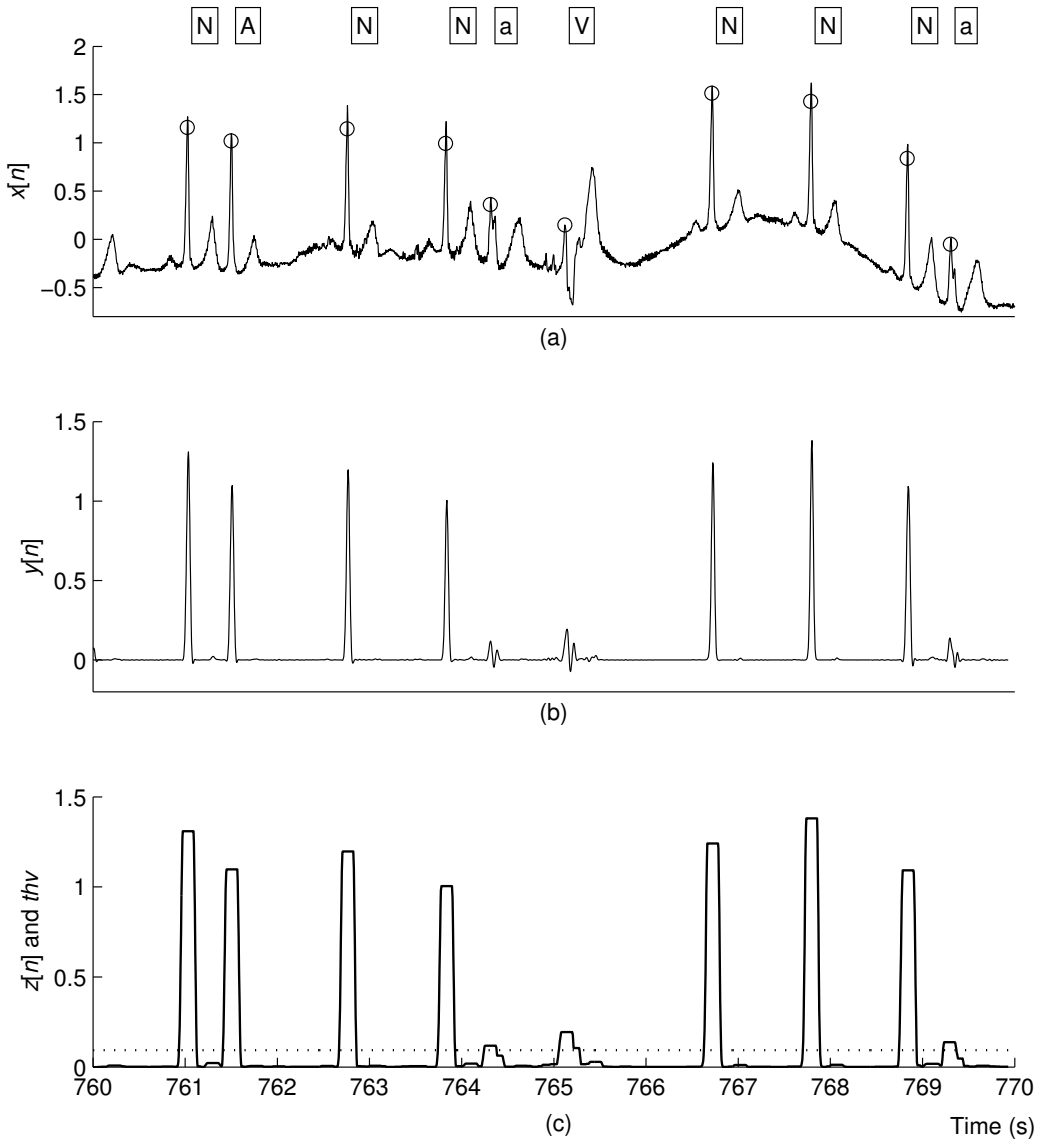

Figure 2.10: Results of the proposed algorithm applied on the ECG signal record 202. (a) The ECG signal before noise removal $x[n]$ overlaid by the circle markers from the expert. "A" stands for an atrial premature beat, "a" for an aberrated atrial premature beat, and "V" for a premature ventricular contraction beat. (b) The ECG signal after noise removal $y[n]$. (c) The envelope signal $z[n]$ (solid line) and the threshold level thv (dotted line).

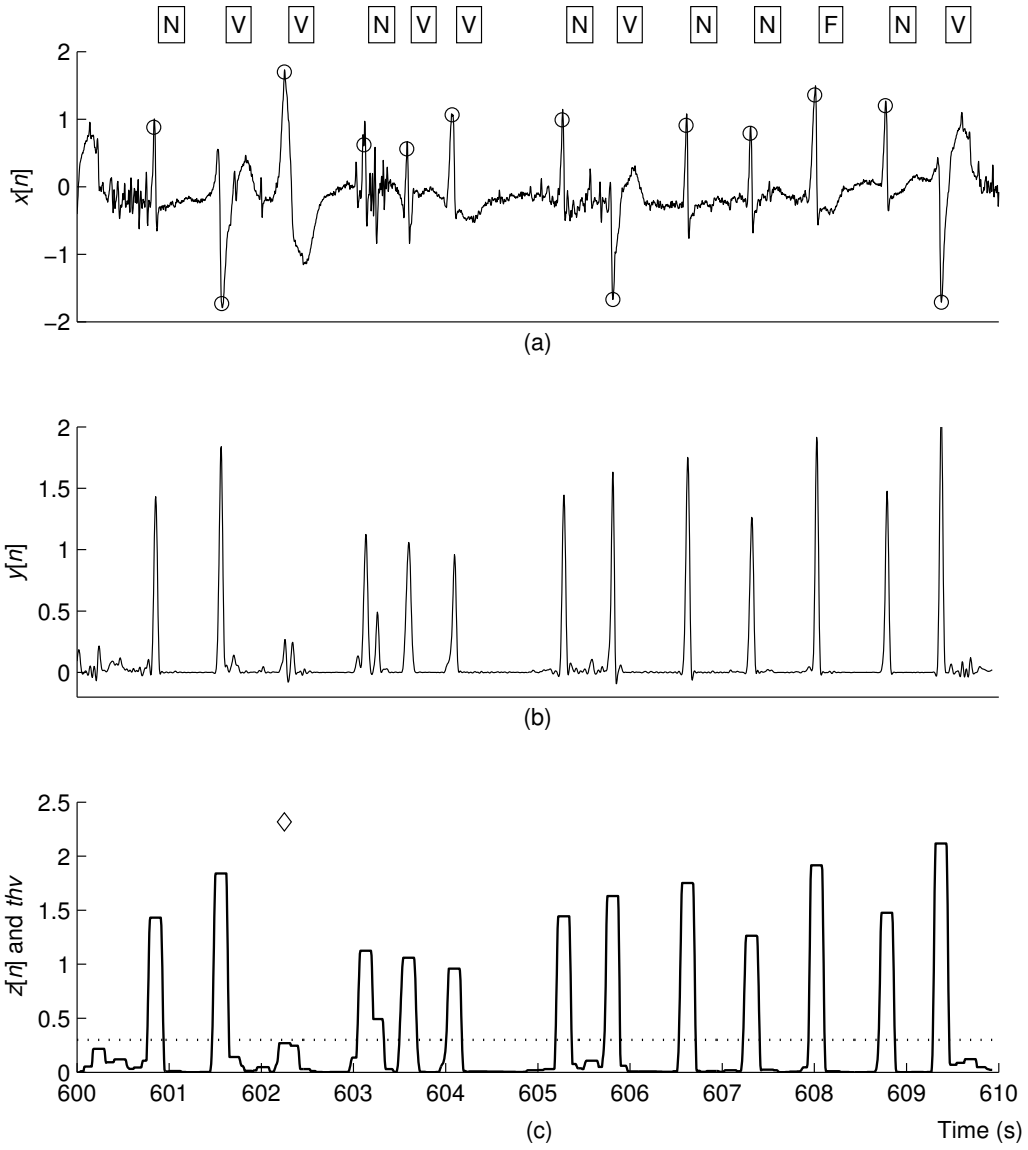

Figure 2.11: Results of the proposed algorithm applied on the ECG signal record 200. (a) The ECG signal before noise removal $x[n]$ overlaid by the circle markers from the expert. "F" stands for a fusion of ventricular and normal beat. (b) The ECG signal after noise removal $y[n]$. (c) The envelope signal $z[n]$ (solid line) and the threshold level thv (dotted line). "$\diamond$" stands for an FN detection.

threshold level thv in this record is higher than the premature ventricular contraction beat after applying with the QF.

Figure 2.12(a) shows the ECG data of record 217 from time 840 s to time 850 s. In addition to normal beats and a premature ventricular contraction, ECG data in this record is composed of fusion of paced and normal beats ("f") and paced beats ("/"). Moreover, we can see abrupt baseline shift at time 846 s. Figure 2.12(c) shows the envelope signal $z[n]$ resulting from the ECG signal after noise removal $y[n]$ in Figure 2.12(b), two FN detections and an FP detection. While the 2 FN detections result from their inherent low amplitudes, the FP detection is caused by the high peak from the abrupt baseline shift after filtering.

Figure 2.13(a) shows the ECG data of record 105 from time 1321 s to time 1331 s. ECG data in this record are contaminated with high-grade noise. Although the QRS complex can be emphasized by the QF as shown in Figure 2.13(b), the high-grade noise is also amplified. The signal after filtering from high-grade noise causes 6 FP detections as shown in Figure 2.13(c).

Figure 2.14(a) shows the ECG data of record 108 from time 1655 s to time 1665 s. We can see that the QRS complexes in this record have low amplitude and are corrupted by muscle noise. The amplitude of noise after filtering from time 1662 s to time 1663 s is higher than that of QRS signals from time 1663 s to time 1665 s as shown in Figure 2.14(b). As a result, the proposed algorithm gives 2 FP detections and 2 FN detections based on the threshold thv shown in Figure 2.14(c).

2.4.3 Performance Evaluation and Comparison

Table 2.1 shows performance evaluation of the proposed algorithm applied on all 48 records of ECG data when the parameters $(\omega_{1k}, \omega_{2l})$, σ_x, , σ_y, and θ of the QF are fixed at (-15, 15), (15, -15) Hz, 1.1, 0.70, and -π/4, respectively. The average DER value is 0.38%. The average values of TP, FN, FP, SEN, and PPR are 109281 beats, 202 beats, 210 beats, 99.82%, and 99.81%, respectively. While the maximum DER value is 4.08 %

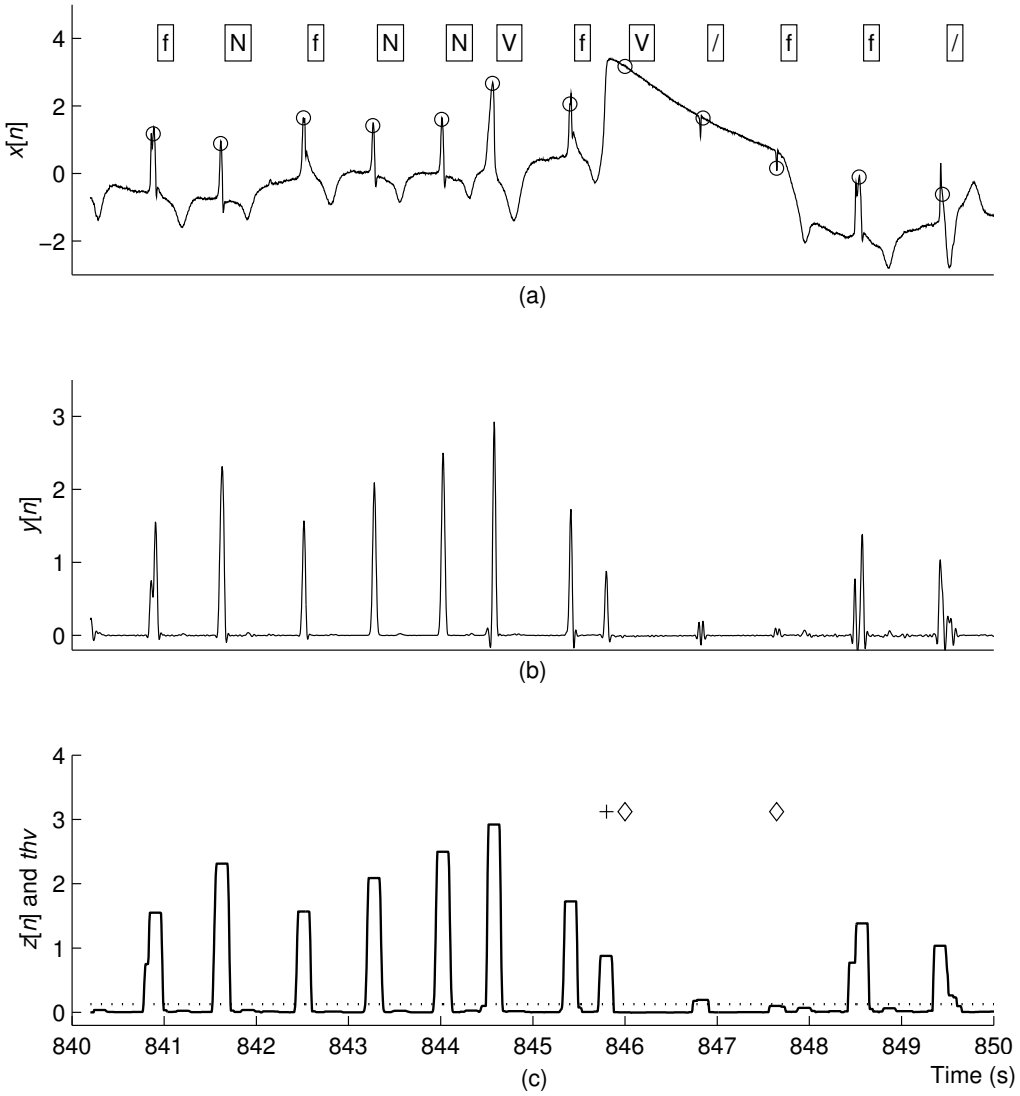

Figure 2.12: Results of the proposed algorithm applied on the ECG signal record 217. (a) The ECG signal before noise removal $x[n]$ overlaid by the circle markers from the expert. "f" stands for a fusion of paced and normal beat and "/" for a paced beat. (b) The ECG signal after noise removal $y[n]$. (c) The envelope signal $z[n]$ (solid line) and the threshold level thv (dotted line). "+" stands for an FP detection.

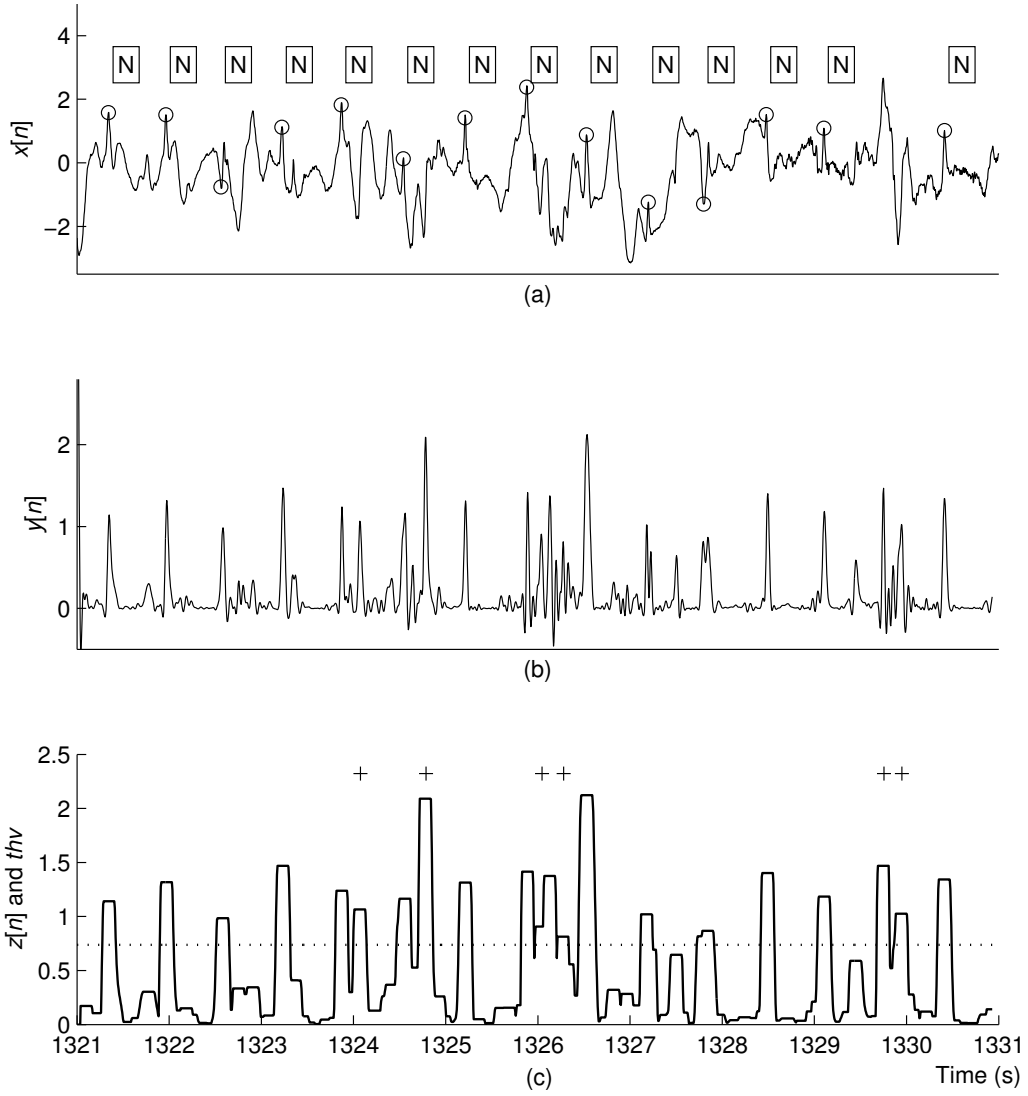

Figure 2.13: Results of the proposed algorithm applied on the ECG signal record 105. (a) The ECG signal before noise removal $x[n]$ overlaid by the circle markers from the expert. (b) The ECG signal after noise removal $y[n]$. (c) The envelope signal $z[n]$ (solid line) and the threshold level thv (dotted line).

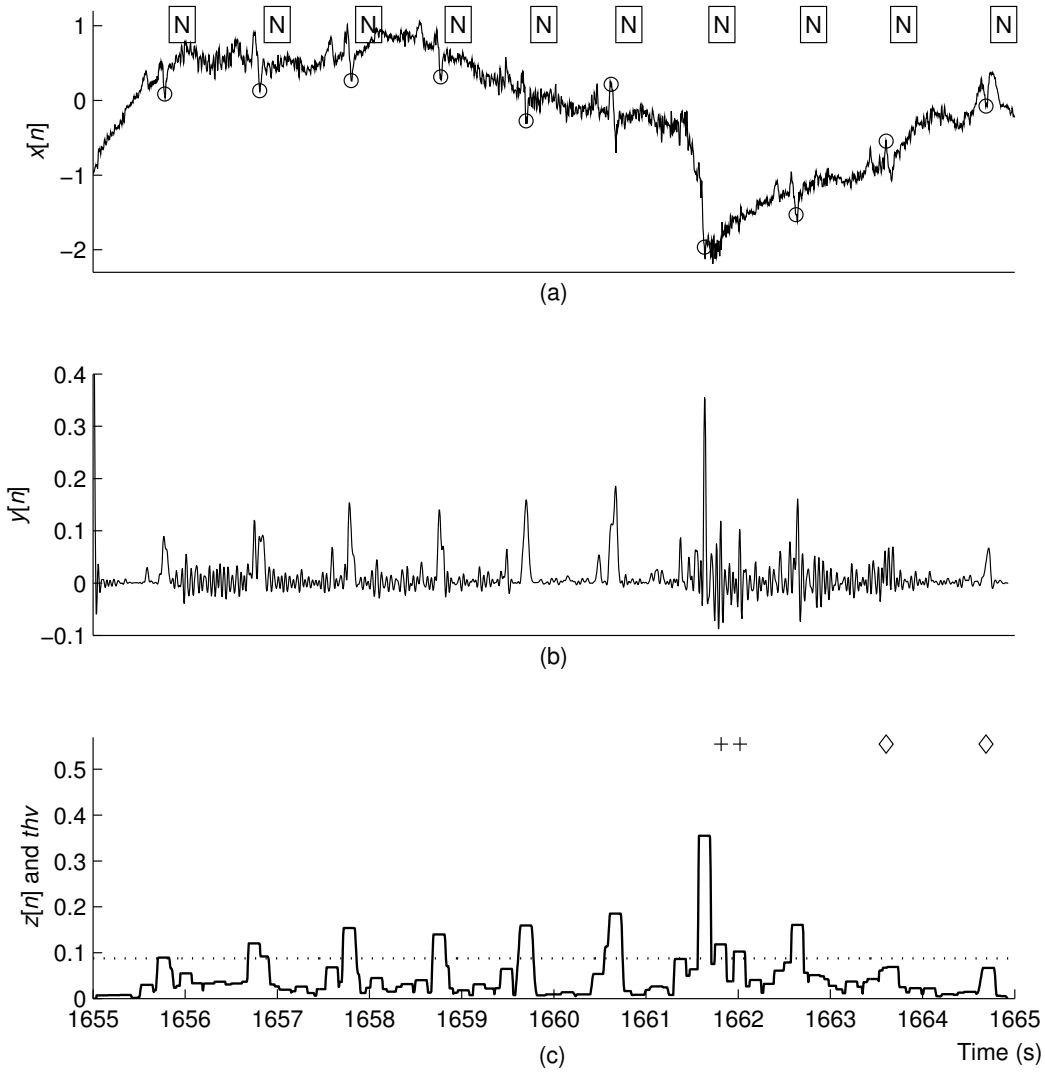

Figure 2.14: Results of the proposed algorithm applied on the ECG signal record 108. (a) The ECG signal before noise removal $x[n]$ overlaid by the circle markers from the expert. (b) The ECG signal after noise removal $y[n]$. (c) The envelope signal $z[n]$ (solid line) and the threshold level thv (dotted line)

from the record 108, the minimum DER value is 0 % from 21 records (record 100, 102, 103, 107, 112, 113, 115, 117, 118, 121-124, 202, 212, 213, 219-221, 230, and 231).

Table 2.2 shows the performance comparison of the proposed algorithm with that from other 7 state-of-the-art papers. The order of each method is sorted from the minimal average DER value to the maximal average DER value. The minimal and maximal average DER values are 0.17% [20] and 0.54% [27], respectively. The average DER value from the proposed algorithm based on noise removal in ECG signals using the QF is 0.38%. This result shows that the QF can significantly increase the QRS signal to noise ratio. As a result, only the use of a single fixed threshold without additional post-processing techniques can yield low average DER value.

Table 2.3 shows comparison results of the DER values of ECG record 121, 202, 200, 217, 105, and 108 from the proposed method with that from other 7 papers. The minimum and maximum DER values for each record are shown using the boldface and italics fonts, respectively. The DER values of ECG record 121 and 202 from the proposed method are minimal at 0.00 %. For other ECG records, the DER values from the proposed method are in the range between minimum and maximum DER values.

For ECG record 121 and 202, the proposed method performs better than the others because of its capability in enhancing QRS signal to noise ratio for challenging situations such as low amplitude ECG data corrupted with baseline drift and various types of abnormal morphologies. As a result, only a simple beat detection step based on a single fixed threshold with no additional post-processing techniques is enough for achieving the DER value of 0 %. However, QRS signal to noise ratio from the QF is not high enough in some situations such as abrupt baseline shift (record 217), high-grade noise (record 105), and low amplitude QRS complex contaminated by muscle noise (record 108). Therefore, FP and FN detections are obtained from the proposed method. Other QRS algorithms overcome these problems using additional computations. On the one hand, the algorithms in some previous publications reduce FN detections using adaptive thresholding techniques [27, 31, 32, 35, 36] and false-noise detection algorithm

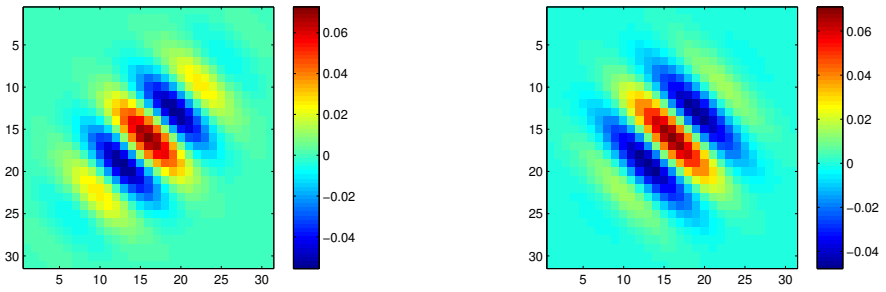

Figure 2.15: Quadratic filters. (Left panel) Original design. (Right panel) Reconstruct from the two largest modes of eigenvalue decomposition.

[20]. On the other hand, some algorithms in previous publications decrease FP detections using the technique based on the refractory period of 200 ms [20, 30, 36]. In other words, two consecutive QRS complexes cannot be detected within 200 ms. Another example used to decrease FP detections is the check up for irregular beat-to-beat interval information algorithm [27].

2.4.4 Computational Complexity Reduction

Figure 2.15(a) shows the quadratic filter from original design with a σ_y value of 0.7. After EVD, its eigenvalues is shown in Figure 2.16. We can see that the first two numbers of eigenvalues are significantly larger than the others. Therefore, for computational complexity reduction, the new quadratic filter is reconstructed from the two largest modes of EVD and shown in Figure 2.15(b). Figure 2.17 shows comparisons of ECG signals after filtering $y[n]$ from original design (solid line) with that from two largest modes of eigenvalue decomposition (dotted line). We can see that both lines are in agreement very well. These results indicate that computational complexity reduction with reconstructing of the new quadratic filter based on EVD is feasible.

2.5 Discussion

This chapter proposed the QRS detection algorithm, which employed the quadratic filter on enhancing QRS signal to noise ratio from ECG signals in preprocessing step. Results

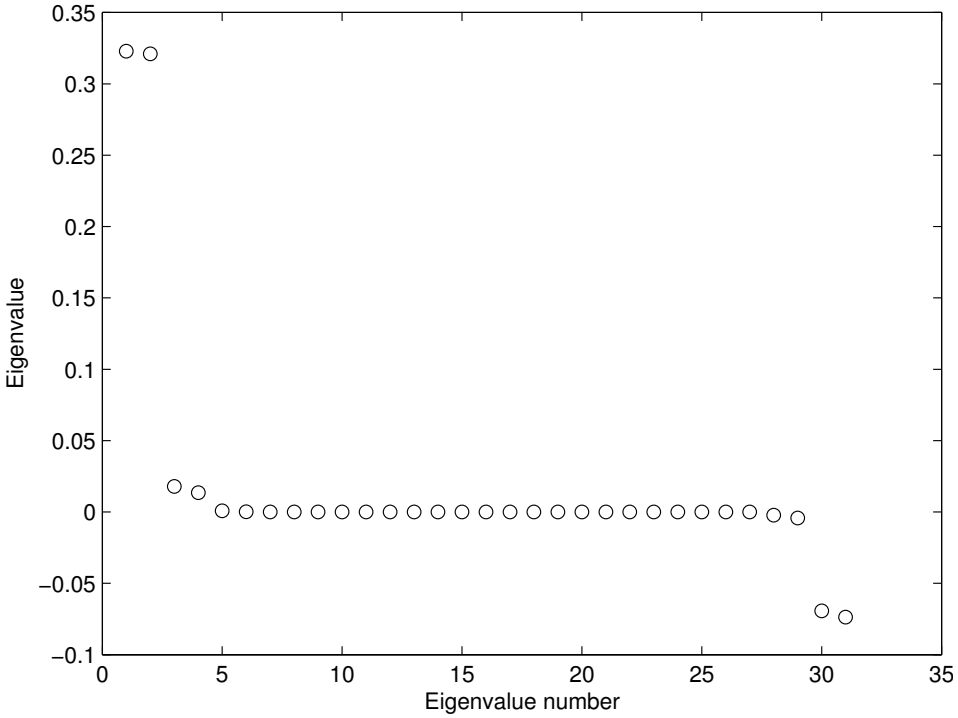

Figure 2.16: Eigenvalue as a function of eigenvalue number.

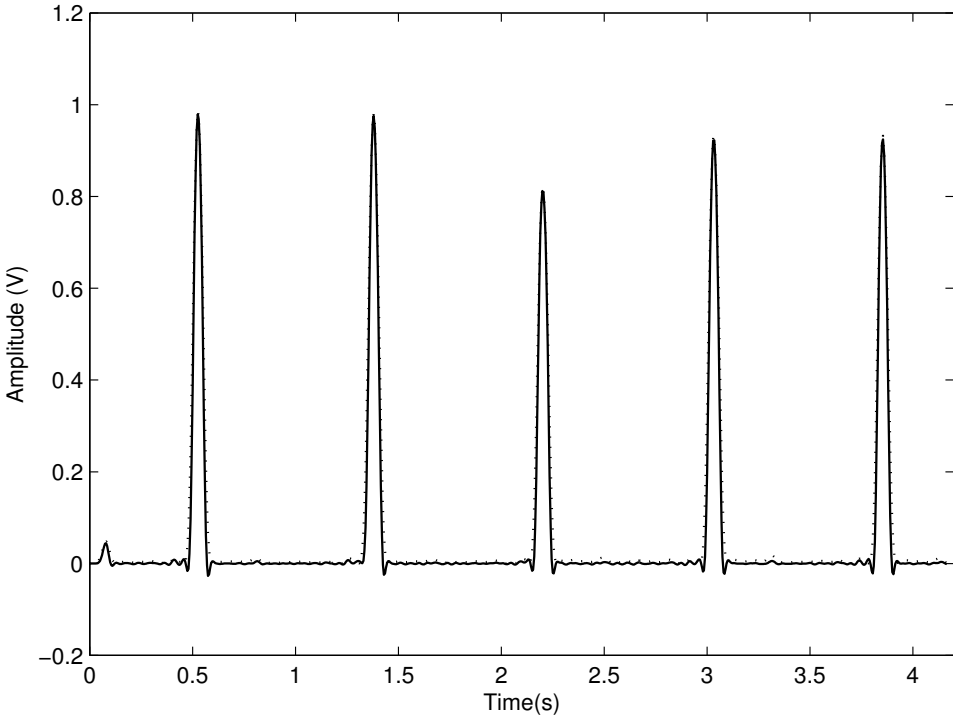

Figure 2.17: Comparisons of ECG signals from record 100 after filtering ($y[n]$) from Solid: Original design. Dotted: Two largest modes of eigenvalue decomposition.

show that the quadratic filter achieves in improving QRS signal to noise ratio for some challenging situations such as low amplitude QRS complex corrupted by baseline drift and a variety of abnormal morphologies such as a fusion of ventricular and normal beat, an atrial premature beat, an aberrated atrial premature beat, a premature ventricular contraction beat, a fusion of paced and normal beat, and a paced beat. Subsequently, the QRS complex is obtained with a simple beat detection algorithm based on an envelope signal and a single fixed threshold without additional post-processing techniques. The proposed algorithm was validated with the MIT-BIH arrhythmia database. The average DER value from 48 records is at 0.38%.

In next chapter, we explore the combination of the Mexican hat wavelet function in enhancing QRS signal to noise ratio in preprocessing step with the maximal filter in reducing FP detection in beat detection step.

Table 2.1: Performance evaluation of proposed algorithm.

Record	Total	TP	FN	FP	SEN(%)	PPR(%)	DER(%)
100	2272	2272	0	0	100.00	100.00	0.00
101	1865	1865	0	4	100.00	99.79	0.21
102	2187	2187	0	0	100.00	100.00	0.00
103	2084	2084	0	0	100.00	100.00	0.00
104	2228	2223	5	20	99.78	99.11	1.12
105	2572	2558	11	28	99.57	98.92	1.52
106	2027	2024	3	4	99.85	99.80	0.35
107	2136	2136	0	0	100.00	100.00	0.00
108	1763	1710	53	19	96.99	98.90	4.08
109	2532	2531	1	0	99.96	100.00	0.04
111	2124	2123	1	0	99.95	100.00	0.05
112	2539	2539	0	0	100.00	100.00	0.00
113	1794	1794	0	0	100.00	100.00	0.00
114	1879	1878	1	5	99.95	99.73	0.32
115	1953	1953	0	0	100.00	100.00	0.00
116	2412	2393	19	2	99.21	99.92	0.87
117	1535	1535	0	0	100.00	100.00	0.00
118	2278	2278	0	0	100.00	100.00	0.00
119	1987	1987	0	1	100.00	99.95	0.05
121	1863	1863	0	0	100.00	100.00	0.00
122	2476	2476	0	0	100.00	100.00	0.00
123	1518	1518	0	0	100.00	100.00	0.00
124	1619	1619	0	0	100.00	100.00	0.00
200	2601	2598	3	2	99.88	99.92	0.19
201	1963	1959	4	3	99.80	99.85	0.36
202	2136	2136	0	0	100.00	100.00	0.00
203	2980	2958	22	35	99.26	98.83	1.91
205	2656	2654	2	0	99.92	100.00	0.08
207	1860	1845	15	26	99.19	98.61	2.20
208	2955	2933	22	13	99.26	99.56	1.18
209	3005	3005	0	1	100.00	99.97	0.03
210	2650	2642	8	7	99.70	99.74	0.57
212	2748	2748	0	0	100.00	100.00	0.00
213	3250	3250	0	0	100.00	100.00	0.00
214	2262	2256	6	0	99.73	100.00	0.27
215	3363	3363	0	1	100.00	99.97	0.03
217	2208	2206	2	4	99.91	99.82	0.27
219	2154	2154	0	0	100.00	100.00	0.00
220	2047	2047	0	0	100.00	100.00	0.00
221	2427	2427	0	0	100.00	100.00	0.00
222	2483	2472	11	13	99.56	99.48	0.97
223	2605	2604	1	1	99.96	99.96	0.08
228	2053	2043	10	16	99.51	99.22	1.27
230	2256	2256	0	0	100.00	100.00	0.00
231	1571	1571	0	0	100.00	100.00	0.00
232	1780	1780	0	1	100.00	99.94	0.06
233	3079	3077	2	3	99.94	99.90	0.16
234	2753	2753	0	1	100.00	99.96	0.04
Total	109483	109281	202	210	99.82	99.81	0.38

Table 2.2: Performance comparison of the proposed algorithm with that from other 7 papers.

Method of noise removal	TP	FN	FP	SEN(%)	PPR(%)	DER(%)
Linear filtering [20]	109401	93	91	99.92	99.92	0.17
S-Transform [36]	108323	171	97	99.84	99.91	0.25
Artificial neural network [35]	109273	210	109	99.82	99.91	0.28
Wavelet transform [30]	109354	140	232	99.87	99.79	0.34
Quadratic filtering (This work)	109281	202	210	99.82	99.81	0.38
Matematical morphology [32]	109297	213	204	99.80	99.81	0.38
Wavelet transform [31]	115945	192	308	99.81	99.70	0.49
Wavelet transform [27]	109118	376	218	99.66	99.80	0.54

Table 2.3: Comparisons of the DER values in percent of ECG record 121, 202, 200, 217, 105, and 108 from the proposed method with that from other 7 papers.

Method of noise removal	121	202	200	217	105	108
Quadratic filtering (This work)	**0.00**	**0.00**	0.19	0.27	1.59	4.08
Wavelet transform [30]	0.10	0.09	0.30	0.23	0.81	8.40
Linear filtering [20]	0.11	0.09	**0.15**	**0.09**	1.25	0.57
S-Transform [36]	0.16	0.09	0.23	0.23	1.24	2.44
Artificial neural network [35]	0.16	0.33	0.31	*0.64*	**0.23**	**0.51**
Wavelet transform [27]	0.16	*0.37*	*1.00*	0.32	2.02	4.71
Wavelet transform [31]	0.32	**0.00**	0.19	0.27	*2.41*	*12.40*
Mathematical morphology [32]	*0.70*	*0.37*	0.50	0.23	1.01	0.68

Chapter 3

QRS Detection Based on Mexican Hat Wavelet Function and Maximal Filter

3.1 Introduction

This chapter proposes a QRS detection algorithm consisting of the Mexican hat wavelet function and the maximal filter. While the Mexican hat wavelet function is capable of enhancing QRS signal to noise ratio, the maximal filter is employed for reducing FP detections. Results show that the excellent detection accuracy can be obtained without the need for adaptive thresholding and post-processing operations.

The rest of this chapter is organized as follows. Section 3.2 presents the background on continuous wavelet transform (CWT). Section 3.3 describes the proposed QRS detection algorithm. Results are given in section 3.4. Finally, discussion is stated in section 3.5.

3.2 Continuous Wavelet Transform

The CWT has been gained popular uses for decomposing signals in many applications including noise removal in ECG signals. Given the input signal $x(t)$, which is the ECG signal in this research project, the CWT of $x(t)$ can be expressed as

$$T_{a,b} = \int_{-\infty}^{\infty} x(t) \frac{1}{\sqrt{a}} \psi^* \left(\frac{t-b}{a} \right) dt, \tag{3.1}$$

where $T_{a,b}$ is the CWT of $x(t)$, a is the dilation or scale parameter, b is the location parameter, and $\psi^*(t)$ is the complex conjugate of the wavelet function. The scale and the wavelet function are two important parameters affecting the performance of noise removal in ECG signals.

There are a variety types of the wavelet function. However, the Maxican hat wavelet function is selected in this research project for removing noises and enhancing QRS signal to noise ratio because its similarity to the shape of the QRS complex from the normal ECG beat [40]. The Maxican hat wavelet function, which is the second derivative of a Gaussian function, is given by

$$\psi(t) = \frac{1}{\sqrt{2\pi}}(1 - t^2)\exp\left(\frac{-t^2}{2}\right). \tag{3.2}$$

3.3 Proposed Algorithm

Based on the block diagram shown in Figure 1.2, the QRS detection algorithm used for evaluating wavelet functions consists of three steps: noise removal using CWT, envelope signal determination, and R peak detection. Details of each step are as follows.

1. Determine the signal after noise removal $y[n]$ from the ECG signal $x[n]$ by processing based on the CWT with the Mexican hat wavelet function, which can be expressed as

$$y[n] = T^2_{a,b}. \tag{3.3}$$

   The scale parameter a was varied in the range of 2 to 4 to find the best scale in maximizing QRS signal to noise ratio.

2. Determine the envelope signal $z[n]$ from $y[n]$ using the maximal filter with the length L as given by

$$z[n] = \max_{k\in[n-L+1,n]} y[k]. \tag{3.4}$$

   The length L was varied in the range of 120 ms to 270 ms to find the best length of the maximal filter in minimizing total false detection (FN+FP) from 48 records

of ECG data.

3. Detect the R peak $r[n]$ in QRS complex using the following steps.

   (a) Define a threshold value thv.

   (b) Find the time duration where $z[n]$ is greater than thv and determine the beginning time t_1 and the ending time t_2.

   (c) Determine the R peak location t_R from time between $[t_1 \ \ t_2]$ in $y[n]$ that gives the maximum amplitude.

3.4 Results

3.4.1 Scale and Filter Length

Figure 3.1 shows the number of total false detection (FP + FN) from 48 records of ECG data as a function of a scale in CWT ranging from 2 to 4. Two examples of total false detections determined using the filter length of 120 ms and 220 ms are shown using the circle and pentagram markers, respectively. Results show that the scale 3 give smaller total false detection compared to those from other scales in both cases. In other words, the Mexican hat wavelet function at scale 3 provides the best QRS signal to noise ratio enhancement. Subsequently, the length of maximal filter was varied to find the minimal total false detection when the scale was fixed at 3.

Figure 3.2 shows the number of FN, FP, and FN+FP from 48 records of ECG data as a function of a filter length L using the cross, circle, and pentagram markers, respectively. Results show the trade-off between FN and FP detections when the filter length increases. In other words, when the filter length increases, the FP detections decrease but the FN detections increase. The minimal false detection rate at 309 FN+FP beats consisting of 111 FN beats and 198 FP beats is obtained when the length of the maximal filter L is 195 ms.

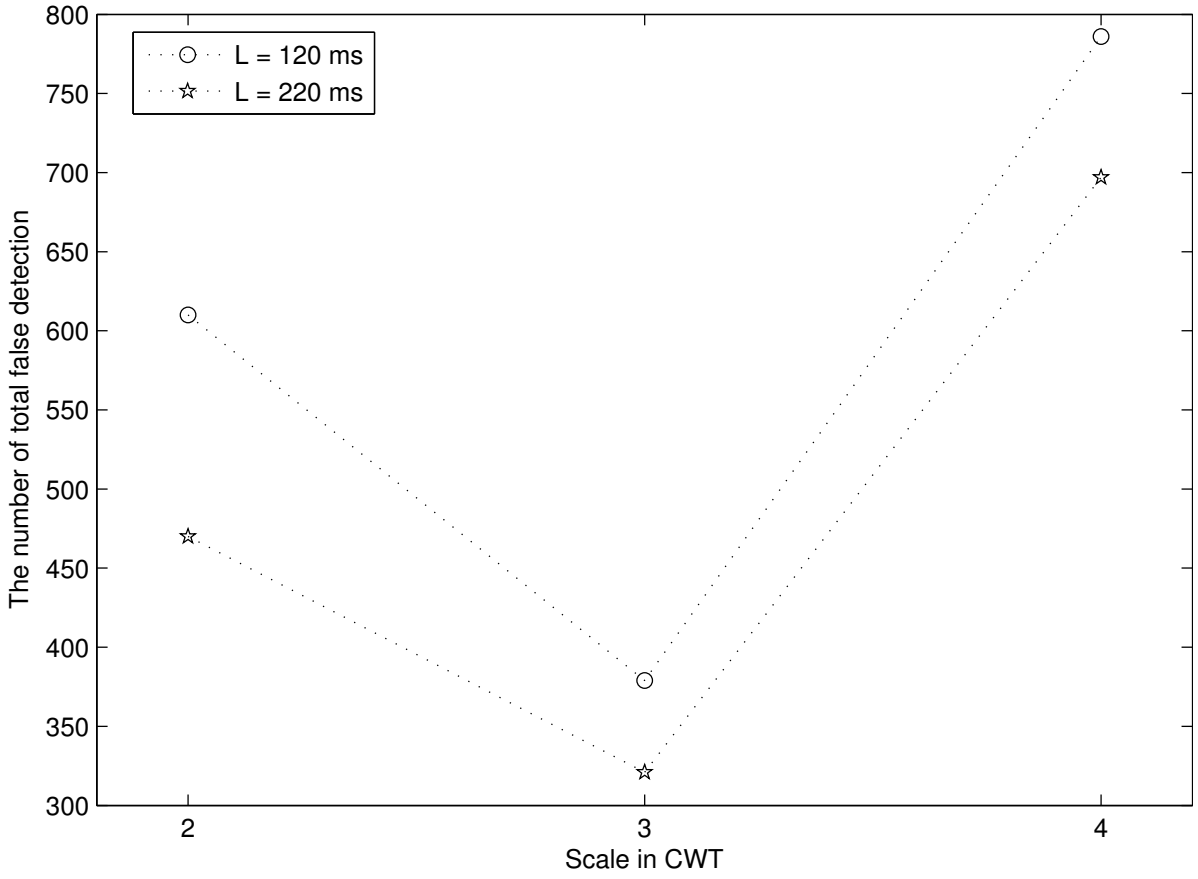

Figure 3.1: The number of total false detection (FP + FN) from 48 records of ECG data as a function of a scale in CWT when filter lengths were fixed at 120 ms (circle) and 220 ms (pentagram).

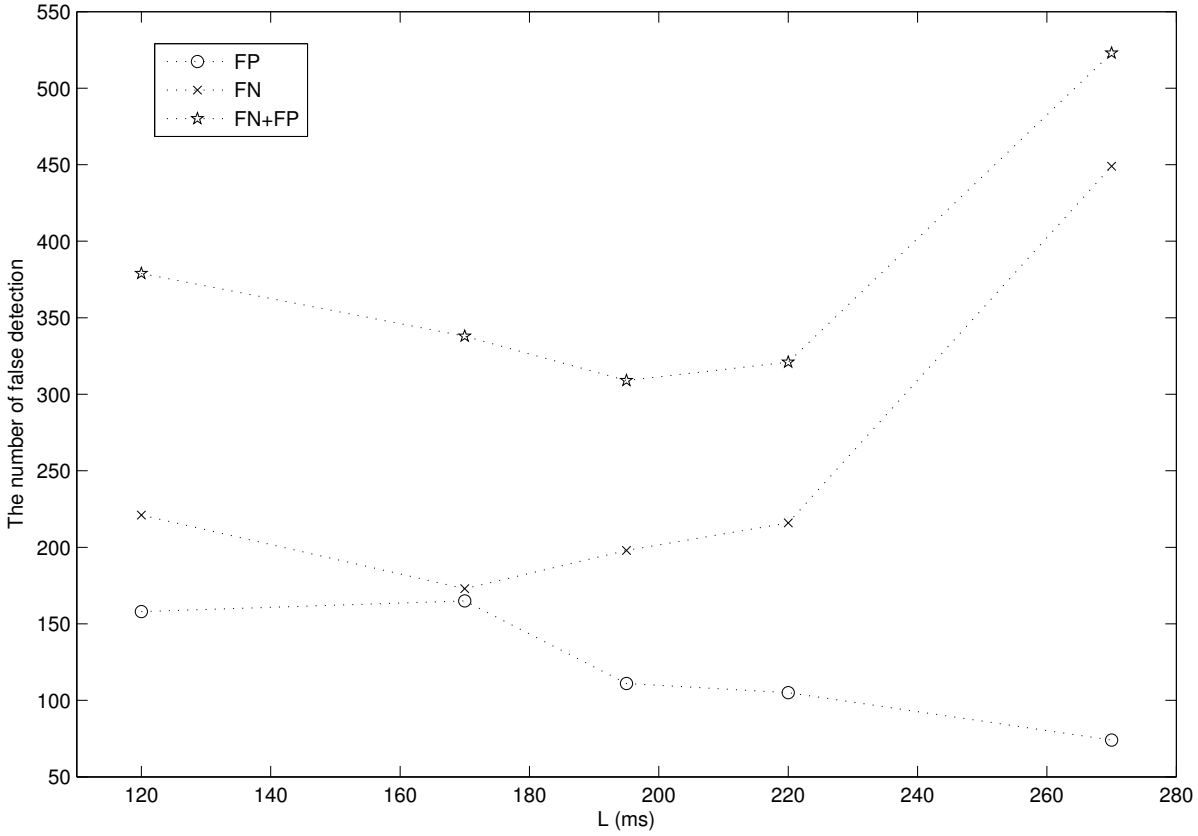

Figure 3.2: The number of FN (cross), FP (circle), and FN+FP (pentagram) from 48 records of ECG data as a function of a filter length L when the scale of Mexican hat wavelet function was fixed at 3.

3.4.2 Signal Characteristic

To illustrate the capability of the combination between Mexican hat wavelet function at scale 3 and the maximal length filter at length 195 ms in enhancing QRS signal to noise ratio, example results from ECG data of record 118, 221, 232, 121, 200, 108, and 105 are demonstrated.

Figure 3.3(a) shows the ECG data of record 118 from time 1381 s to time 1391 s consisting of 9 right bundle branch block beats, a premature ventricular contraction beat, and an atrial premature beat. Figure 3.3(b) shows the output signals from the Mexican hat wavelet function. It can be clearly seen that the QRS signal to noise ratio enhancement is obtained. Figure 3.3(c) shows the envelope signal $z[n]$ with a solid line and the threshold level thv with a dotted line. We can see that the threshold value thv is appropriate with the envelope signal $z[n]$. As a result, all beats are correctly detected as shown in Figure 3.3(d).

Figure 3.4(a) shows the ECG data of record 221 from time 838 s to time 848 s consisting of 11 normal beats and 4 premature ventricular contraction beats. In addition, 3 beats of ventricular tachycardia can be observed at time 842-843 s. Enhancement of QRS signal to noise ratio can be observed from the ECG signal after noise removal $y[n]$ shown in Figure 3.4(b). Based on the envelope signal $z[n]$ and the threshold level thv shown in Figure 3.4(c), all ECG beats are correctly detected as shown in Figure 3.4(d).

Figure 3.5(a) shows the ECG data of record 232 from time 717 s to time 727 s consisting of 11 atrial premature beats and a right bundle branch block beat contaminated by noise. Figure 3.5(b) shows the ECG signal after noise removal $y[n]$ with the improvement in QRS signal to noise ratio. Figure 3.5(c) shows the envelope signal $z[n]$ using a solid line and the threshold level thv using a dotted line. Figure 3.5(d) shows all correct beat detections from the proposed algorithm using a square marker compared to those from the expert using an asterisk marker.

Figure 3.6(a) shows the ECG data of record 121 from time 1650 s to time 1660

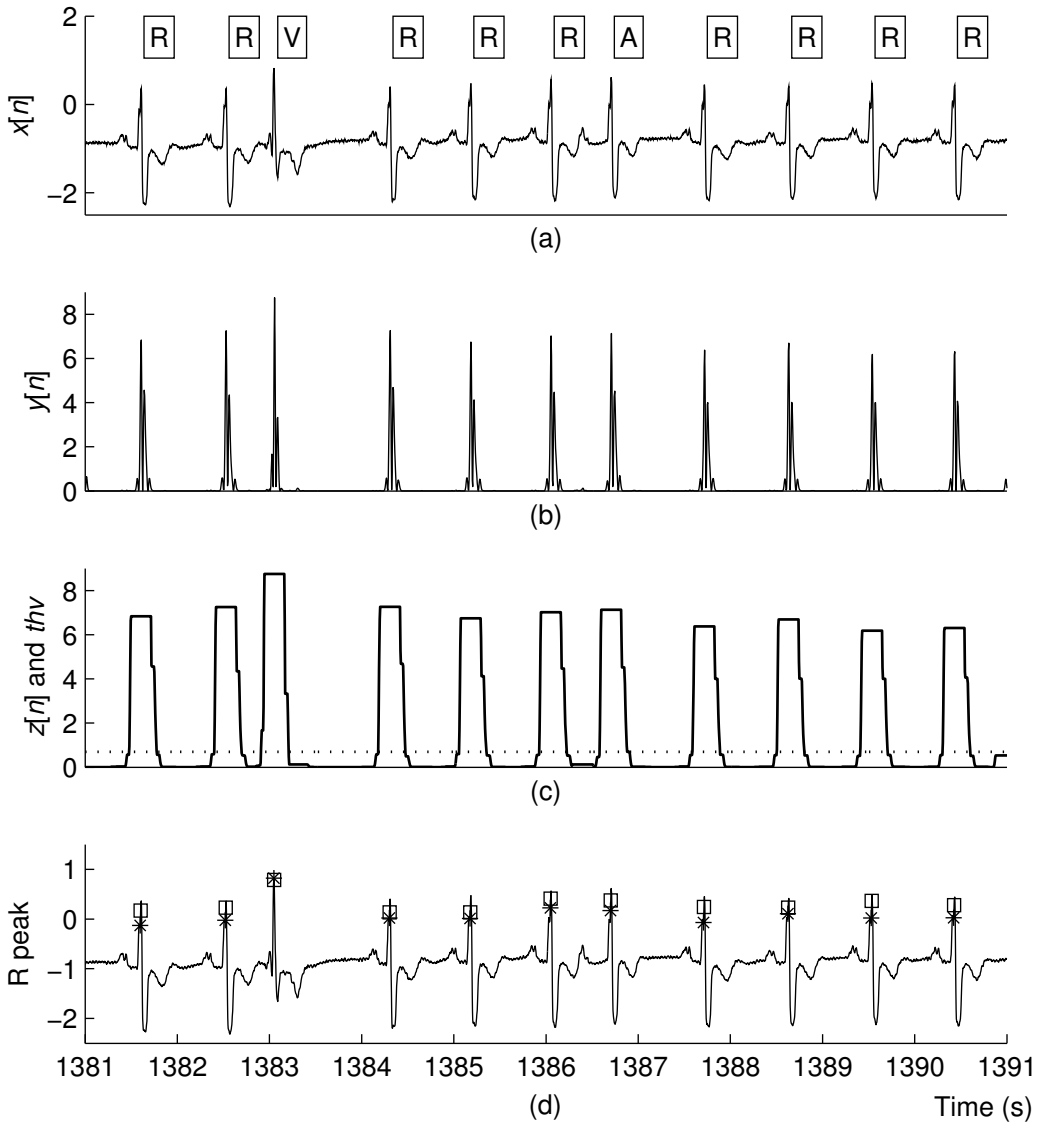

Figure 3.3: Results of the proposed algorithm applied on the ECG signal record 118. (a) The ECG signal before noise removal $x[n]$. "R" stands for a right bundle branch block beat, "V" for a premature ventricular contraction beat, and "A" for an atrial premature beat. (b) The ECG signal after noise removal $y[n]$. (c) The envelope signal $z[n]$ shown in a solid line and the threshold level thv shown in a dotted line. (d) The ECG signal overlaid by the markers from the proposed algorithm (square) and the expert (asterisk).

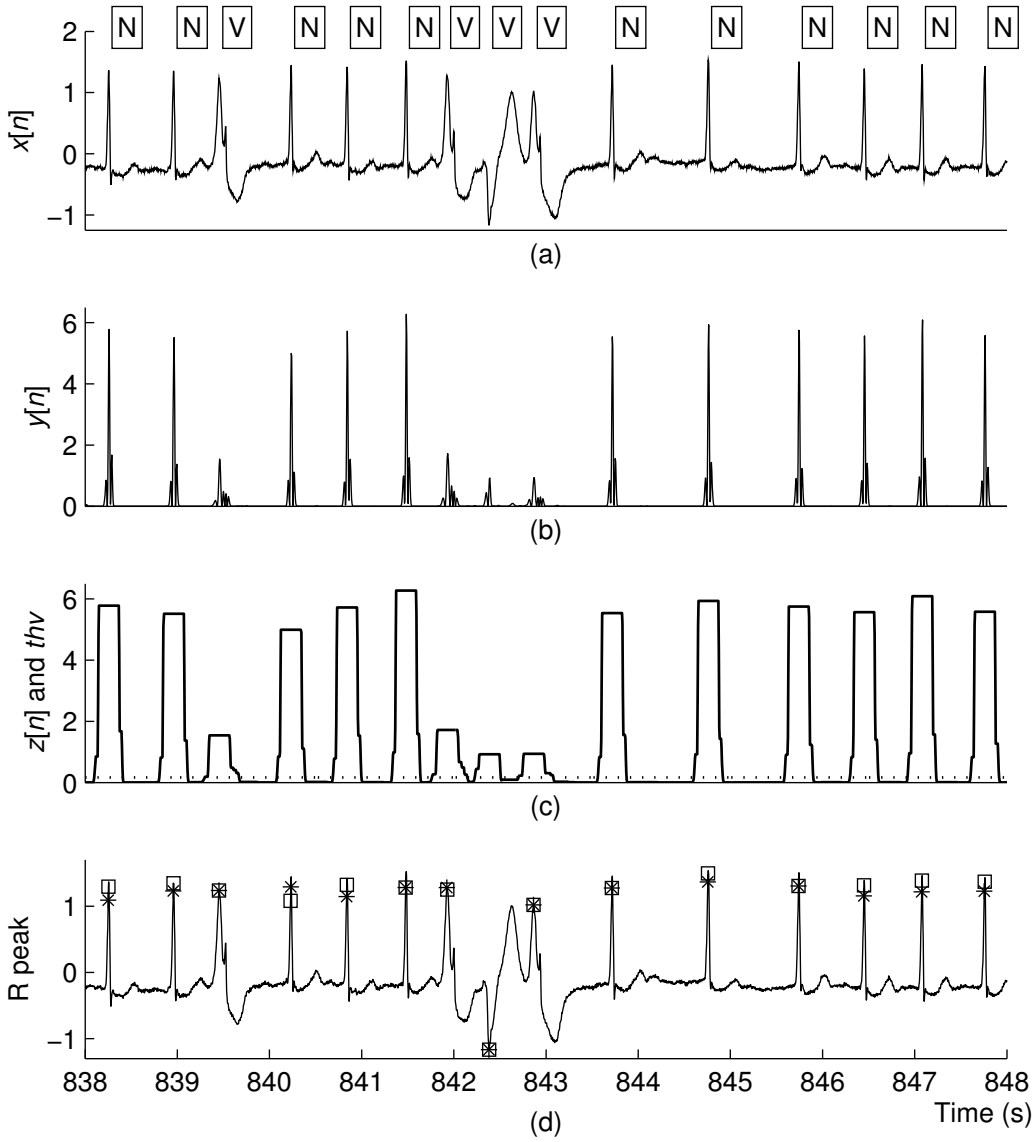

Figure 3.4: Results of the proposed algorithm applied on the ECG signal record 221. (a) The ECG signal before noise removal $x[n]$. "N" stands for a normal beat. (b) The ECG signal after noise removal $y[n]$. (c) The envelope signal $z[n]$ shown in a solid line and the threshold level thv shown in a dotted line. (d) The ECG signal overlaid by the markers from the proposed algorithm (square) and the expert (asterisk).

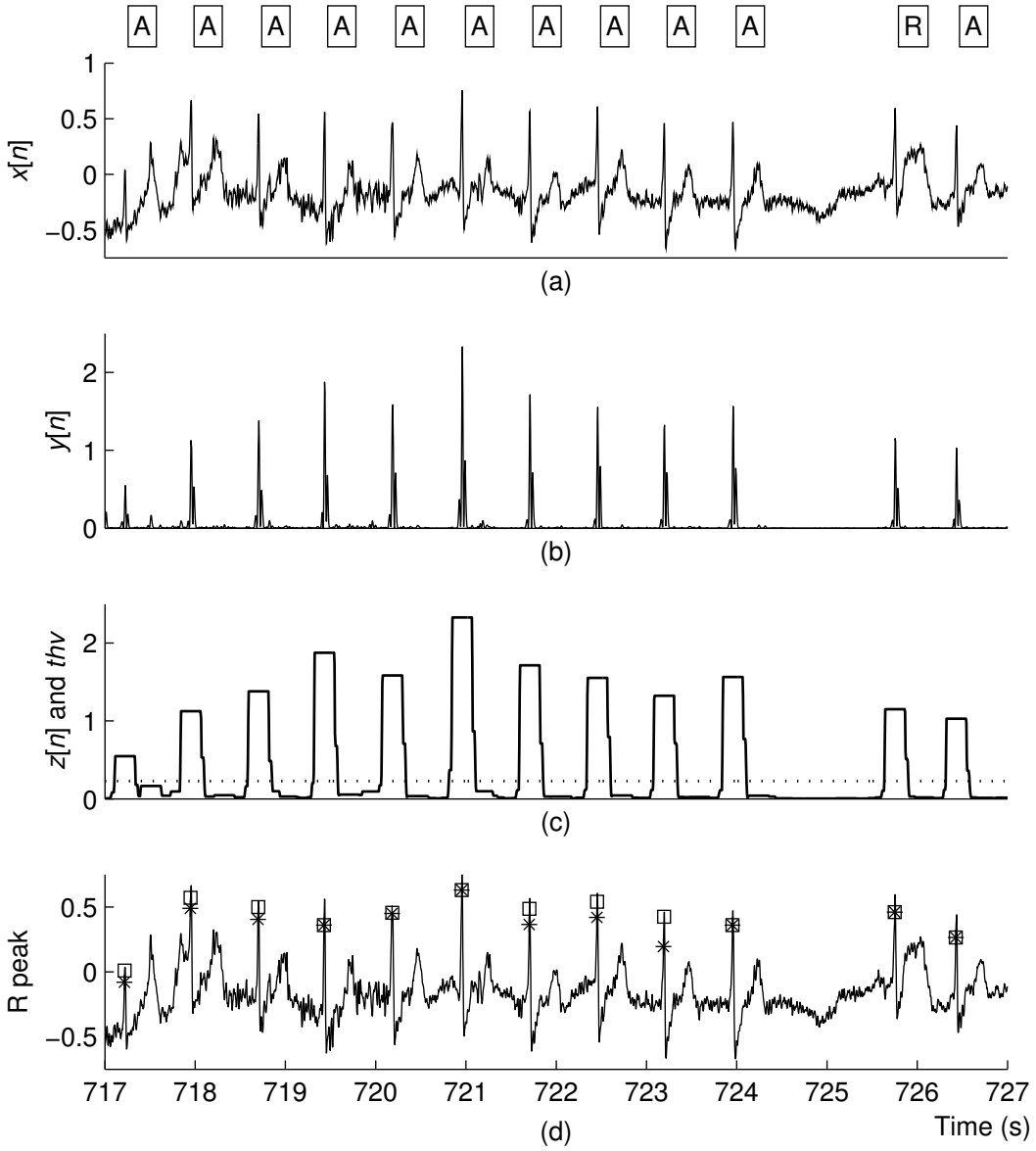

Figure 3.5: Results of the proposed algorithm applied on the ECG signal record 232. (a) The ECG signal before noise removal $x[n]$. (b) The ECG signal after noise removal $y[n]$. (c) The envelope signal $z[n]$ shown in a solid line and the threshold level thv shown in a dotted line. (d) The ECG signal overlaid by the markers from the proposed algorithm (square) and the expert (asterisk).

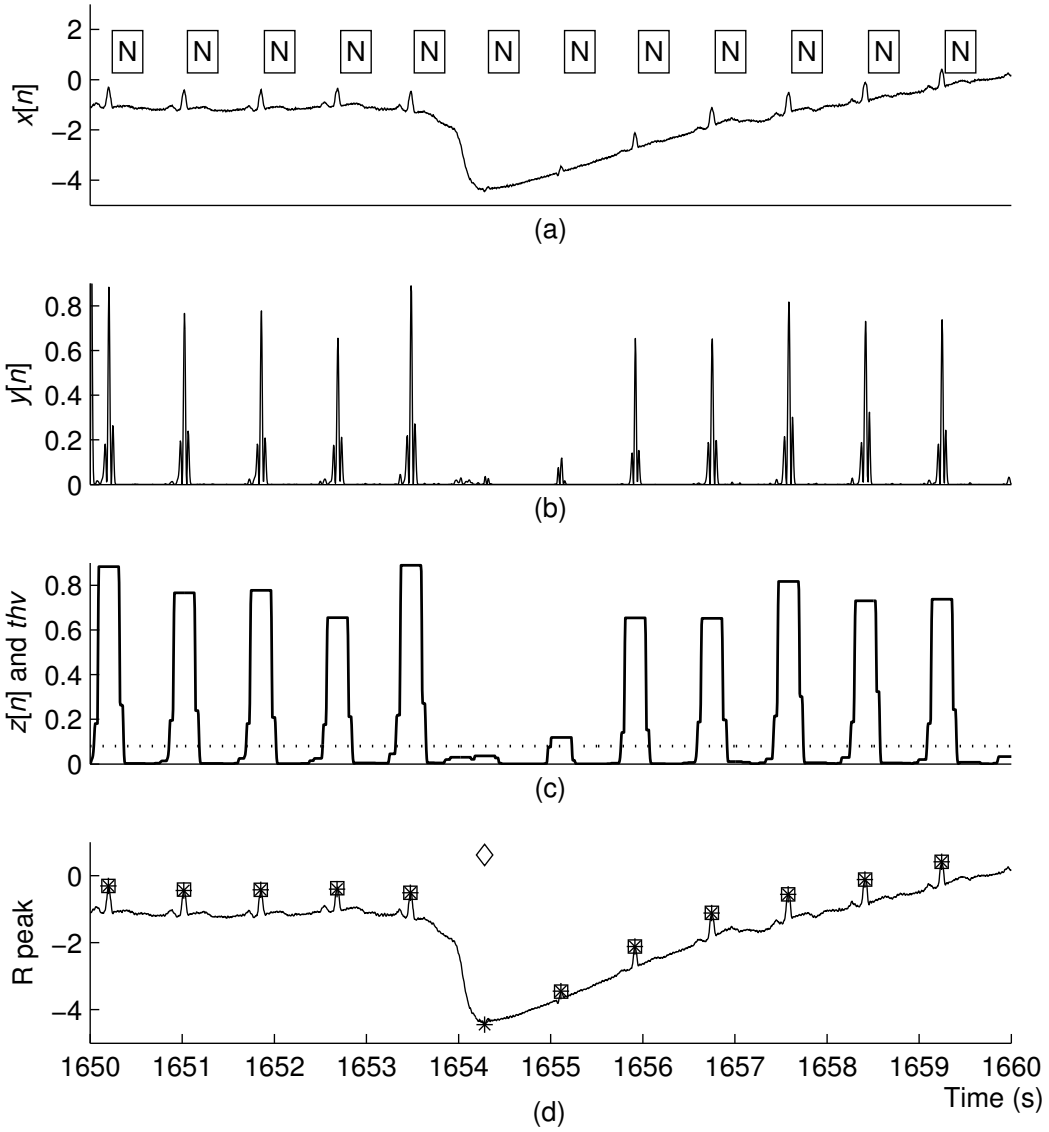

Figure 3.6: Results of the proposed algorithm applied on the ECG signal record 121. (a) The ECG signal before noise removal $x[n]$. (b) The ECG signal after noise removal $y[n]$. (c) The envelope signal $z[n]$ shown in a solid line and the threshold level thv shown in a dotted line. (d) The ECG signal overlaid by the markers from the proposed algorithm (square) and the expert (asterisk). "$\diamond$" stands for an FN detection.

s. ECG data in this record are corrupted by baseline drift and some QRS complexes have very low amplitude. Figure 3.6(b) shows significant improvement in QRS signal to noise ratio of the ECG signal after noise removal $y[n]$. The corresponding envelope signal $z[n]$ and the threshold value thv are shown in Figure 3.6(c). There is an FN detection shown in Figure 3.6(c) using a diamond marker at time 1654.2 s because the threshold level thv in this record is higher than the normal beat after applying with the CWT.

Figure 3.7(a) shows the ECG data of record 200 from time 1070 s to time 1080 s consisting of 7 normal beats, 7 premature ventricular contraction beats, and a fusion of ventricular and normal beat. Note that the fusion of ventricular and normal beat has very low amplitude. Figure 3.7(b) and (c) show the ECG signal after noise removal $y[n]$ and the corresponding envelope signal $z[n]$ as well as the threshold value thv, respectively. Figure 3.7(d) shows an FN detection at time 1072 s because of the low amplitude of fusion of ventricular and normal beat after QRS signal to noise ratio enhancement with CWT.

Figure 3.8(a) shows the ECG data of record 108 from time 1710 s to time 1720 s., which are contaminated by the respiratory related rhythms and muscle artifacts. The high degree of noise cannot be completely removed as shown in Figure 3.8(b). Figure 3.8(c) shows the envelope signal $z[n]$ with a solid line and the threshold level thv with a dotted line. We can see that the amplitudes of noises within the envelop signals at time 1712 and 1713 s are higher than those of ECG signals. As a result, two FN beats and two FP beats are detected and shown in Figure 3.8(d).

Figure 3.9(a) shows the ECG data of record 105 from time 1321 s to time 1331 s. ECG data in this record are contaminated with high-grade noise. Although the QRS complex can be emphasized by the CWT as shown in Figure 3.9(b), the high-grade noise is also amplified. Figure 3.9(c) shows the envelope signal $z[n]$ and the threshold level thv. The signal after filtering from high-grade noise causes 2 FP detections and an FN detections as shown in Figure 3.9(d).

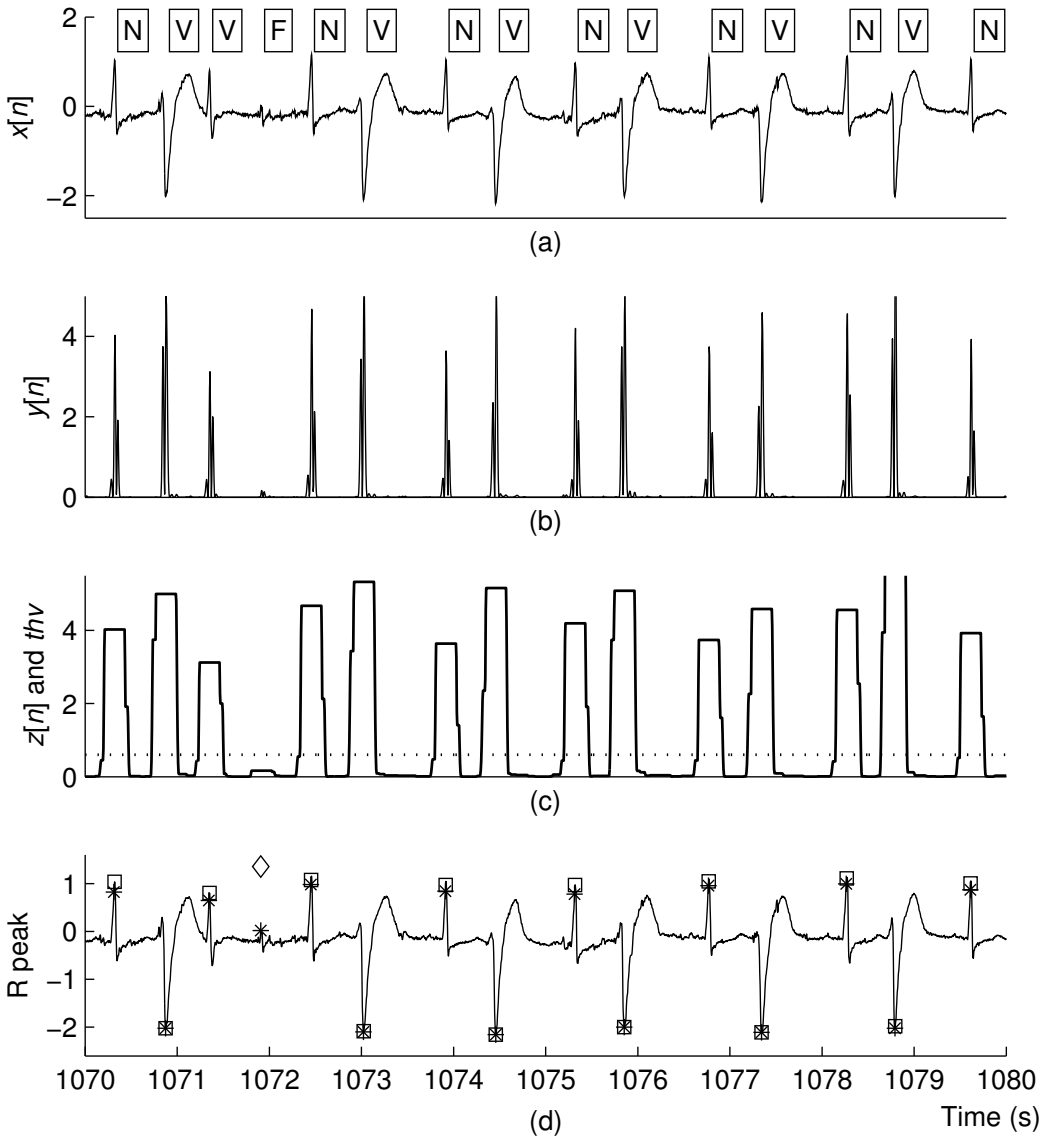

Figure 3.7: Results of the proposed algorithm applied on the ECG signal record 200. (a) The ECG signal before noise removal $x[n]$. "F" stands for a fusion of ventricular and normal beat. (b) The ECG signal after noise removal $y[n]$. (c) The envelope signal $z[n]$ shown in a solid line and the threshold level thv shown in a dotted line. (d) The ECG signal overlaid by the markers from the proposed algorithm (square) and the expert (asterisk).

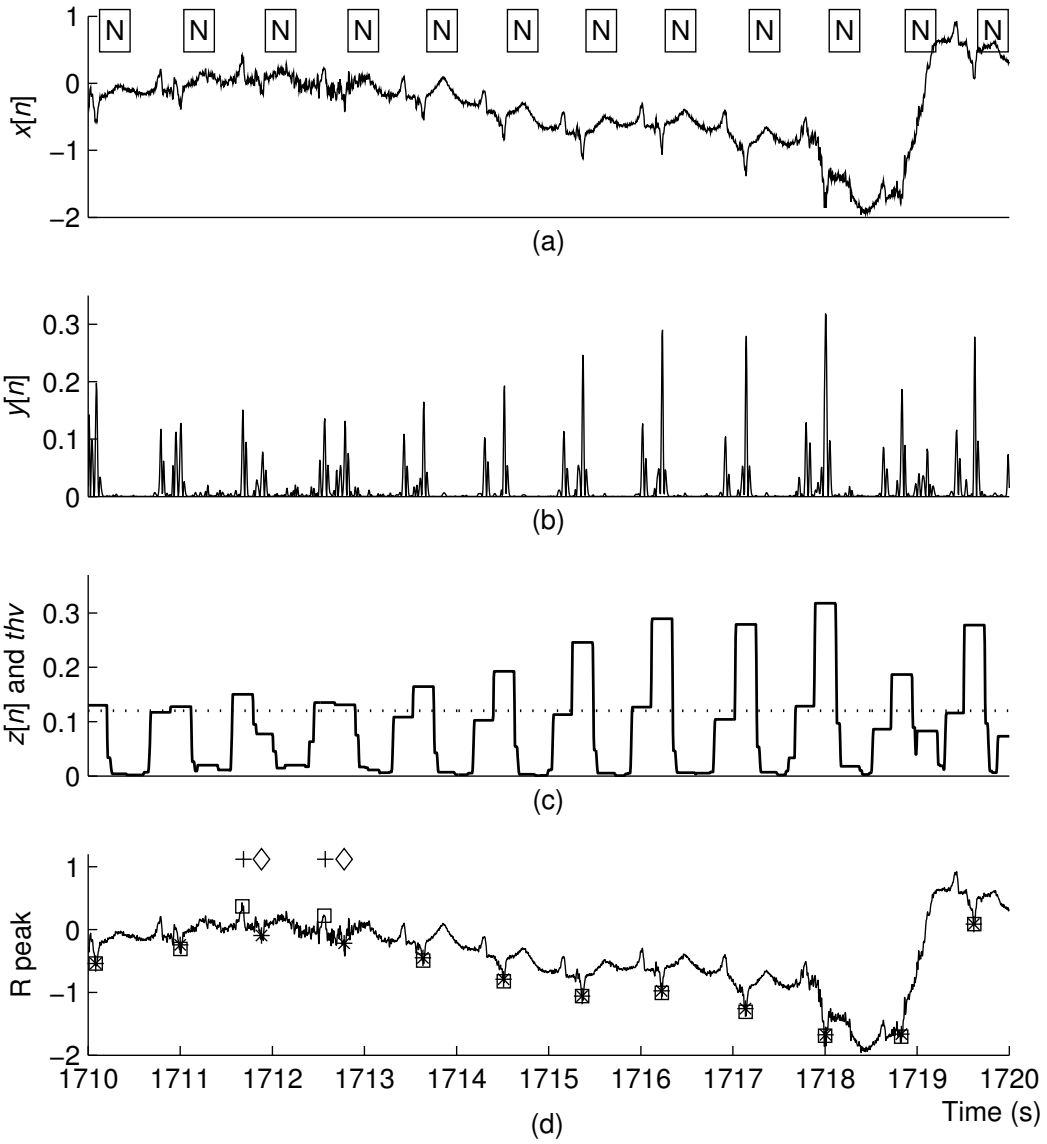

Figure 3.8: Results of the proposed algorithm applied on the ECG signal record 108. (a) The ECG signal before noise removal $x[n]$. (b) The ECG signal after noise removal $y[n]$. (c) The envelope signal $z[n]$ shown in a solid line and the threshold level thv shown in a dotted line. (d) The ECG signal overlaid by the markers from the proposed algorithm (square) and the expert (asterisk). "+" stands for an FP detection.

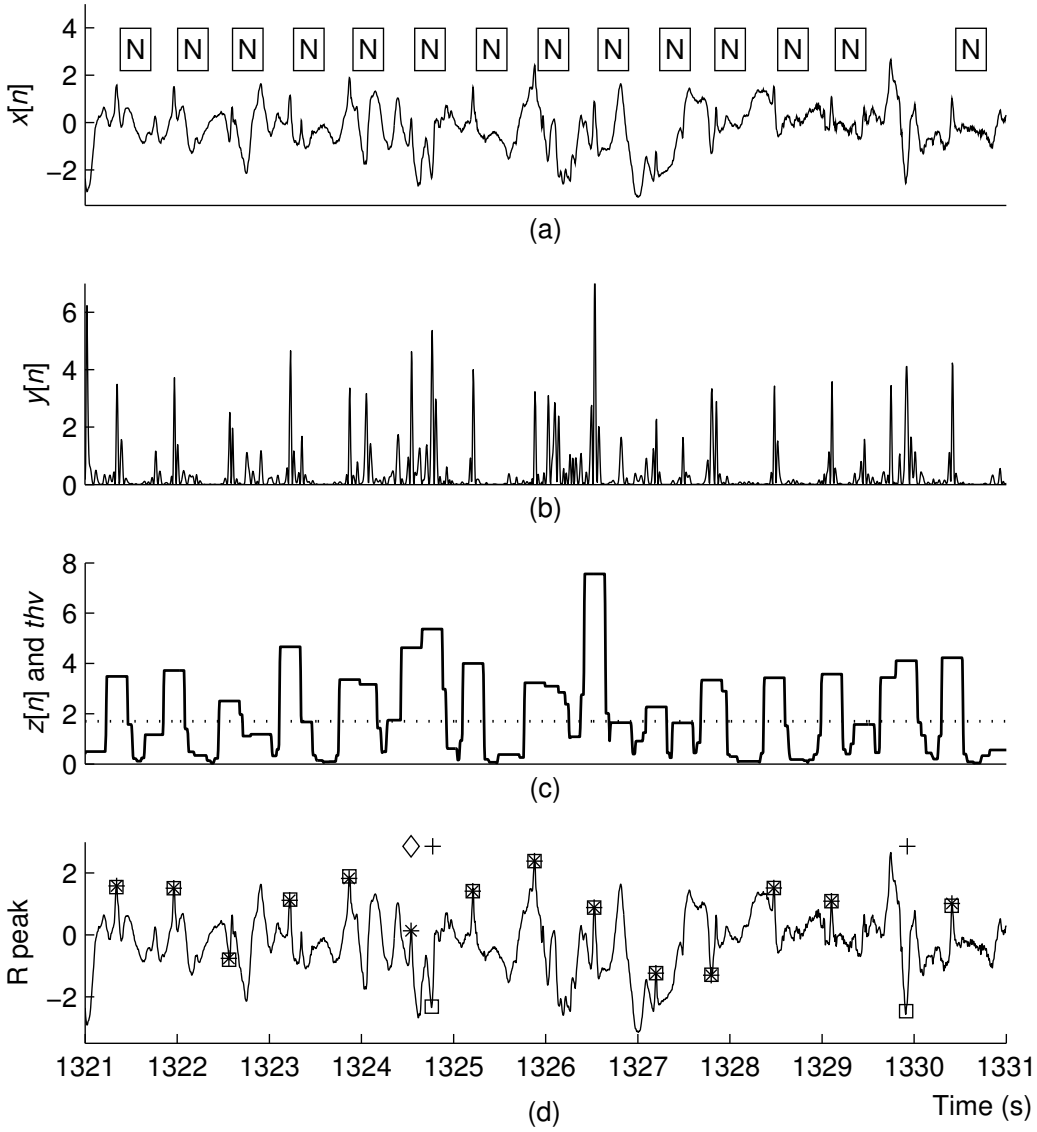

Figure 3.9: Results of the proposed algorithm applied on the ECG signal record 105. (a) The ECG signal before noise removal $x[n]$. (b) The ECG signal after noise removal $y[n]$. (c) The envelope signal $z[n]$ shown in a solid line and the threshold level thv shown in a dotted line. (d) The ECG signal overlaid by the markers from the proposed algorithm (square) and the expert (asterisk).

3.4.3 Performance Evaluation and Comparison

Table 3.1 shows performance evaluation of the proposed algorithm applied on all 48 records of ECG data when the scale of wavelet function and the length of the maximal filter are fixed at 3 and 195 ms, respectively. The average DER value is 0.27%. The values of total TP, FN, and FP beats are 109293 beats, 198 beats, 111 beats, respectively. The average values of SEN and PPR are 99.83% and 99.90%, respectively. While the maximum DER value is 2.15% from the record 203, the minimum DER value is 0% from 20 records, i.e. record 100, 102, 103, 107, 109, 112, 113, 115, 117, 118, 122-124, 212, 219, 220, 221, 230, 231, and 234.

Table 3.2 shows the performance comparison of the proposed algorithm with that from other 7 state-of-the-art papers. The order of each method is sorted from the minimal average DER value to the maximal average DER value. The minimal and maximal average DER values are 0.17% [20] and 0.54% [27], respectively. The average DER value from the proposed algorithm based on the combination of Mexican hat wavelet function at scale 3 and the maximal filter at length 195 ms is 0.27%. This result shows that the Mexican hat wavelet function at scale 3 can significantly increase the QRS signal to noise ratio and the maximal filter at length 195 ms can efficiently reduce FP detections. As a result, only the use of a single fixed threshold without additional post-processing techniques can yield low average DER value.

Table 3.3 shows comparison results of the DER values of ECG record 118, 221, 232, 121, 200, 108, and 105 from the proposed method with that from other 7 papers. The minimum and maximum DER values for each record are shown using the boldface and italics fonts, respectively. The DER values of ECG record 118 and 221 from the proposed method are minimal at 0%. For other ECG records, the DER values from the proposed method are in the range between minimum and maximum DER values.

3.5 Discussion

This chapter proposes the QRS detection algorithm employing the efficient cascade of two combination steps, i.e., the Mexican hat wavelet function on enhancing QRS signal to noise ratio in preprocessing step and the maximal filter on reducing FP detections in beat detection step. Results show that the proposed algorithm achieved in enhancing QRS signal to noise ratio from a variety of beat types such as a right bundle branch block beat, a premature ventricular contraction beat, an atrial premature beat, and a fusion of ventricular and normal beat. The subsequent beat detection step based on the maximal filter is capable of reducing FP detection into a same level among the top previous publications. Using a single threshold without any additional post-processing techniques, the proposed algorithm can achieve DER value of 0.27% validated with 48 records of MIT-BIH arrhythmia database.

In addition to a single scale wavelet function used in the QRS detection algorithm as shown in this chapter, in next chapter we investigate the utilization of wavelet functions at various scales in the preprocessing step of QRS detection algorithm to improve QRS signal to ratio and QRS detection accuracy. Moreover, quantitative measurement of efficiency of wavelet function types in enhancing QRS signal to noise ratio is also studied.

Table 3.1: Performance evaluation of proposed algorithm.

Record	Total	TP	FN	FP	SEN(%)	PPR(%)	DER(%)
100	2273	2273	0	0	100.00	100.00	0.00
101	1865	1865	0	4	100.00	99.79	0.21
102	2187	2187	0	0	100.00	100.00	0.00
103	2084	2084	0	0	100.00	100.00	0.00
104	2228	2223	1	8	99.96	99.64	0.40
105	2572	2554	18	16	99.30	99.38	1.32
106	2027	2025	2	4	99.90	99.80	0.30
107	2136	2136	0	0	100.00	100.00	0.00
108	1763	1748	15	12	99.15	99.32	1.53
109	2532	2532	0	0	100.00	100.00	0.00
111	2124	2123	1	0	99.95	100.00	0.05
112	2539	2539	0	0	100.00	100.00	0.00
113	1794	1794	0	0	100.00	100.00	0.00
114	1879	1876	3	4	99.84	99.79	0.37
115	1953	1953	0	0	100.00	100.00	0.00
116	2412	2392	20	2	99.17	99.92	0.91
117	1535	1535	0	0	100.00	100.00	0.00
118	2278	2278	0	0	100.00	100.00	0.00
119	1987	1987	0	1	100.00	99.95	0.05
121	1863	1862	1	1	99.95	99.95	0.11
122	2476	2476	0	0	100.00	100.00	0.00
123	1518	1518	0	0	100.00	100.00	0.00
124	1619	1619	0	0	100.00	100.00	0.00
200	2601	2598	3	0	99.88	100.00	0.12
201	1963	1953	10	3	99.49	99.85	0.66
202	2136	2135	1	1	99.95	99.95	0.09
203	2980	2928	52	12	98.26	99.59	2.15
205	2656	2651	5	0	99.81	100.00	0.19
207	1860	1850	10	17	99.46	99.09	1.45
208	2955	2939	16	9	99.46	99.69	0.85
209	3005	3005	0	1	100.00	99.97	0.03
210	2650	2644	6	4	99.77	99.85	0.38
212	2748	2748	0	0	100.00	100.00	0.00
213	3251	3248	3	2	99.91	99.94	0.15
214	2262	2257	5	0	99.78	100.00	0.22
215	3363	3359	4	0	99.88	100.00	0.12
217	2208	2205	3	1	99.86	99.95	0.18
219	2154	2154	0	0	100.00	100.00	0.00
220	2047	2047	0	0	100.00	100.00	0.00
221	2427	2427	0	0	100.00	100.00	0.00
222	2483	2477	6	1	99.76	99.96	0.28
223	2605	2604	1	0	99.96	100.00	0.04
228	2053	2044	9	7	99.56	99.66	0.78
230	2256	2256	0	0	100.00	100.00	0.00
231	1571	1571	0	0	100.00	100.00	0.00
232	1780	1780	0	1	100.00	99.94	0.06
233	3079	3076	3	0	99.90	100.00	0.10
234	2753	2753	0	0	100.00	100.00	0.00
Total	109491	109293	198	111	99.83	99.90	0.27

Table 3.2: Performance comparison of the proposed algorithm with that from other 7 papers.

Method of noise removal	TP	FN	FP	SEN(%)	PPR(%)	DER(%)
Linear filtering [20]	109401	93	91	99.92	99.92	0.17
S-Transform [36]	108323	171	97	99.84	99.91	0.25
This work	109293	198	111	99.83	99.90	0.27
Artificial neural network [35]	109273	210	109	99.82	99.91	0.28
Wavelet transform [30]	109354	140	232	99.87	99.79	0.34
Matematical morphology [32]	109297	213	204	99.80	99.81	0.38
Wavelet transform [31]	115945	192	308	99.81	99.70	0.49
Wavelet transform [27]	109118	376	218	99.66	99.80	0.54

Table 3.3: Comparisons of the DER values in percent of ECG record 118, 221, 232, 121, 200, 108, and 105 from the proposed method with that from other 7 papers.

Method of noise removal	118	221	232	121	200	108	105
This work	**0.00**	**0.00**	**0.06**	0.11	**0.12**	1.53	1.32
Wavelet transform [30]	0.08	0.08	0.11	**0.10**	0.30	8.40	0.81
Linear filtering [20]	0.04	**0.00**	**0.06**	0.11	0.15	0.57	1.25
S-Transform [36]	*0.22*	0.16	**0.06**	0.16	0.23	2.44	1.24
Artificial neural network [35]	**0.00**	0.33	*0.62*	0.16	0.31	**0.51**	**0.23**
Wavelet transform [27]	*0.22*	0.16	**0.06**	0.16	*1.00*	4.71	2.02
Wavelet transform [31]	0.04	0.04	0.11	0.32	0.19	*12.40*	*2.41*
Mathematical morphology [32]	*0.22*	*0.49*	0.09	*0.70*	0.50	0.68	1.01

Chapter 4

QRS Signal to Noise Ratio and Wavelet Functions

4.1 Introduction

The algorithm of R peak detection in the QRS complex is composed of two main steps, i.e. ECG pre-processing and ECG beat detection. The objective of the ECG pre-processing step is to remove a variety of noises in the ECG signal, such as the muscle noise, the power line noise, and the baseline drift noise. Examples of the methods used for noise removal in the ECG signal include the linear filtering technique [9], the wavelet transform technique [28], and mathematical morphology technique [33]. In ECG beat detection step, the envelope signal is obtained from the ECG signal after noise removal and the threshold is defined to determine the time period where the QRS complex locates. The R peak can be detected from the time position where the amplitude of the ECG signal after noise removal is maximum.

Generally, more complicated threshold techniques such as multiple levels fixed threshold and the single level adaptive threshold are used because the ECG signals after noise removal from different beat types, such as normal beat and premature ventricular contraction beat, have significant difference in their amplitudes due to their difference in frequency components. All wavelet functions in previous publications were selected based on their efficiency in removing noise. However, their effects on QRS signal to noise ratio and the detection accuracy are not yet considered. Therefore, the proposed

comparison measurements of the wavelet function in CWT are presented in section 4.2 of this chapter to demonstrate both QRS signal to noise ratio enhancement and detection accuracy so that the reduction in the computational complexity of the algorithm in the R peak detection step can be obtained.

Moreover, the ECG pre-processing step is very important because if noises in the ECG signal can be effectively removed in this step, the computational complexity of the algorithm in the ECG beat detection step can be reduced. Therefore, we proposed the noise removal algorithm based on the dual-band continuous wavelet transform (CWT) in section 4.2 of this chapter to effectively remove noises in the ECG signal.

The rest of this chapter is organized as follows. While section 4.2 presents the method and evaluation results of wavelet functions on QRS signal to noise ratio, section 4.3 describes possible method and results of enhancing QRS signal to noise ratio based on dual-band CWT. Finally, discussion is given in section 4.4.

4.2 Effect of Wavelet Functions on QRS Signal to Noise Ratio

4.2.1 QRS Detection Algorithm

Based on the block diagram shown in Figure 1.2, the QRS detection algorithm used for evaluating wavelet functions consists of three steps: noise removal using CWT, envelope signal determination, and R peak detection. Details of each step are as follows.

1. Determine the signal after noise removal $y[n]$ from the ECG signal $x[n]$ by processing based on the CWT, which can be expressed as

$$y[n] = T^2_{a,b}. \tag{4.1}$$

There are various types of the wavelet functions that are successfully used for removing noises in ECG signals from previous publications including Bior1.3 [21], Db10 [27], and Mexican hat wavelet [41] functions. This section proposes to study

and quantitatively compare the performance of these three wavelet functions on their capability in enhancing QRS signal to noise ratio and demonstrate its potential application in QRS detection algorithm of ECG data.

2. Determine the envelope signal $z[n]$ from $y[n]$ using the maximum filter with the length $L = 120$ ms as given by

$$z[n] = \max_{k \in [n-L+1, n]} y[k]. \tag{4.2}$$

3. Detect the R peak $r[n]$ in QRS complex using the following steps.

   (a) Define a threshold value thv.

   (b) Find the time duration where $z[n]$ is greater than thv and determine the beginning time t_1 and the ending time t_2.

   (c) Determine the R peak location t_R from time between $[t_1 \;\; t_2]$ in $y[n]$ that gives the maximum amplitude.

Figure 4.1 shows an example of signal characteristics determined from the QRS detection algorithm. Figure 4.1(b) shows an example of two beats of the ECG signal $x[n]$. While the beat on the left hand side is a normal ECG beat, the beat on the right hand side is a premature ventricular contraction beat. The noises in the ECG signal $x[n]$ are removed based on the CWT to obtain $y[n]$. Figure 4.1(a) shows an example of the ECG signal after noise removal $y[n]$ as described in the first step of the algorithm using a thin line. While the normal beat has a single peak after noise removal, the premature ventricular contraction beat has double peaks. Subsequently, the envelope signal $z[n]$ is calculated from $y[n]$ as described in the second step of the algorithm and is shown in Figure 4.1(a) using a dotted line. Then, the threshold value thv is defined as shown in Figure 4.1(a) using a thick line. Finally, the R peak in the QRS complex $r[n]$ is determined from the time where the maximum peak occurs within the time period defined by $z[n]$ and the threshold value as described in the third step of the algorithm.

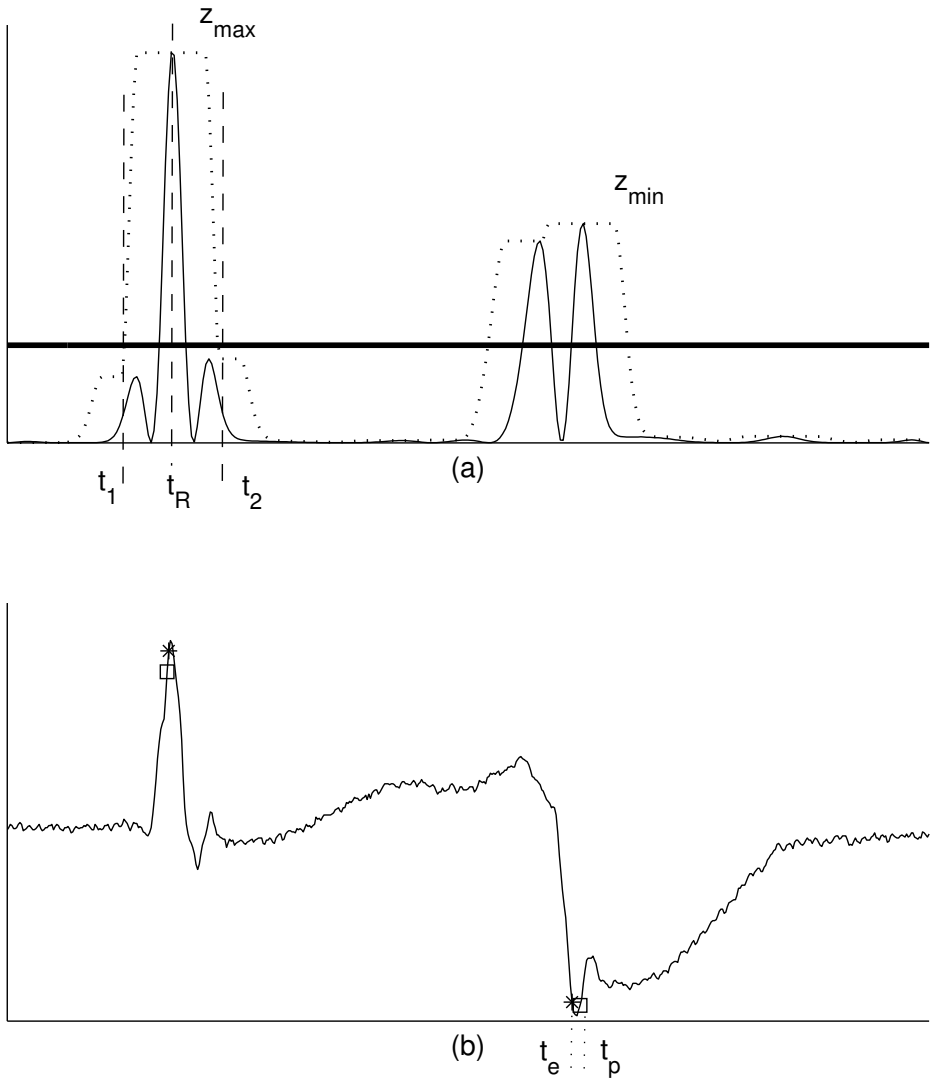

Figure 4.1: Signal characteristics in QRS detection algorithm. (a) Thin line: ECG signal after noise removal $y[n]$. Dotted line: Envelope signal $z[n]$. Thick line: Threshold value line. (b) ECG signal overlaid by the markers from the algorithm (square) and the expert (asterisk). While the signal on the left hand side is a normal ECG beat, the signal on the right hand side is a premature ventricular contraction beat.

Figure 4.1(a) shows an example of the beginning time t_1, the ending time t_2, and the time t_R where the maximum peak locates. The z_{max} and z_{min} are maximum beat amplitude and minimum beat amplitude, respectively. In addition, the ECG signal overlaid by the markers from the proposed algorithm (square) and the expert (asterisk) is shown in Figure 4.1(b). The time t_p and t_e are the position of R peak given by the algorithm and the position of R peak given by the expert, respectively.

4.2.2 Performance Measurement

Three parameters were used in evaluating the performance of the wavelet function in the CWT consisting of the ratio of the maximum beat amplitude z_{max} to the minimum beat amplitude z_{min} (RMM), the sum of absolute of time error (MATE), and the figure of merit (FOM). Their details are as follows.

- RMM: The RMM can be expressed as

$$\text{RMM} = \frac{z_{max}}{z_{min}}. \tag{4.3}$$

  If the value of RMM is closed to 1, the amplitude of all beats in the envelope signal $z[n]$ is almost equal. In other words, the QRS signal to noise ratio is maximized. As a result, the single fixed threshold technique can be used instead of the adaptive threshold technique. This is important because it can reduce the computational complexity of QRS detection algorithm.

- MATE: The MATE in the unit of millisecond (ms) is given by

$$\text{MATE} = \frac{1}{N}\sum_{k=1}^{N}|t_p(k) - t_e(k)|, \tag{4.4}$$

  where N is the total number of ECG beats under considerations, $t_p(k)$ is the time where the R peak locates determined from the algorithm and $t_e(k)$ is the time where the R peak locates determined from the expert. The best value of MATE is 0, which means that all R peaks in the QRS complex are correctly detected by the algorithm.

- FOM: The FOM can be defined by

$$\text{FOM} = \frac{1}{\text{RMM} \times \text{MATE}}. \tag{4.5}$$

FOM is determined using the combination of RMM and MATE. The higher FOM, the more appropriate for the wavelet function in removing noises from the ECG signal and equalizing the amplitude of ECG beats after processing with the CWT.

4.2.3 Results

Comparisons of Wavelet Functions

We measure the performance of wavelet functions Bior1.3, Db10, and Mexican hat with the ECG data record 207 containing the mixture of normal beats and premature ventricular contraction beats from MIT-BIH arrhythmia database [38]. The QRS complex is detected using the ECG signal from channel 1 or lead II only. In other words, the ECG signal from channel 1 was represented by $x[n]$.

Figure 4.2 shows the results of RMM as a function of the scale from 1 to 8 applied on the ECG signal record 207 from time 12.6 s to 22.6 s. In other words, the CWT processing method is $T^2_{a,b}$ when the scale a is varied from 1 to 8. Results from the Bior1.3, Db10, and Mexican hat wavelet functions are shown using square, circle, and asterisk markers, respectively. The RMM values from all wavelet functions tend to decrease when the scales increase from 1 to 8. The RMM values from the Db10 wavelet function are greater than those from other wavelet functions at same scale (Except the scale 1). The maximum RMM is 11.69 at the scale 4 of the Db10 wavelet function and the minimum RMM is 1.51 at the scale 8 of the Mexican hat wavelet function.

Figure 4.3 shows the results of MATE as a function of the scale from 1 to 8 applied on the ECG signal record 207 from time 12.6 s to 22.6 s. Results from the Bior1.3, Db10, and Mexican hat wavelet functions are shown using square, circle, and asterisk markers, respectively. The MATE values from all wavelet functions tend to increase when the scales increase from 1 to 8. The MATE values from the Db10 wavelet

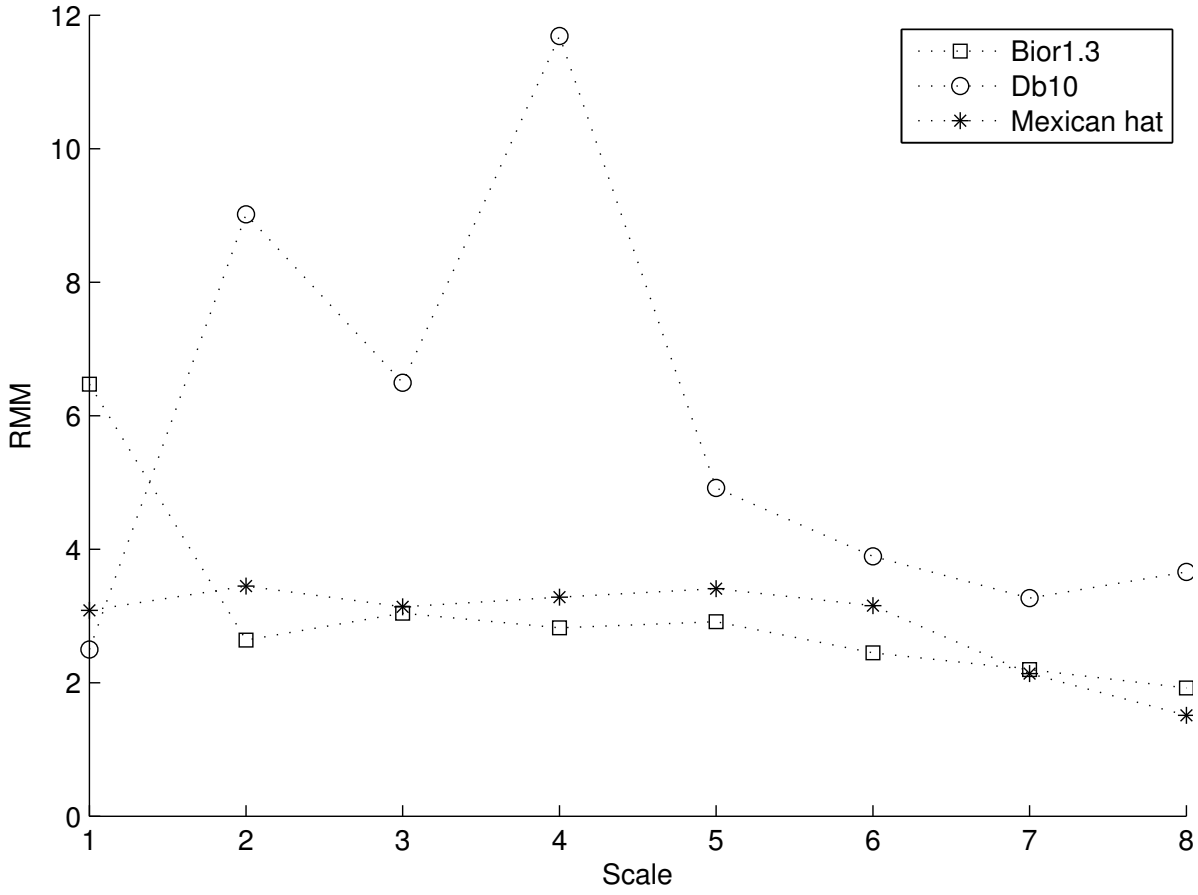

Figure 4.2: Comparisons of the RMM value as a function of scale from three wavelet functions. Results from the Bior1.3, Db10, and Mexican hat wavelet functions are shown using square, circle, and asterisk markers, respectively.

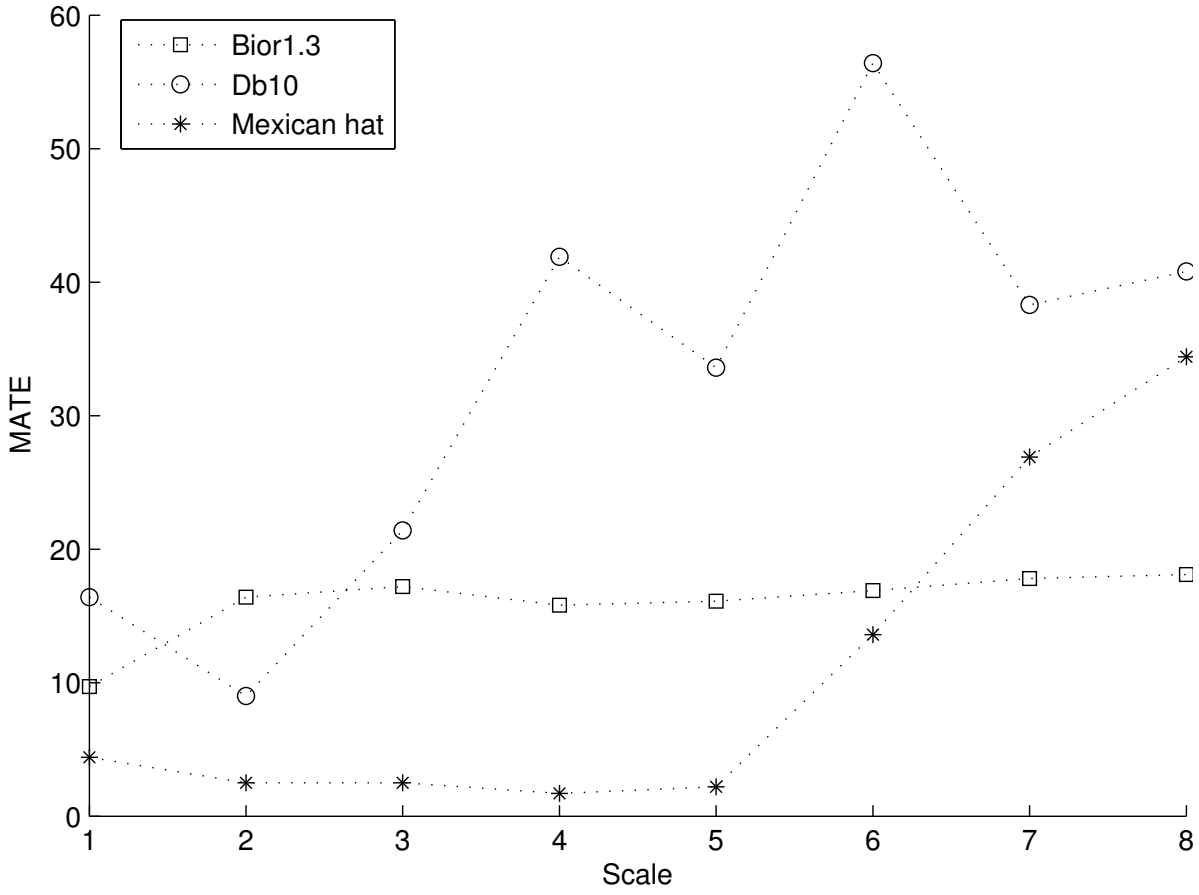

Figure 4.3: Comparisons of the MATE value as a function of scale from three wavelet functions. Results from the Bior1.3, Db10, and Mexican hat wavelet functions are shown using square, circle, and asterisk markers, respectively.

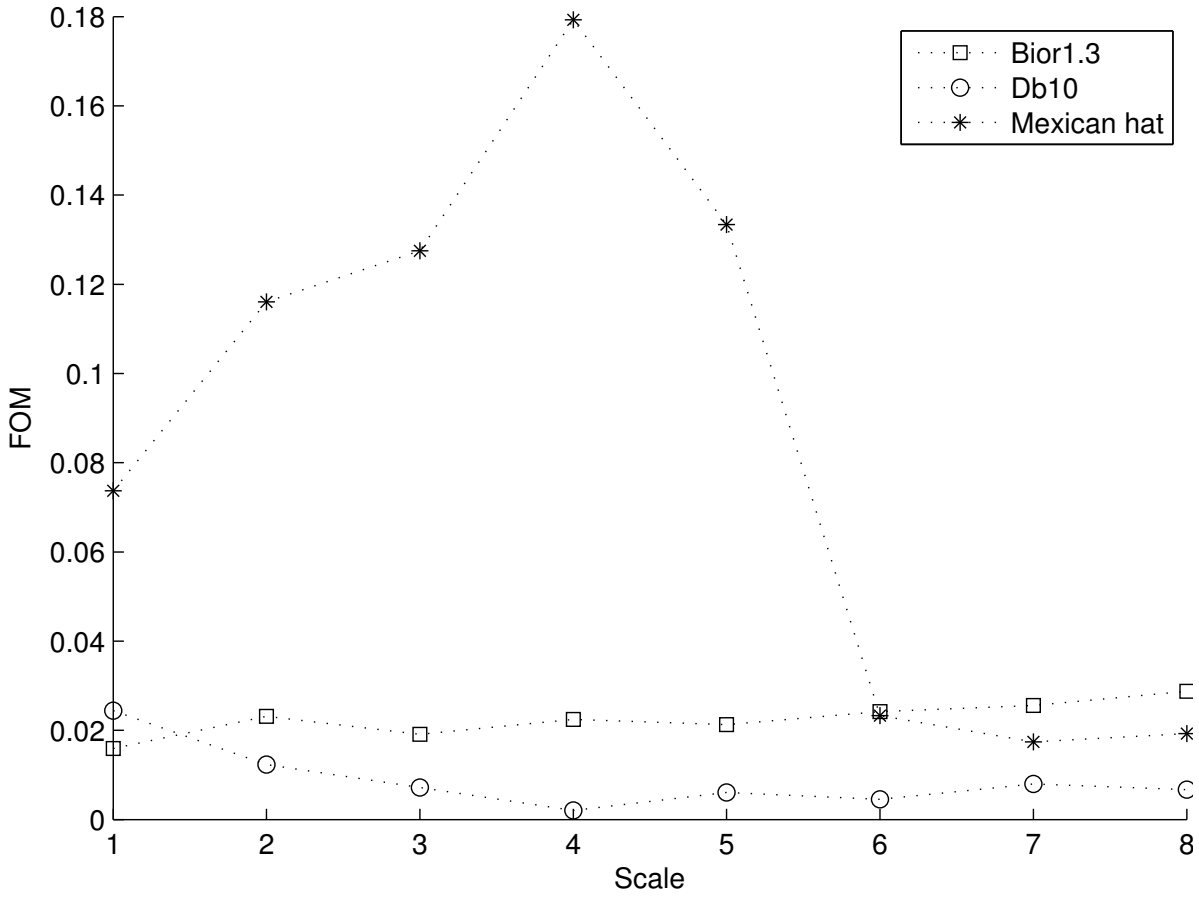

Figure 4.4: Comparisons of the FOM value as a function of scale from three wavelet functions. Results from the Bior1.3, Db10, and Mexican hat wavelet functions are shown using square, circle, and asterisk markers, respectively.

function are greater than those from other wavelet functions at same scale (Except the scale 2). The maximum MATE is 56.4 ms at the scale 6 of the Db10 wavelet function and the minimum MATE is 1.7 ms at the scale 4 of the Mexican hat wavelet function.

Figure 4.4 shows the results of FOM as a function of the scale from 1 to 8 applied on the ECG signal record 207 from time 12.6 s to 22.6 s. Results from the Bior1.3, Db10, and Mexican hat wavelet functions are shown using square, circle, and asterisk markers, respectively. The FOM values from first five scales of the Mexican hat wavelet function are greater than those from other wavelet functions at the same scale. However, at the scale 6, 7 and 8, the FOM values from the Bior1.3 wavelet function are greater than those from other wavelet functions.

Signal Characteristics

To gain more insight of the performance measurement, signal characteristics from the scale 8 of the Mexican hat wavelet function, the scale 4 of the Mexican hat wavelet function, and the scale 4 of the Db10 wavelet function are shown and discussed. While the signal characteristics from the scale 8 and 4 of the Mexican hat wavelet function are the representation for the best RMM and MATE, respectively, the signal characteristics from the scale 4 of the Db10 wavelet function are the representation of the worst FOM.

Figure 4.5 shows signal characteristics of the proposed algorithm from the scale 8 of the Mexican hat wavelet function applied on the ECG signal record 207. Figure 4.5(a) shows the ECG signal before noise removal $x[n]$ from time 12.6 s to 22.6 s. The ECG signal $x[n]$ consists of 5 normal beats and 5 premature ventricular contraction beats. Figure 4.5(b) shows the ECG signal after noise removal $y[n]$. While the normal beat has a single peak amplitude, the premature ventricular contraction beat comprises double peak amplitudes where the left peak is greater than the right peak. Figure 4.5(c) shows the envelope signal $z[n]$. While the fifth beat has maximum amplitude, the forth beat has minimum amplitude. As a result, the best RMM value of 1.51 is determined. Figure 4.5(d) shows the ECG signal overlaid by the markers from the proposed algorithm (square) and the expert (asterisk). While all R peaks in QRS complex of normal beats are correctly detected, all R peaks in QRS complex of premature ventricular contraction beats are slightly incorrectly detected because the algorithm detects the left peak, which is greater than the right peak in all premature ventricular contraction beats. This leads to the MATE value of 34.3 ms. The corresponding FOM value in this case is 0.02.

Figure 4.6 shows signal characteristics resulting from the scale 4 of the Mexican hat wavelet function applied on the ECG signal record 207. Figure 4.6(b) shows the ECG signal after noise removal $y[n]$. Similar to the case in Figure 4.5, while the normal beat has single peak amplitude, the premature ventricular contraction beat comprises double peak amplitudes. However, the position of the larger peak amplitude in each

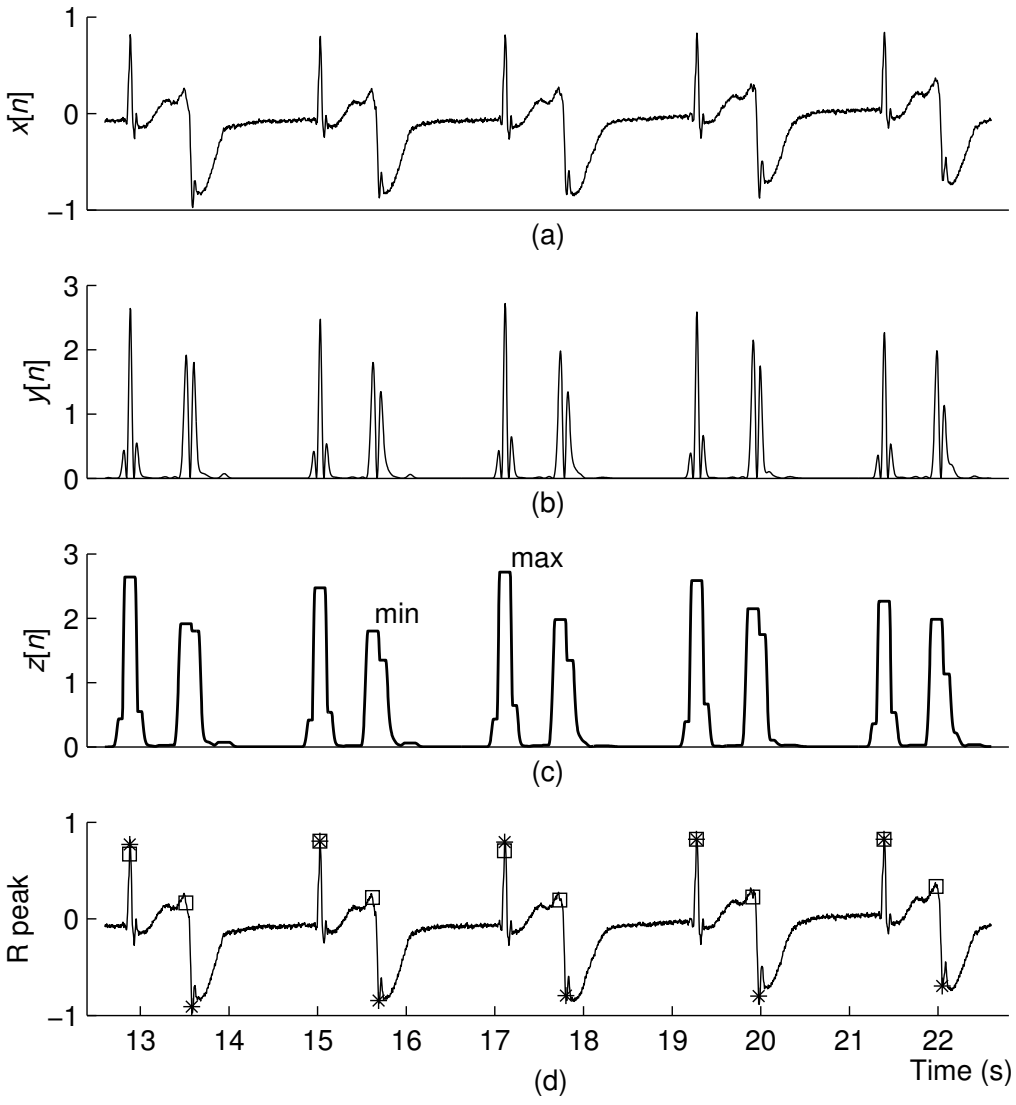

Figure 4.5: Signal characteristics from the scale 8 of the Mexican hat wavelet function applied on the ECG signal record 207. (a) The ECG signal before noise removal $x[n]$. (b) The ECG signal after noise removal $y[n]$. (c) The envelope signal $z[n]$. (d) The ECG signal overlaid by the markers from the proposed algorithm (square) and the expert (asterisk).

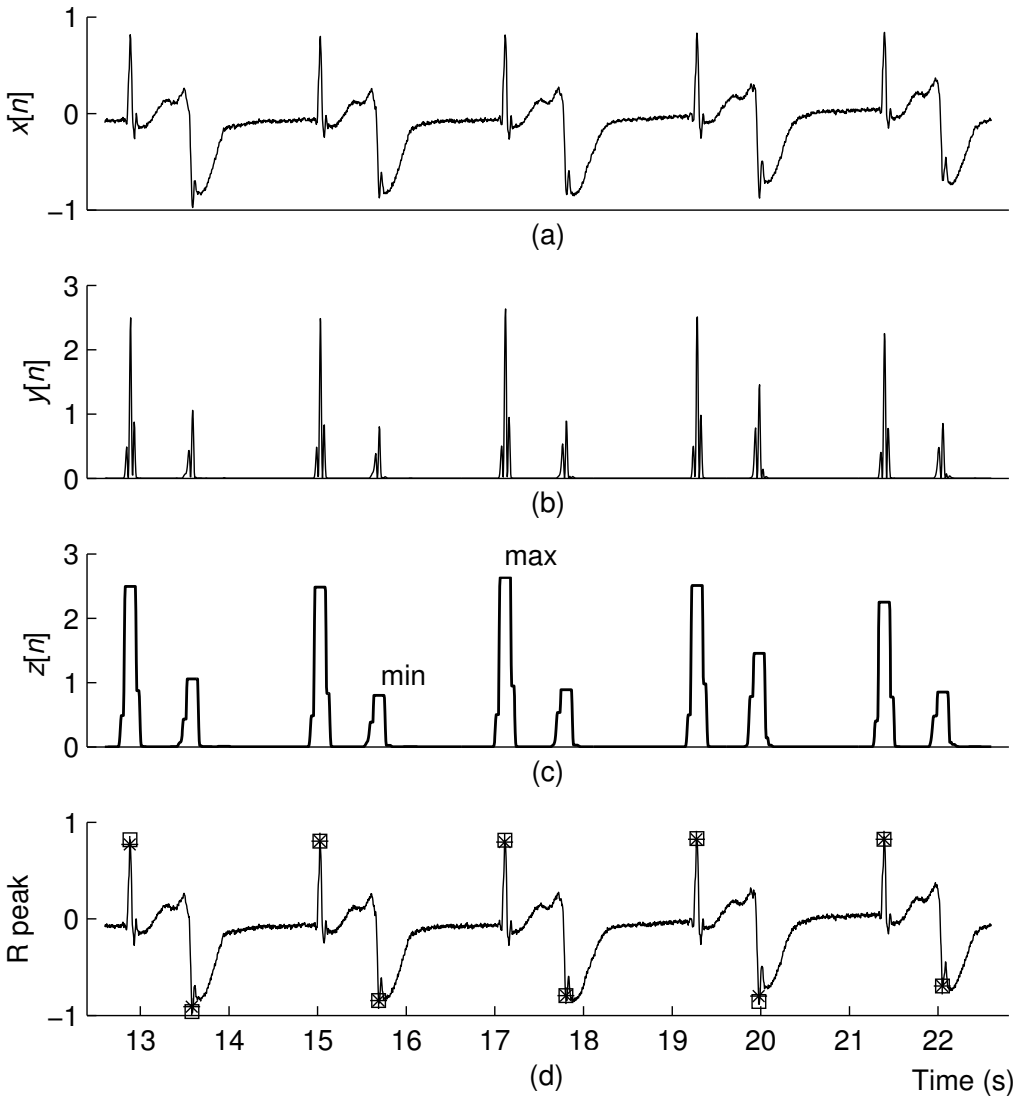

Figure 4.6: Signal characteristics from the scale 4 of the Mexican hat wavelet function applied on the ECG signal record 207. (a) The ECG signal before noise removal $x[n]$. (b) The ECG signal after noise removal $y[n]$. (c) The envelope signal $z[n]$. (d) The ECG signal overlaid by the markers from the proposed algorithm (square) and the expert (asterisk).

premature ventricular contraction beat is on the right hand side. Figure 4.6(c) shows that the maximum beat amplitude and the minimum beat amplitude locate at the forth beat and the fifth beat, respectively. Consequently, the RMM value of 3.28 is obtained. Figure 4.6(d) shows the ECG signal overlaid by the markers from the proposed algorithm (square) and the expert (asterisk). All R peaks in QRS complex of both normal beats and premature ventricular contraction beats are almost correctly detected. All R peaks in QRS complex of premature ventricular contraction beats are correctly detected because the proposed algorithm detects the right peak, which is greater than the left peak in all premature ventricular contraction beats. As a result, the best value of MATE 1.7 ms is achieved. In addition, the corresponding value of FOM in this case is the best at 0.18.

Figure 4.7 shows signal characteristics resulting from the scale 4 of the Db10 wavelet function applied on the ECG signal record 207. Figure 4.7(b) shows the ECG signal after noise removal $y[n]$ consisting of multiple peaks, which are different from double peaks in the case of Mexican hat wavelet function. Figure 4.7(c) show the envelope signal $z[n]$. The position of maximum $z[n]$ and the position of minimum $z[n]$ are at the fifth beat and the eighth beat, respectively. This results in the worst RMM value of 11.69. Figure 4.7(d) shows the ECG signal overlaid by the markers from the proposed algorithm (square) and the expert (asterisk). All R peaks in QRS complex of both normal beats and premature ventricular contraction beats are incorrectly detected. Therefore, the high value of MATE at 41.9 ms is obtained. Moreover, the corresponding value of FOM in this case is the worst at 0.002.

Performance Comparisons

To demonstrate the potential of selected wavelet functions, we apply the QRS detection algorithm to the whole ECG data of record 207. Table 4.1 shows the performance comparisons of the algorithm with those from other 3 papers ([26, 27, 42]), which use the wavelet transform, single level adaptive thresholding techniques, and additional post processing methods in QRS detection algorithms such as irregular RR interval checkup

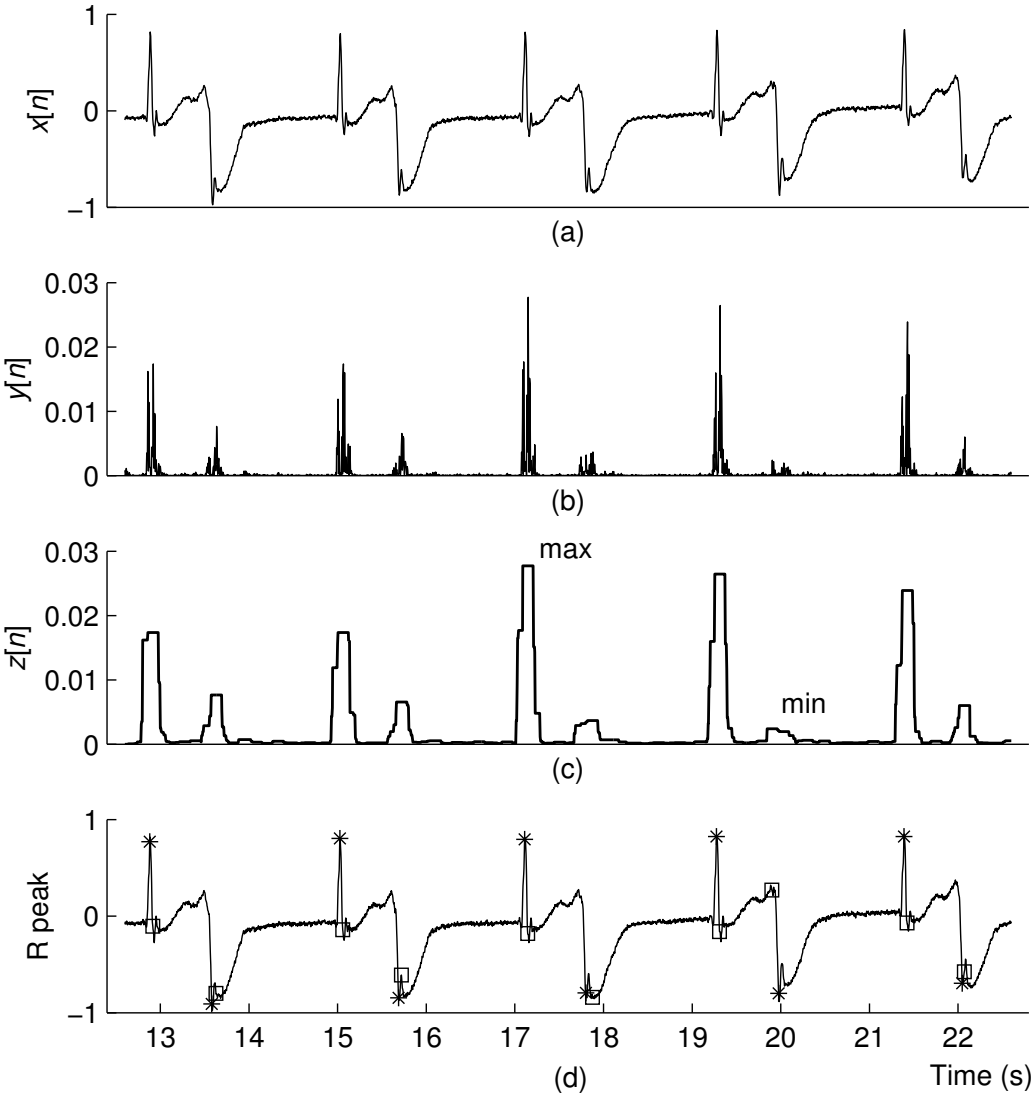

Figure 4.7: Signal characteristics from the scale 4 of the Db10 wavelet function applied on the ECG signal record 207. (a) The ECG signal before noise removal $x[n]$. (b) The ECG signal after noise removal $y[n]$. (c) The envelope signal $z[n]$. (d) The ECG signal overlaid by the markers from the proposed algorithm (square) and the expert (asterisk).

Table 4.1: Performance comparisons of the algorithm from scale 4 and 8 of the Mexican hat wavelet functions with those from other 3 publications.

Method	Total	TP	FN	FP	SEN(%)	PPR(%)	DER(%)
Scale 4	1860	1852	8	12	99.57	99.36	1.08
Scale 8	1860	1843	17	7	99.09	99.62	1.29
Choi [27]	1860	1848	12	10	99.35	99.46	1.18
Chen [26]	1863	1860	3	24	99.84	98.72	1.45
Zidelmala [42]	1872	1860	12	8	99.36	99.57	1.08

strategy [27]. Note that each R peak from the proposed algorithm is considered as a correct detection when it locates within ±50 ms from the position of the R peak given by the expert. The DER value from the scale 4 of the Mexican hat wavelet function (1.08%) is smaller than that from the scale 8 of the Mexican hat wavelet function (1.29%). Results show that the DER values from both wavelet functions are in the same range as those from other publications. However, the proposed algorithm uses only a single fixed threshold without any additional post-processing techniques.

4.3 QRS Signal to Noise Ratio Enhancement and Dual-Band CWT

4.3.1 Proposed Algorithm

Based on the block diagram shown in Figure 1.2, the ECG signal $x[n]$ is determined from the ECG signal $x(t)$ at a sampling rate of 200 Hz. Details of the QRS detection algorithm used for enhancing signal to noise ratio with dual-band CWT are as follows.

1. Determine the signal after noise removal $y[n]$ from the ECG signal $x[n]$ by processing based on the CWT, which can be expressed as

$$y[n] = T^2_{a_1,b} + T^2_{a_2,b}. \tag{4.6}$$

2. Determine the envelope signal $z[n]$ from $y[n]$ using the maximum filter with the length $L = 120$ ms as given by

$$z[n] = \max_{k\in[n-L+1,n]} y[k]. \tag{4.7}$$

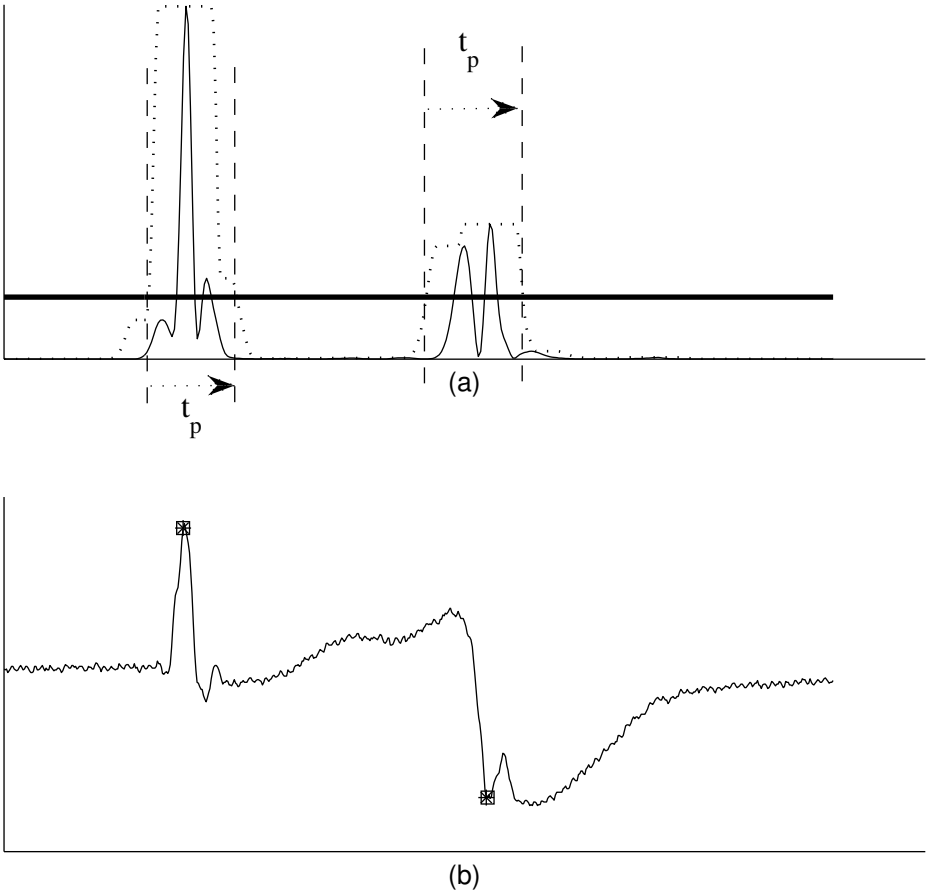

Figure 4.8: ECG beat detection algorithm. (a) Thin line: ECG signal after noise removal $y[n]$. Dotted line: Envelope signal $z[n]$. Thick line: Threshold value line. (b) ECG signal overlaid by the markers from the proposed algorithm (square) and the expert (asterisk). While the signal in the left hand side is a normal ECG beat, the signal in the right hand side is a premature ventricular contraction beat.

3. Detect the R peak $r[n]$ in QRS complex using the following steps.

   (a) Define a threshold value thv.

   (b) Find the time duration where $z[n]$ is greater than thv and determine the beginning time t_1 and the ending time t_2.

   (c) Determine the R peak location t_R from time between $[t_1 \ \ t_2]$ in $y[n]$ that gives the maximum amplitude.

Figure 4.8(b) shows an example of two beats of the ECG signal $x[n]$. While the beat in the left hand side is a normal ECG beat, the beat in the right hand side is a premature ventricular contraction beat. Then, the noises in the ECG signal $x[n]$ are removed based on the CWT to obtain $y[n]$. Three types of the CWT processing method are explored and compared as follows:

- A: $T_{3,b}^2 + T_{3,b}^2$
- B: $T_{6,b}^2 + T_{6,b}^2$
- C: $T_{3,b}^2 + T_{6,b}^2$.

While case A and case B are the representative of a single-band CWT processing method, case C is the representative of a dual-band CWT processing method. Figure 4.8(a) shows an example of the ECG signal after noise removal $y[n]$ with the CWT method of case C using a thin line. While the normal beat has a single peak after noise removal, the premature ventricular contraction beat has double peaks. Subsequently, the envelope signal $z[n]$ is calculated from $y[n]$ as shown in Figure 4.8(a) using a dotted line. Then, the threshold value is defined as shown in Figure 4.8(a) using a thick line. Finally, the R peak in the QRS complex $r[n]$ is determined from the time where the maximum peak occurs within the time period defined by $z[n]$ and the threshold value. Figure 4.8(a) shows an example the time period t_p where the maximum peak locates. In addition, the ECG signal overlaid by the markers from the proposed algorithm (square) and the expert (asterisk) is shown in Figure 4.8(b).

4.3.2 Results

Scale Adjustment

Figure 4.9 shows results of the proposed algorithm case A applied on the ECG signal record 207. Figure 4.9(a) shows the ECG signal before noise removal $x[n]$ from time 17 s to 27 s. The ECG signal $x[n]$ consists of 5 normal beats and 5 premature ventricular contraction beats. Figure 4.9(b) shows the ECG signal after noise removal $y[n]$. While the normal beat has a single peak amplitude, the premature ventricular contraction beat comprises double peak amplitudes. Figure 4.9(c) shows the envelope signal $z[n]$ using a solid line and the threshold level thv using a dotted line. While the first beat has maximum amplitude, the last beat has minimum amplitude. Figure 4.9(d) shows the ECG signal overlaid by the markers from the proposed algorithm (square) and the expert (asterisk). In this case, all R peaks in QRS complex are correctly detected.

Figure 4.10 shows results of the proposed algorithm case B applied on the ECG signal record 207. Figure 4.10(b) shows the ECG signal after noise removal $y[n]$. Similar to case A, the normal beat has a single peak amplitude and the premature ventricular contraction beat comprises double peak amplitudes. However, the position of maximum peak in each premature ventricular contraction beat is different from that in case A except the second beat. Figure 4.10(c) shows that the maximum beat and the minimum beat locate at the first beat and the second beat, respectively. Figure 4.10(d) shows that there are four wrong beat detections.

Figure 4.11 shows results of the proposed algorithm case C applied on the ECG signal record 207. The ECG signal after noise removal $y[n]$ and the envelope signal $z[n]$ shown in Figure 4.11(b) and (c) are slightly different from those in case A and case B in terms of both the position of the maximum peak in $y[n]$ and the maximum beat and the minimum beat in $z[n]$. In addition, there is a single false detection in the last beat shown in Figure 4.11(d). As more quantitative details on performance comparisons, Table 4.2 shows the values of z_{max}, z_{min}, RMM, and MATE from all cases. Case A gives the best

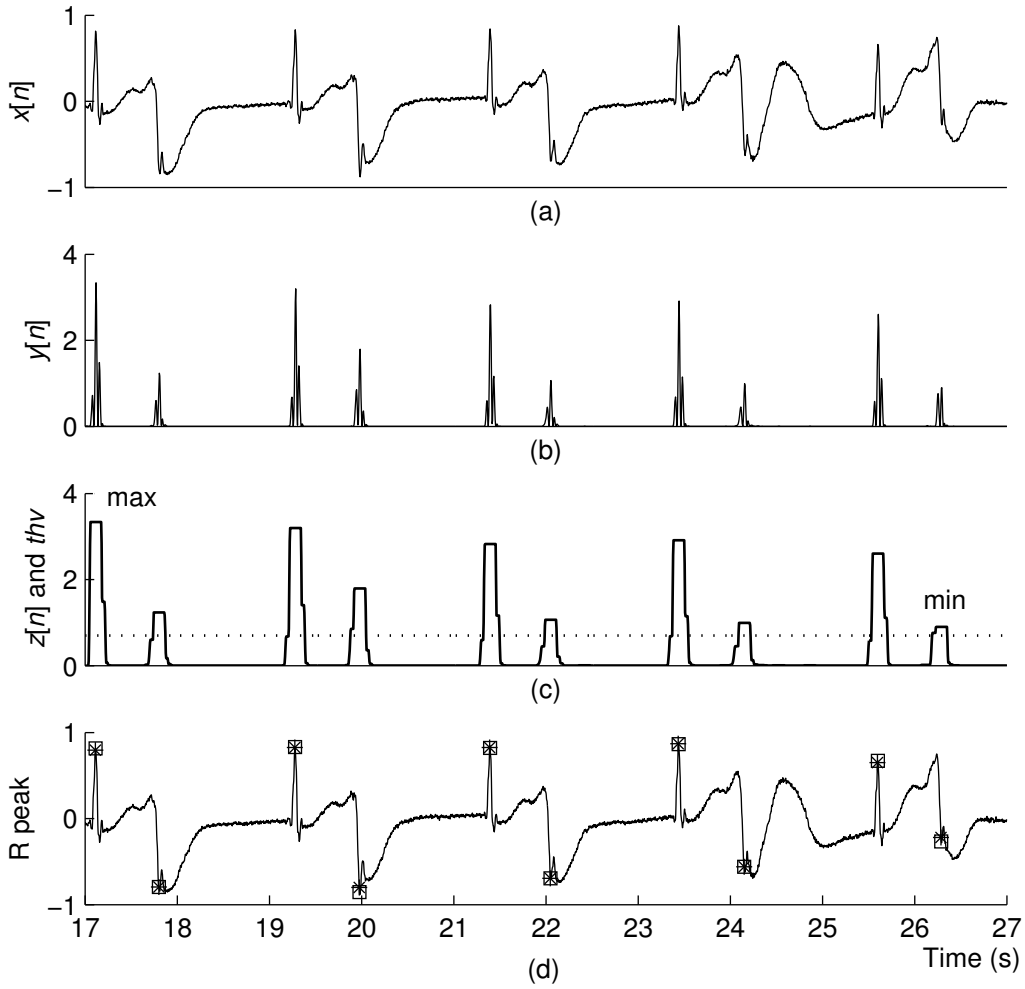

Figure 4.9: Results of the proposed algorithm case A applied on the ECG signal record 207. (a) The ECG signal before noise removal $x[n]$. (b) The ECG signal after noise removal $y[n]$. (c) The envelope signal $z[n]$ shown in a solid line and the threshold level thv shown in a dotted line. (d) The ECG signal overlaid by the markers from the proposed algorithm (square) and the expert (asterisk).

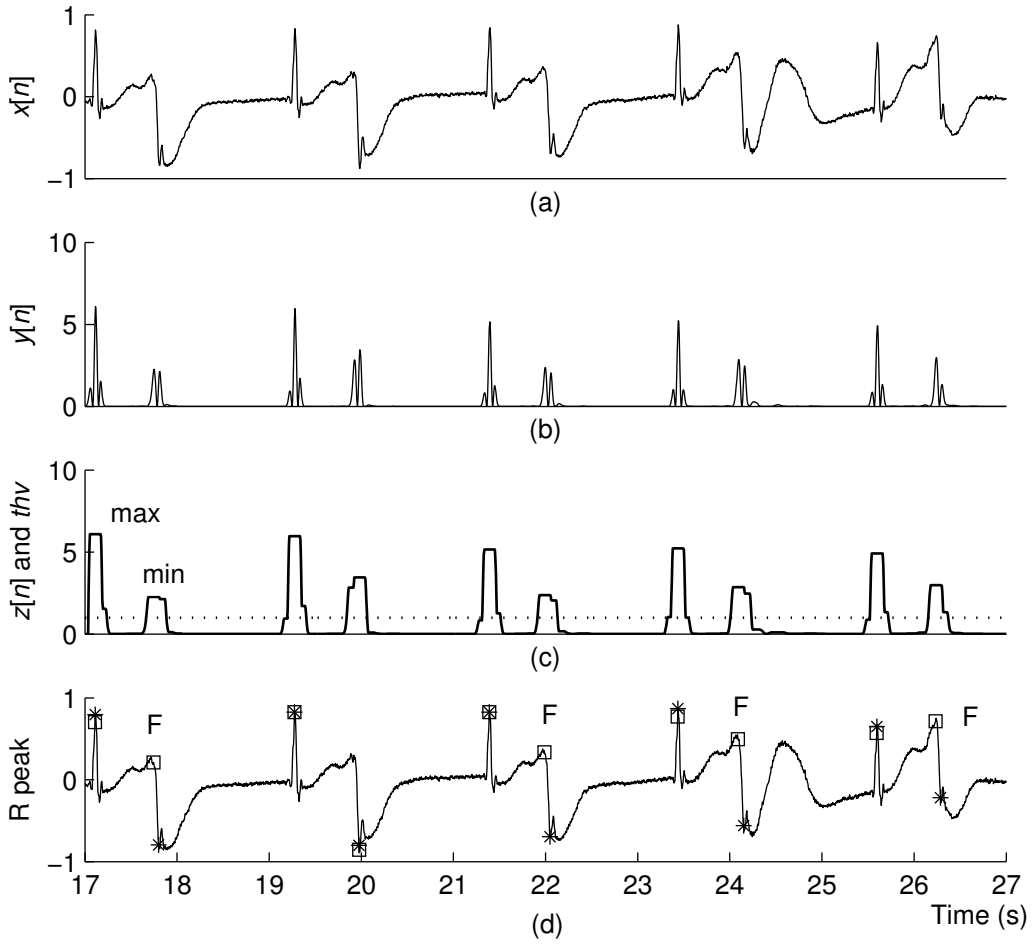

Figure 4.10: Results of the proposed algorithm case B applied on the ECG signal record 207. (a) The ECG signal before noise removal $x[n]$. (b) The ECG signal after noise removal $y[n]$. (c) The envelope signal $z[n]$ shown in a solid line and the threshold level thv shown in a dotted line. (d) The ECG signal overlaid by the markers from the proposed algorithm (square) and the expert (asterisk).

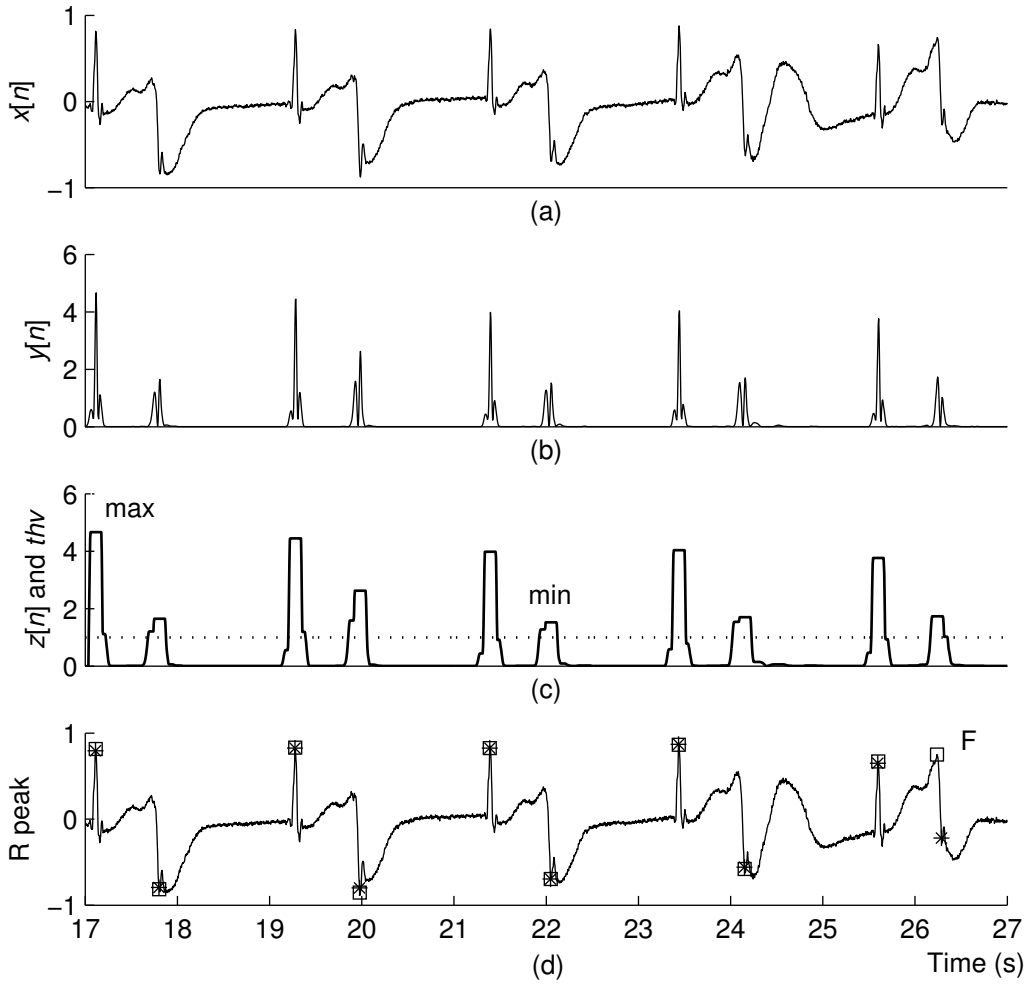

Figure 4.11: Results of the proposed algorithm case C applied on the ECG signal record 207. (a) The ECG signal before noise removal $x[n]$. (b) The ECG signal after noise removal $y[n]$. (c) The envelope signal $z[n]$ shown in a solid line and the threshold level thv shown in a dotted line. (d) The ECG signal overlaid by the markers from the proposed algorithm (square) and the expert (asterisk).

Table 4.2: Performance comparison of the proposed algorithm.

Method	z_{max}	z_{min}	RMM	MATE
A	3.32	0.91	3.65	0.25
B	6.05	2.25	2.69	2.39
C	4.69	1.54	3.05	0.69

MATE among all cases at an expense of the worst RMM. In contrast, case B gives the best RMM among all cases at an expense of the worst MATE. However, with the use of the dual-band CWT processing technique (case C), the improvement in terms of both the RMM and the MATE is possible as shown in the third row of Table 4.2. In other words, while the RMM of case C decreases from 3.65 to 3.05 compared to case A, the MATE of case C decreases from 2.39 to 0.69 compared to case B.

Figure 4.12(a) shows the results of RMM as a function of the second scale from 1 to 8 applied on the ECG signal record 207. In other words, the CWT processing method is $T^2_{3,b} + T^2_{a,b}$ when the first scale is fixed at 3 and the second scale is varied from 1 to 8. The maximum RMM is 3.91 at the second scale 4 and the minimum RMM is 2.16 at the second scale 8. Figure 4.12(b) shows the results of MATE as a function of the second scale from 1 to 8. The maximum MATE is 2.69 at the second scale 8 and the minimum MATE is 0.25 at the second scale 3. These results show that the second scale 6 is the optimized selection because it can achieve both RMM and MATE.

Wavelet Function

In addition to the scale and scale combination, the type of wavelet function is another important parameter affecting the SNR. Figure 4.13 shows the results from the Haar wavelet function. The RMM and MATE are 2.38 and 18.1, respectively. Figure 4.14 shows the results from the 2.2 reverse biorthogonal wavelet function with the RMM and MATE of 3.72 and 0.25, respectively. These results confirm the importance of the wavelet function selection.

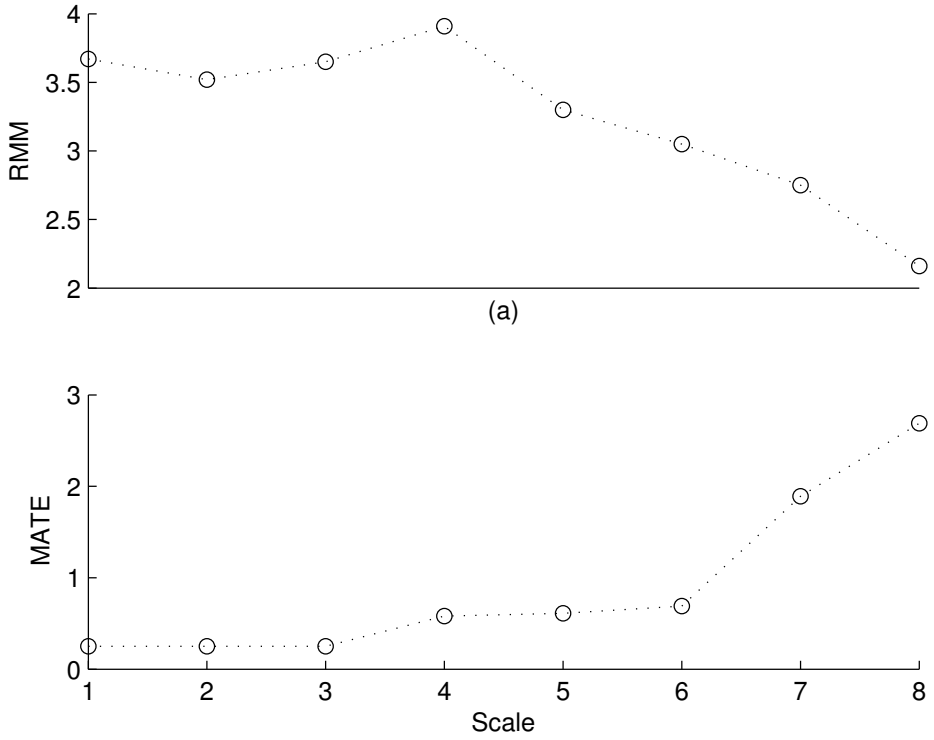

Figure 4.12: (a) RMM as a function of the second scale from 1 to 8. (b) MATE as a function of the second scale from 1 to 8.

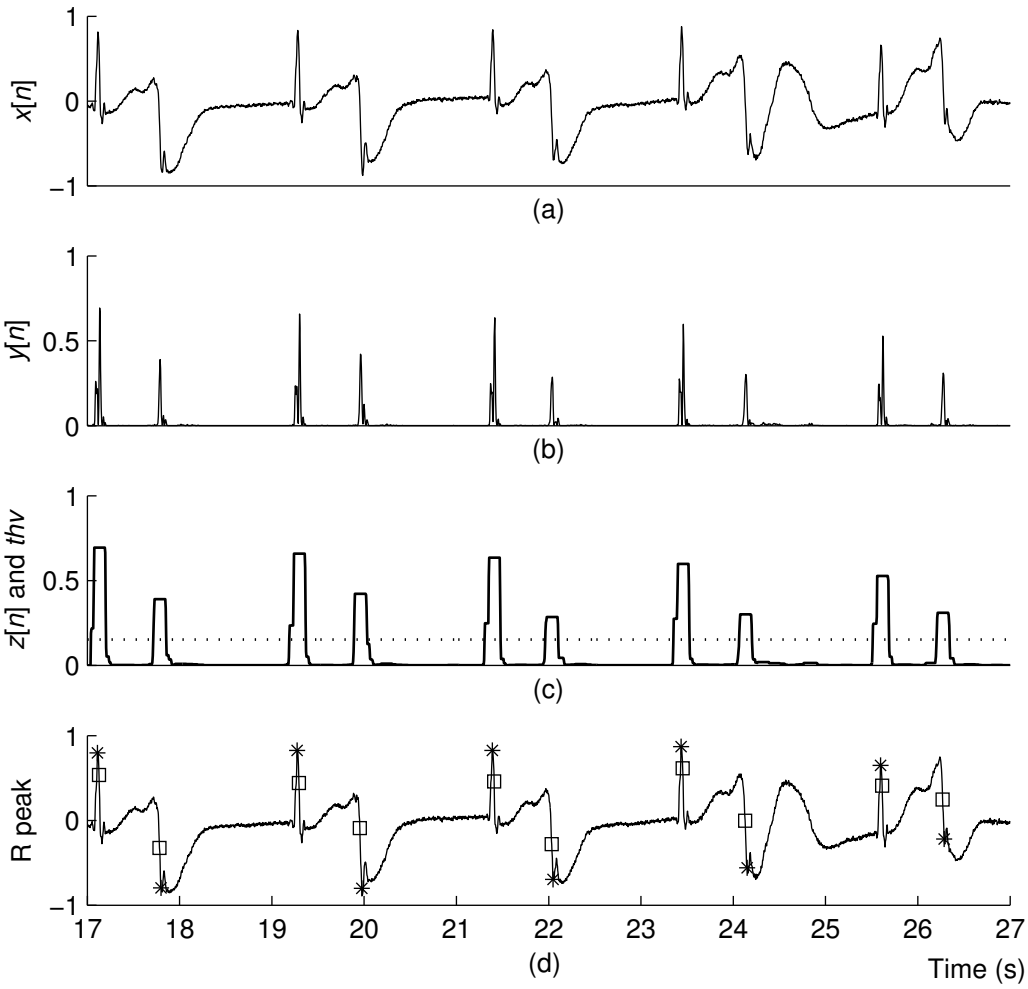

Figure 4.13: Results of the proposed algorithm with the Haar wavelet function.

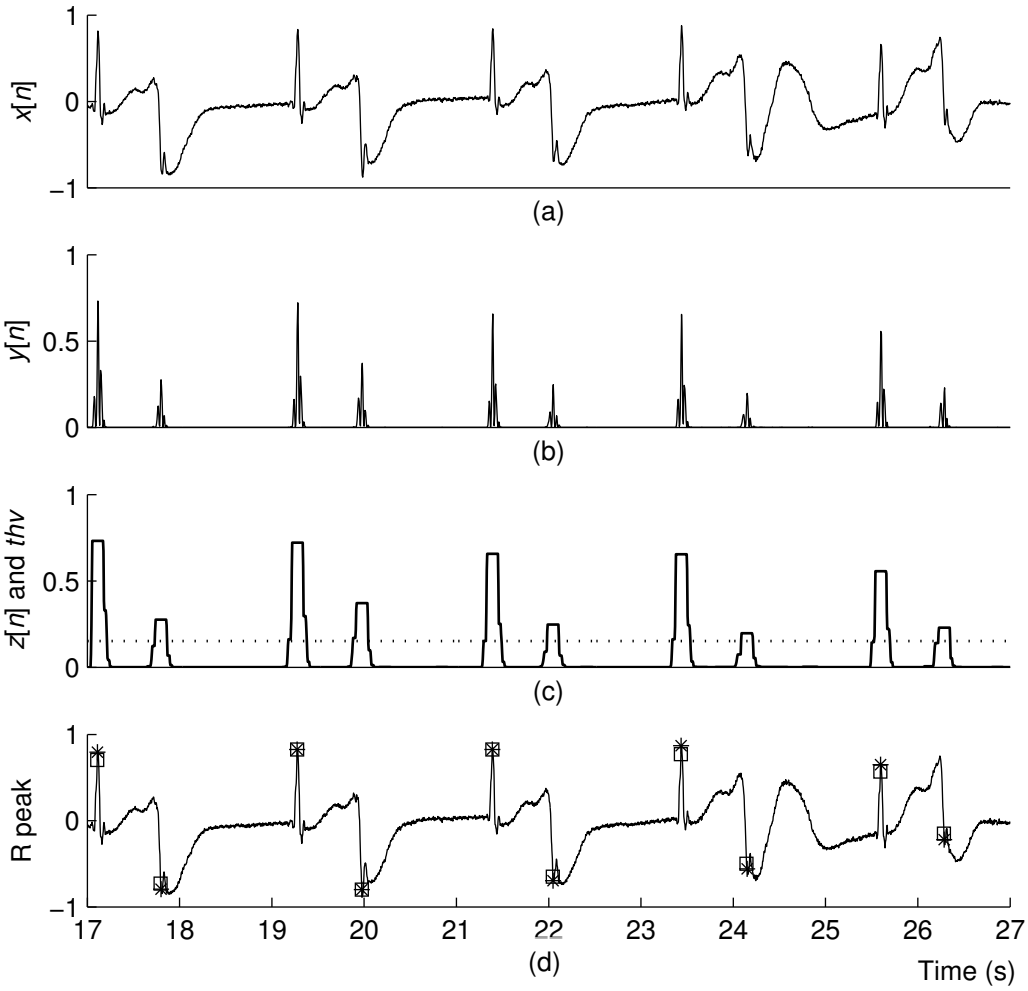

Figure 4.14: Results of the proposed algorithm with the 2.2 reverse biorthogonal wavelet function.

4.4 Discussion

We compare the capability of wavelet functions used for noise removal in QRS detection algorithm as details shown in section 4.2 of this chapter. The effects of the wavelet function on the performance in terms of QRS signal to noise ratio enhancement and detection accuracy are carefully studied and evaluated using three measurement parameters, i.e., RMM, MATE, and FOM. Three wavelet functions from previous publications are explored consisting of the Bior1.3, Db10, and Mexican hat wavelets functions. Results show that the Mexican hat wavelet function is the most appropriate for the QRS detection algorithm because it can give good results in terms of both QRS signal to noise ratio enhancement (scale 8 of the Mexican hat wavelet function) and detection accuracy (scale 4 of the Mexican hat wavelet function), which opens the opportunity for the use of a single level fixed threshold for all records of ECG data.

Moreover, we present the improvement of signal to noise ratio in ECG signals based on dual-band CWT as details shown in section 4.3 of this chapter. The ECG signal after noise removal using the dual-band CWT at dilation parameter combination of 3 and 6 shows the feasibility of the method in maximizing the signal to noise ratio without the loss of accuracy compared to the single-band CWT at the dilation parameter of 3 and the dilation parameter of 6.

In this chapter we show the opportunity in improving the QRS signal to noise ratio based on the separable band CWT and the dual-band CWT, which can be obtained for increasing the QRS detection accuracy. In next chapter, the conclusions and recommendations for future work of this research project will be presented.

Chapter 5

Conclusions and Recommendations for Future Work

5.1 Conclusions

We develop a QRS detection algorithm in the electrocardiogram (ECG) signals, which provides very important information on the state of the heart used for medical monitoring and diagnosis, based on advanced signal processing methods in this research project. Two advanced signal processing methods used in this research project are the quadratic filter (QF) and the wavelet transform.

The QRS detection algorithm based on the QF presented in chapter 2 is capable of enhancing QRS signal to noise ratio from ECG signals in preprocessing step. Results show that the QF achieves in improving QRS signal to noise ratio for some challenging situations such as low amplitude QRS complex corrupted by baseline drift and a variety of abnormal morphologies such as a fusion of ventricular and normal beat, an atrial premature beat, an aberrated atrial premature beat, a premature ventricular contraction beat, a fusion of paced and normal beat, and a paced beat. In beat detection step, the QRS complex is simply obtained based on an envelope signal and a single fixed threshold without additional post-processing techniques. The average DER value validated with 48 records of ECG signals from the MIT-BIH arrhythmia database is at 0.38%.

To improve QRS detection accuracy, the QRS detection algorithm employing the efficient cascade of two combination steps, i.e., the Mexican hat wavelet function

on enhancing QRS signal to noise ratio in preprocessing step and the maximal filter on reducing FP detections in beat detection step was developed in chapter 3. Results show that the proposed algorithm is successful in enhancing QRS signal to noise ratio from a variety of abnormal beat types such as a right bundle branch block beat, a premature ventricular contraction beat, an atrial premature beat, and a fusion of ventricular and normal beat. The subsequent beat detection step based on the maximal filter is capable of reducing FP detections into a same level among the top previous publications. Using a single threshold without any additional post-processing techniques, the proposed algorithm can achieve DER value of 0.27% validated with 48 records of ECG signals from MIT-BIH arrhythmia database.

To gain more improvement in detection accuracy, we propose the QRS detection algorithms based on the separable band continuous wavelet transform (CWT) and the dual-band CWT in preprocessing step described in chapter 4. Results show that both proposed methods are feasible. In other words, for the separable band CWT, while the scale 8 of the Mexican hat wavelet function gives the best QRS signal to noise ratio enhancement, the scale 4 of the Mexican hat wavelet function provides the best detection accuracy. This opens an opportunity in using one scale of wavelet function in preprocessing step and using another scale of wavelet function in beat detection step. For the dual-band CWT, the enhancement of QRS signal to noise ratio is obtained from the combination of two wavelet functions with dilation parameters of 3 and 6.

5.2 Recommendations for Future Study

There are several ways for improving the accuracy of QRS algorithm detection. We categorize the methods of improvement into two directions, i.e. the ways of improvement in preprocessing step and the ways of improvement in beat detection step. Details are as follows.

Improvement in Preprocessing Step

To achieve a better detection accuracy of the QRS detection algorithm, we may use more sophisticated signal processing techniques in enhancing QRS signal to noise ratio in preprocessing step. Examples include the separable band CWT and the dual-band CWT presented in chapter 4. The results from chapter 4 suggest combine wavelet functions from multiple scales instead of using a single scale wavelet function as published in previous literature. In other words, the combination of multiple scale wavelet functions may simultaneously allow for both the enhancement QRS signal to noise ratio and the increase in detection accuracy. However, more studies on other combinations of dilation parameters should be performed and performance evaluation to all records of ECG data in MIT-BIH arrhythmia database should be investigated. In addition, others wavelet functions should be carefully considered.

Improvement in Beat Detection Step

To achieve a better detection accuracy of the QRS detection algorithm for abrupt baseline shift, high-grade noise, and low amplitude QRS complex contaminated by muscle noise, more computations in beat detection step may be added. The employment of more sophisticated thresholding techniques such as the multiple levels of fixed threshold, the single level of adaptive threshold, and the multiple levels of adaptive threshold may be used for decreasing FN detections. Moreover, FP detections may be reduced using the algorithm based on the refractory period of 200 ms.

Bibliography

[1] M. Korrek and B. Doan, "ECG beat classification using particle swarm optimization and radial basis function neural network," *Expert Systems with Applications*, vol. 37, no. 12, pp. 7563–7569, 2010.

[2] S. Dutta, A. Chatterjee, and S. Munshi, "Correlation technique and least square support vector machine combine for frequency domain based ECG beat classification," *Medical Engineering and Physics*, vol. 32, no. 10, pp. 1161–1169, 2010.

[3] Y. Kutlu and D. Kuntalp, "Feature extraction for ECG heartbeats using higher order statistics of WPD coefficients," *Computer Methods and Programs in Biomedicine*, vol. 105, no. 3, pp. 257–267, 2012.

[4] A. Yildiz, M. Akn, and M. Poyraz, "An expert system for automated recognition of patients with obstructive sleep apnea using electrocardiogram recordings," *Expert Systems with Applications*, vol. 38, no. 10, pp. 12880–12890, 2011.

[5] S. Babaeizadeh, D. P. White, S. D. Pittman, and S. H. Zhou, "Automatic detection and quantification of sleep apnea using heart rate variability," *Journal of Electrocardiology*, vol. 43, no. 6, pp. 535–541, 2010.

[6] S. N. Yu and M. Y. Lee, "Bispectral analysis and genetic algorithm for congestive heart failure recognition based on heart rate variability," *Computers in Biology and Medicine*, vol. 42, no. 8, pp. 816–825, 2012.

[7] S. N. Yu and M. Y. Lee, "Conditional mutual information-based feature selection for congestive heart failure recognition using heart rate variability," *Computer Methods and Programs in Biomedicine*, vol. 108, no. 1, pp. 299–309, 2012.

[8] D. H. Shih, H. S. Chiang, B. Lin, and S. B. Lin, "An embedded mobile ECG reasoning system for elderly patients," *IEEE Transactions on Information Technology in Biomedicine*, vol. 14, no. 3, pp. 854–865, 2010.

[9] J. Pan and W. J. Tompkins, "A real-time QRS detection algorithm," *IEEE Transactions on Biomedical Engineering*, vol. BME-32, no. 3, pp. 230–236, 1985.

[10] P. S. Hamilton and W. J. Tompkins, "Quantitative investigation of QRS detection rules using the MIT/BIH arrhythmia database," *IEEE Transactions on Biomedical Engineering*, vol. BME-33, no. 12, pp. 1157–1165, 1986.

[11] R. Poli, S. Cagnoni, and G. Valli, "Genetic design of optimum linear and nonlinear QRS detectors," *IEEE Transactions on Biomedical Engineering*, vol. 42, no. 11, pp. 1137–1141, 1995.

[12] D. Benitez, P. A. Gaydecki, A. Zaidi, and A.P. Fitzpatrick, "The use of the Hilbert transform in ECG signal analysis," *Computers in Biology and Medicine*, vol. 31, no. 5, pp. 399–406, 2001.

[13] J. W. Lee, K. S. Kim, B. S. Lee, B. C. Lee, and M. H. Lee, "A real time QRS detection using delay-coordinate mapping for the microcontroller implementation," *Annals of Biomedical Engineering*, vol. 30, no. 9, pp. 1140–1151, 2002.

[14] B. U. Kohler, C. Hennig, and R. Orglmeister, "QRS detection using zero crossing counts," *Progress in Biomedical Research*, vol. 8, no. 3, pp. 138–145, 2003.

[15] Y. C. Yeh and W. J. Wang, "QRS complexes detection for ECG signal: The difference operation method," *Computer Methods and Programs in Biomedicine*, vol. 91, no. 3, pp. 245–254, 2008.

[16] N. M. Arzeno, Z. D. Deng, and C. S. Poon, "Analysis of first-derivative based QRS detection algorithms," *IEEE Transactions on Biomedical Engineering*, vol. 55, no. 2, pp. 478–484, 2008.

[17] M. Adnane, Z. Jiang, and S. Choi, "Development of QRS detection algorithm designed for wearable cardiorespiratory system," *Computer Methods and Programs in Biomedicine*, vol. 93, no. 1, pp. 20–31, 2009.

[18] Z. E. H. Slimane and A. N. Ali, "QRS complex detection using empirical mode decomposition," *Digital Signal Processing*, vol. 20, no. 4, pp. 1221–1228, 2010.

[19] M. S. Manikandan and K. P. Soman, "A novel method for detecting R-peaks in electrocardiogram (ECG) signal," *Biomedical Signal Processing and Control*, vol. 7, no. 2, pp. 118–128, 2012.

[20] H. Zhu and J. Dong, "An R-peak detection method based on peaks of Shannon energy envelope," *Biomedical Signal Processing and Control*, vol. 8, pp. 466–474, 2013.

[21] B. Abibullaev and H. D. Seo, "A new QRS detection method using wavelets and artificial neural networks," *Journal of Medical Systems*, vol. 35, no. 4, pp. 683–691, 2011.

[22] J. P. V. Madeiro, P. C. Cortez, J. A. L. Marques, C. R. V. Seisdedos, and C. R. M. R. Sobrinho, "An innovative approach of QRS segmentation based on first-derivative, Hilbert and wavelet transforms," *Medical Engineering and Physics*, vol. 34, no. 9, pp. 1236–1246, 2012.

[23] C. Li, C. X. Zheng, and C. F. Tai, "Detection of ECG characteristic points using wavelet transforms," *IEEE Transactions on Biomedical Engineering*, vol. 42, no. 1, pp. 21–28, 1995.

[24] M. Bahoura, M. Hassani, and M. Hubin, "DSP implementation of wavelet transform for real time ECG waveforms detection and heart rate analysis," *Computer Methods and Programs in Biomedicine*, vol. 52, no. 1, pp. 35–44, 1997.

[25] V. X. Afonso, W. J. Tompkins, T. Q. Nguyen, K. Michler, and S. Luo, "ECG beat detection using filter banks," *IEEE Transactions on Biomedical Engineering*, vol. 46, no. 2, pp. 192–202, 1999.

[26] S. W. Chen, H. C. Chen, , and H. L. Chan, "A real-time QRS detection method based on moving-averaging incorporating with wavelet denoising," *Computer Methods and Programs in Biomedicine*, vol. 82, no. 3, pp. 187–195, 2006.

[27] S. Choi, M. Adnane, G. J. Lee, H. Jang, Z. Jiang, and H. K. Park, "Development of ECG beat segmentation method by combining lowpass filter and irregular RR interval checkup strategy," *Expert Systems with Applications*, vol. 37, no. 7, pp. 5208–5218, 2010.

[28] Z. Zidelmala, A. Amiroua, M. Adnaneb, and A. Belouchranib, "QRS detection based on wavelet coefficients," *Computer Methods and Programs in Biomedicine*, vol. 107, no. 3, pp. 490–496, 2012.

[29] S. A. Chouakri, F. B. Reguig, and A. T. Ahmed, "QRS complex detection based on multi wavelet packet decomposition," *Applied Mathematics and Computation*, vol. 217, no. 23, pp. 9508–9525, 2011.

[30] F. Bouaziz, D. Boutana, and M. Benidir, "Multiresolution wavelet-based QRS complex detection algorithm suited to several abnormal morphologies," *IET Signal Processing*, vol. 8, no. 7, pp. 774–782, 2014.

[31] A. Karimipour and M. R. Homaeinezhad, "Real-time electrocardiogram P-QRS-T detection-delineation algorithm based on quality-supported analysis of characteristic templates," *Computers in Biology and Medicine*, vol. 52, pp. 153–165, 2014.

[32] F. Zhang and Y. Lian, "QRS detection based on multi-scale mathematical morphology for wearable ECG device in body area networks," *IEEE Transaction on Biomedical Circuits and Systems*, vol. 3, no. 4, pp. 220–228, 2009.

[33] F. Zhang and Y. Lian, "QRS detection based on morphological filter and energy envelope for applications in body sensor networks," *Journal of Signal Processing Systems*, vol. 64, no. 2, pp. 187–194, 2011.

[34] C. F. Zhang and T. W. Bae, "VLSI friendly ECG QRS complex detector for body sensor networks," *IEEE Journal on Emerging and Selected Topics on Circuits and Systems*, vol. 2, no. 1, pp. 52–59, 2012.

[35] K. Arbateni and A. Bennia, "Sigmoidal radial basis function ANN for QRS complex detection," *Neurocomputing*, vol. 145, pp. 438–450, 2014.

[36] Z. Zidelmal, A. Amirou, D. Ould-Abdeslamb, A. Moukadem, and A. Dieterlen, "QRS detection using S-Transform and Shannon energy," *Computer Methods and Programs in Biomedicine*, vol. 116, pp. 1–9, 2014.

[37] G. B. Moody and R. G. Mark, "The impact of the MIT-BIH Arrhythmia Database," *IEEE Engineering in Medicine and Biology*, vol. 20, no. 3, pp. 45–50, 2001.

[38] A. L. Goldberger, L. A. N. Amaral, L. Glass, J. M. Hausdorff, P. Ch. Ivanov, R. G. Mark, J. E. Mietus, G. B. Moody, C. K. Peng, and H. E. Stanley, "PhysioBank, PhysioToolkit, and PhysioNet: Components of a new research resource for complex physiologic signals," *Circulation*, vol. 101, no. 23, pp. e215–e220, 2000.

[39] P. Phukpattaranont and C. Limsakul, "Optimum quadratic filters for nonlinear ultrasonic imaging," *Japanese Journal of Applied Physics*, vol. 48, no. 7, pp. 07GJ02: 1–7, 2009.

[40] I. R. Legarreta, P. S. Addison, N. R. Grubb, G. R. Clegg, C. E. Roberson, and J. N. Watson, "A comparison of continuous waveket transforms modulus maxima

analysis of characteristic ecg features," *Computer in Cardiology*, vol. 32, pp. 755–758, 2005.

[41] M. Rooijakkers, C. Rabotti, S. G. Oei, and M. Mischi, "Low-complexity R-peak detection for ambulatory fetal monitoring," *Physiological Measurement*, vol. 33, pp. 1135–1150, 2012.

[42] J. P. V. Madeiro, P. C. Cortez, J. A. L. Marques, C. R. V. Seisdedos, and C. R. M. R. Sobrinho, "An innovative approach of qrs segmentation based on first-derivative, hilbert and wavelet transforms," *Medical Engineering and Physics*, vol. 34, pp. 1236–1246, 2012.

Output จากโครงการวิจัยที่ได้รับทุนจาก สกว.

1 ผลงานตีพิมพ์ในวารสารวิชาการนานาชาติ (ระบุชื่อผู้แต่ง ชื่อเรื่อง ชื่อวารสาร ปี เล่มที่ เลขที่ และหน้า) พร้อมแจ้งสถานะของการตีพิมพ์ เช่น submitted, accepted, in press, published

มีจำนวน 1 เรื่อง ดังรายละเอียดต่อไปนี้

- Pornchai Phukpattaranont, “QRS detection algorithm based on the quadratic filter,” *Expert Systems with Applications* (*ESA*), vol. 42, no. 11, pp. 4867-4877, Jul., 2015, DOI No: 10.1016/j.eswa.2015.02.012 **[impact factor 1.965, Q1 in JCR® Category]**

2 การนำผลงานวิจัยไปใช้ประโยชน์

- เชิงพาณิชย์ (มีการนำไปผลิต/ขาย/ก่อให้เกิดรายได้ หรือมีการนำไปประยุกต์ใช้โดยภาคธุรกิจ/บุคคลทั่วไป)

-

- เชิงนโยบาย (มีการกำหนดนโยบายอิงงานวิจัย/เกิดมาตรการใหม่/เปลี่ยนแปลงระเบียบข้อบังคับหรือวิธีทำงาน)

-

- เชิงสาธารณะ (มีเครือข่ายความร่วมมือ/สร้างกระแสความสนใจในวงกว้าง)

-

- เชิงวิชาการ (มีการพัฒนาการเรียนการสอน/สร้างนักวิจัยใหม่)

-

3 อื่นๆ (เช่น ผลงานตีพิมพ์ในวารสารวิชาการในประเทศ การเสนอผลงานในที่ประชุมวิชาการ หนังสือ การจดสิทธิบัตร)

การเสนอผลงานในที่ประชุมวิชาการ

- Pornchai Phukpattaranont, “Improvement of signal to noise ratio (SNR) in ECG signals based on dual-band continuous wavelet transform,” in *Proceedings of Asia-Pacific Signal and Information Processing Association Annual Summit and Conference* (*APSIPA ASC 2014*), Siem Reap, Cambodia, Dec. 10-12, 2014.

ภาคผนวก

Pornchai Phukpattaranont, “QRS detection algorithm based on the quadratic filter,” *Expert Systems with Applications* (*ESA*), vol. 42, no. 11, pp. 4867-4877, Jul., 2015, DOI No: 10.1016/j.eswa.2015.02.012 **[impact factor 1.965, Q1 in JCR® Category]**

Expert Systems with Applications 42 (2015) 4867–4877

Contents lists available at ScienceDirect

Expert Systems with Applications

journal homepage: www.elsevier.com/locate/eswa

QRS detection algorithm based on the quadratic filter

Pornchai Phukpattaranont *

Department of Electrical Engineering, Faculty of Engineering, Prince of Songkla University, Thailand

ARTICLE INFO

Article history:
Available online 19 February 2015

Keywords:
Electrocardiography (ECG)
ECG beat detection
QRS detection
Signal processing
Quadratic filter
Volterra filter

ABSTRACT

QRS detection in the electrocardiogram signal is very crucial as a preliminary step for obtaining QRS complex, beat segmentation, and beat-to-beat intervals. Two main problems in QRS detection are a variety of noise types and various types of abnormal morphologies. We propose a QRS detection algorithm consisting of the quadratic filter for enhancing QRS signal to noise ratio. Results show that significant improvement in QRS signal to noise ratio can be obtained from challenging situations including low amplitude QRS complexes corrupted by baseline drift and abnormal morphologies such as an aberrated atrial premature beat, a premature ventricular contraction beat, a fusion of ventricular and normal beat, and a fusion of paced and normal beat. The enhancements in QRS signal to noise ratio allow us to use a single fixed threshold without any additional post-processing techniques in beat detection step. The performance of proposed algorithm was evaluated with the electrocardiogram data from MIT-BIH arrhythmia database. Results show that the quadratic filter is capable of enhancing QRS signal to noise very well leading to the average detection error rate of 0.38% from 48 records.

1. Introduction

The electrocardiogram (ECG) provides very important information on the state of the heart, which can be used for medical monitoring and diagnosis. Each beat of ECG consists of P wave, QRS complex, and T wave. An automatic QRS detection algorithm is very crucial as a preliminary step for obtaining QRS complex, beat segmentation, and beat-to-beat intervals. Further processing of these preliminary steps can be employed for a variety of medical applications. QRS complex can be used for monitoring the electrical activity of the heart during the ventricular contraction. After beat segmentation, each individual beat can be further categorized into different types of arrhythmia, such as normal beats, premature ventricular contraction beats, atrial premature beats, and other beats (Dutta, Chatterjee, & Munshi, 2010; Korürek & Dogan, 2010; Kutlu & Kuntalp, 2012). Series of beat-to-beat intervals is a basis used in analyzing heart rate variability. Heart rate variability analysis is an inexpensive and noninvasive tool for a variety of medical diagnoses such as obstructive sleep apnea syndrome (Babaeizadeh, White, Pittman, & Zhou, 2010; Yildiz, Akin, & Poyraz, 2011) and congestive heart failure (Yu & Lee, 2012a, 2012b). In addition, the automatic QRS detection algorithm can be applied for discovering an abnormal ECG activity in a mobile ECG monitoring and alert system for elderly patients (Shih, Chiang, Lin, & Lin, 2010).

To accurately detect the QRS complex, two steps of processing algorithms are needed, i.e., ECG preprocessing and ECG beat detection. The aim of ECG preprocessing is to remove noises in ECG signals. The main noises in ECG signal can be divided into two types: low frequency noises and high frequency noises. While the low frequency noises are the T-wave noise and the baseline wander noise, the high frequency noises are the muscle noise and the power line noise. Based on previous publications, the noise removal algorithms in preprocessing step can be classified into 2 main categories: linear filtering and wavelet transform.

The preprocessing operation in many previous publications employs linear filtering techniques for noise removal in ECG signals (Adnane, Jiang, & Choi, 2009; Arzeno, Deng, & Poon, 2008; Benitez, Gaydecki, Zaidi, & Fitzpatrick, 2001; Hamilton & Tompkins, 1986; Kohler, Hennig, & Orglmeister, 2003; Lee, Kim, Lee, Lee, & Lee, 2002; Manikandan & Soman, 2012; Pan & Tompkins, 1985; Poli, Cagnoni, & Valli, 1995; Slimane & Ali, 2010; Yeh & Wang, 2008; Zhu & Dong, 2013). Its main processing is based on a bandpass filter with a cutoff frequency 5–36 Hz, which is corresponding to the bandwidth of QRS interval in the ECG signal. In addition, signals after filtering are further processed with a variety of methods for calculating the envelope signal, for example, moving average filter (Hamilton & Tompkins, 1986; Pan & Tompkins, 1985; Slimane & Ali, 2010), differential equation (Adnane et al., 2009; Arzeno et al., 2008; Benitez et al., 2001;

* Address: Department of Electrical Engineering, Faculty of Engineering, Prince of Songkla University, 110/5 Kanjanavanit Road, Kohong, Hat Yai, Songkhla 90112, Thailand. Tel.: +66 74 558831.
E-mail address: pornchai.p@psu.ac.th

http://dx.doi.org/10.1016/j.eswa.2015.02.012
0957-4174/

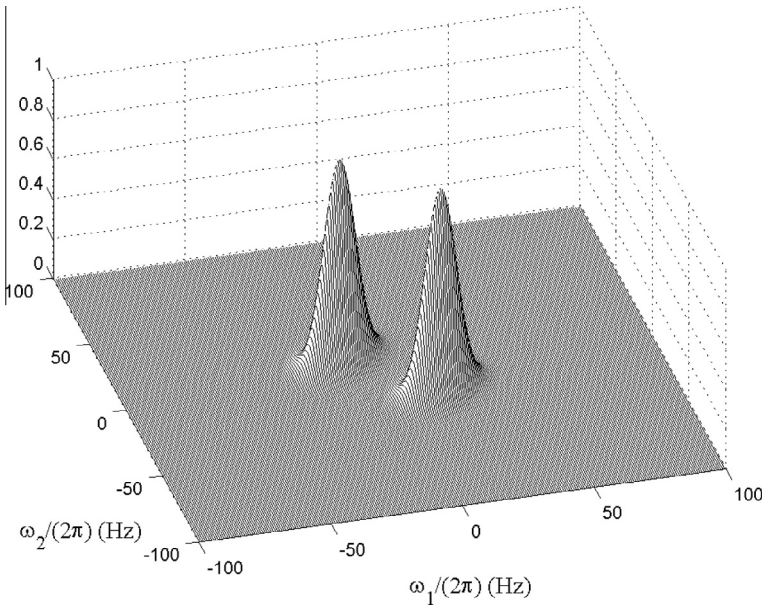

Fig. 1. The modified 2D Gaussian function in the frequency domain.

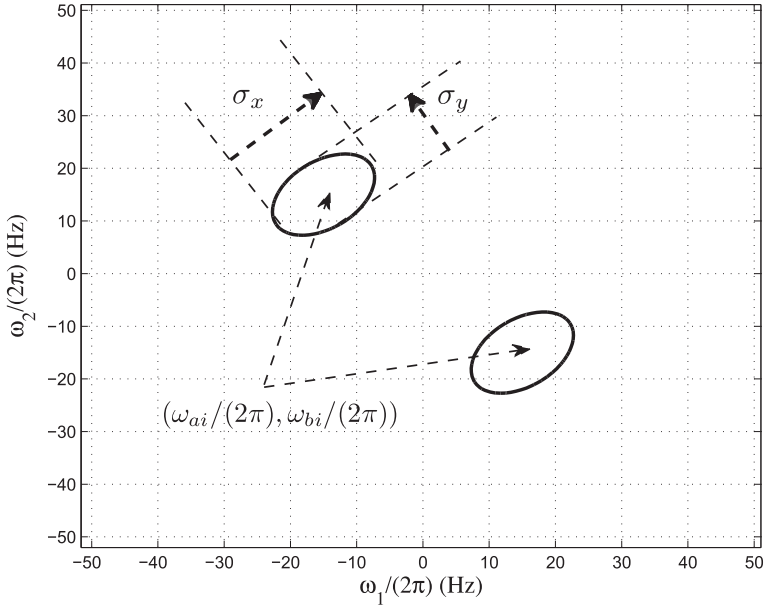

Fig. 2. The contour plot at −6 dB showing parameters in the design of the QF: Passband width and center points.

Hamilton & Tompkins, 1986; Pan & Tompkins, 1985), squaring function (Adnane et al., 2009; Arzeno et al., 2008; Hamilton & Tompkins, 1986; Pan & Tompkins, 1985), genetic algorithm (Poli et al., 1995), Hilbert transform (Benitez et al., 2001), and zero crossing (Kohler et al., 2003).

Preprocessing algorithms based on wavelet transform are popularly used for removing noises in ECG signals (Abibullaev & Seo, 2011; Afonso, Tompkins, Nguyen, Michler, & Luo, 1999; Bahoura, Hassani, & Hubin, 1997; Bouaziz, Boutana, & Benidir, 2014; Chen, Chen, & Chan, 2006; Choi et al., 2010; Chouakri, Reguig, & Ahmed, 2011; Karimipour & Homaeinezhad, 2014; Li, Zheng, & Tai, 1995; Madeiro, Cortez, Marques, Seisdedos, & Sobrinho, 2012; Zidelmala, Amiroua, Adnaneb, & Belouchranib, 2012). After the output from wavelet transform is obtained, further processing methods used for determining the envelope signal include differential equation (Choi et al., 2010; Madeiro et al., 2012), moving average filter (Chen et al., 2006; Chouakri et al., 2011), filter bank (Afonso et al., 1999), and zero crossing (Bahoura et al., 1997).

In addition to linear filtering and wavelet transform, other noise removal techniques include mathematical morphology (Zhang & Bae, 2012; Zhang & Lian, 2009, 2011), artificial neural network (Arbateni & Bennia, 2014), and S-transform (Zidelmal, Amirou, Ould-Abdeslamb, Moukadem, & Dieterlen, 2014). Further processing techniques after mathematical morphology are differential equation (Zhang & Lian, 2009) and wavelet transform (Zhang & Lian, 2011).

After the noises in the ECG signal are removed in the preprocessing operation, the envelope signal is extracted, and the QRS complex is detected in the ECG beat detection process. In this step,

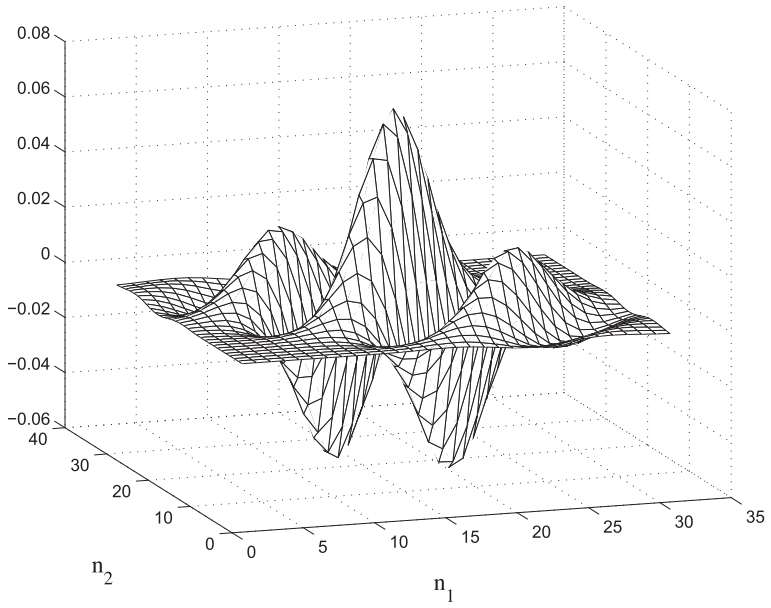

Fig. 3. Coefficients of the QF shown in time domain.

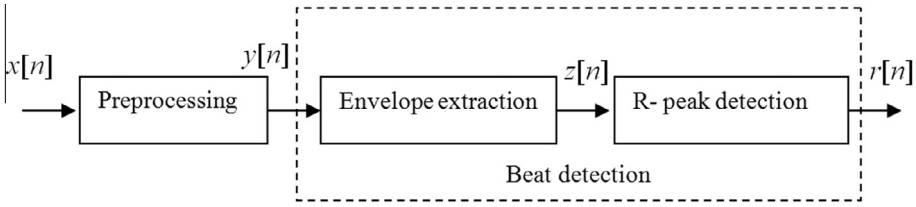

Fig. 4. Schematic diagram of QRS detection algorithm.

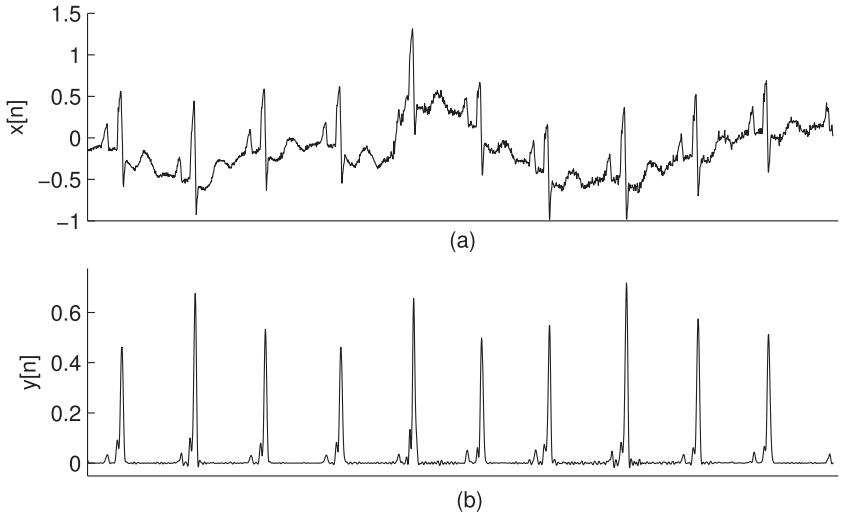

Fig. 5. Noise removal in preprocessing operation. (a) ECG signal before noise removal $x[n]$. (b) ECG signal after noise removal $y[n]$.

a threshold is a very important parameter. The threshold can be classified into two types: fixed threshold and adaptive threshold. The fixed threshold has an advantage of low computational complexity at an expense of detection accuracy. There are two categories of fixed threshold, i.e., single level (Abibullaev & Seo, 2011; Zidelmala et al., 2012) and multiple levels (Afonso et al., 1999; Chouakri et al., 2011; Yeh & Wang, 2008). To achieve better detection accuracy, the adaptive threshold is used. Similar to the fixed threshold, the adaptive threshold can be categorized into single level (Benitez et al., 2001; Chen et al., 2006; Choi et al., 2010; Kohler et al., 2003; Madeiro et al., 2012; Zhang & Bae, 2012; Zhang & Lian, 2009, 2011) and multiple levels (Adnane et al., 2009; Hamilton & Tompkins, 1986; Lee et al., 2002; Pan & Tompkins, 1985; Poli et al., 1995). In addition, some post-processing algorithms are used to achieve better detection rate. These post-processing algorithms include the checkup for irregular

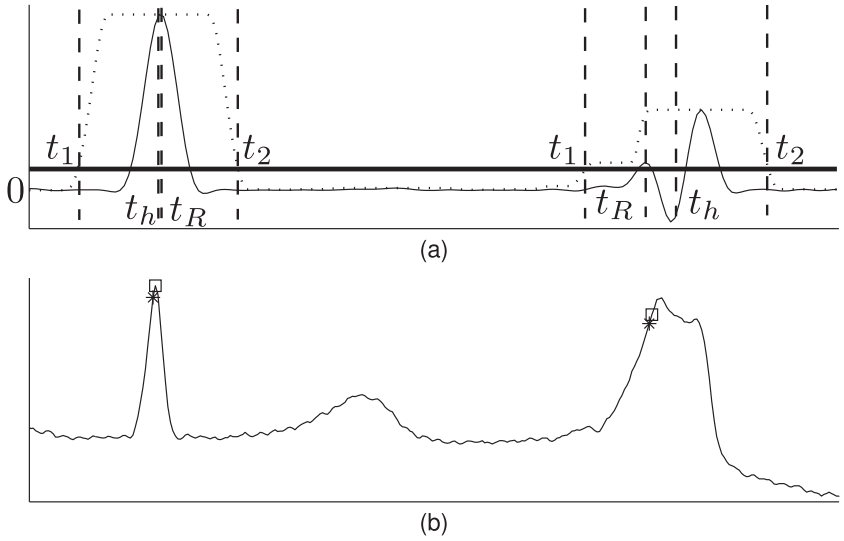

Fig. 6. ECG beat detection algorithm. (a) Thin line: ECG signal after noise removal $y[n]$. Dotted line: Envelope signal $z[n]$. Thick line: Threshold value line. (b) ECG signal overlaid by the markers from the proposed algorithm (square) and the expert (asterisk). While the signal on the left hand side is a normal ECG beat, the signal on the right hand side is a premature ventricular contraction beat.

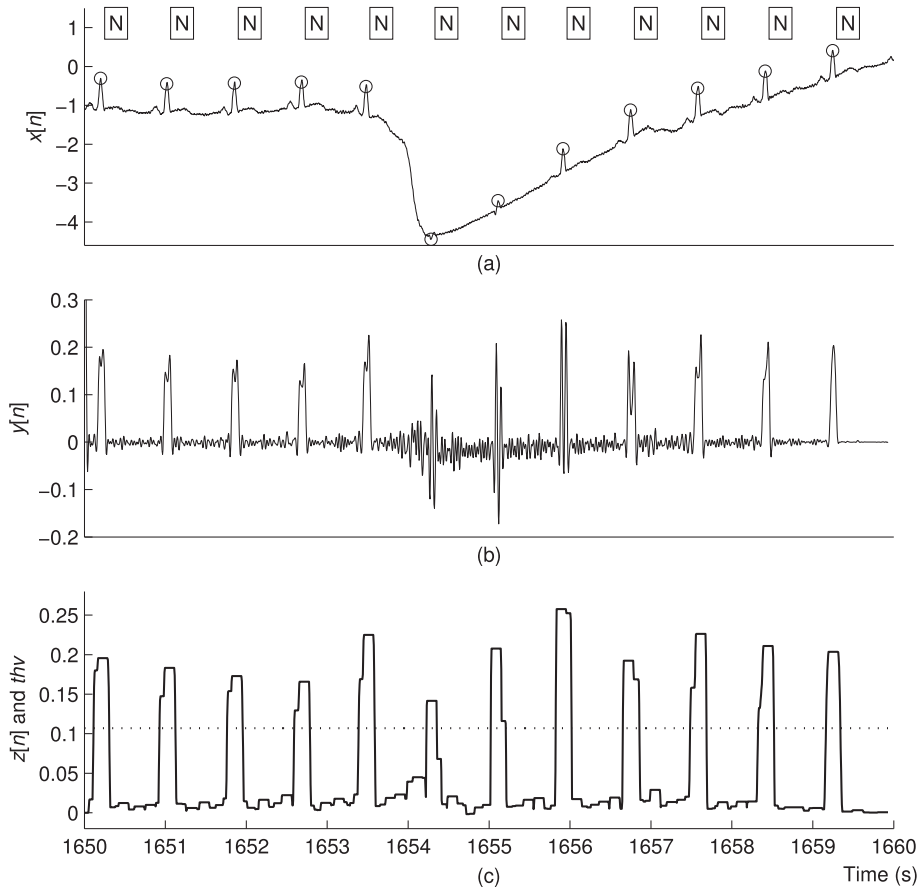

Fig. 7. Results of the proposed algorithm applied on the ECG signal record 121. (a) The ECG signal before noise removal $x[n]$ overlaid by the circle markers from the expert. "N" stands for a normal beat. (b) The ECG signal after noise removal $y[n]$. (c) The envelope signal $z[n]$ (solid line) and the threshold level *thv* (dotted line).

beat-to-beat interval information (Adnane et al., 2009; Choi et al., 2010; Pan & Tompkins, 1985).

The main focus of this work is to propose the QRS detection algorithm consisting of the quadratic filter (QF) capable of enhancing QRS signal to noise ratio in preprocessing operation. Results show that the QRS complex can be emphasized by the preprocessing operation based on the QF because of the significant increase in the QRS signal to noise ratio. As a result, the detection accuracy can be obtained without the need for adaptive thresholding and post-processing operations.

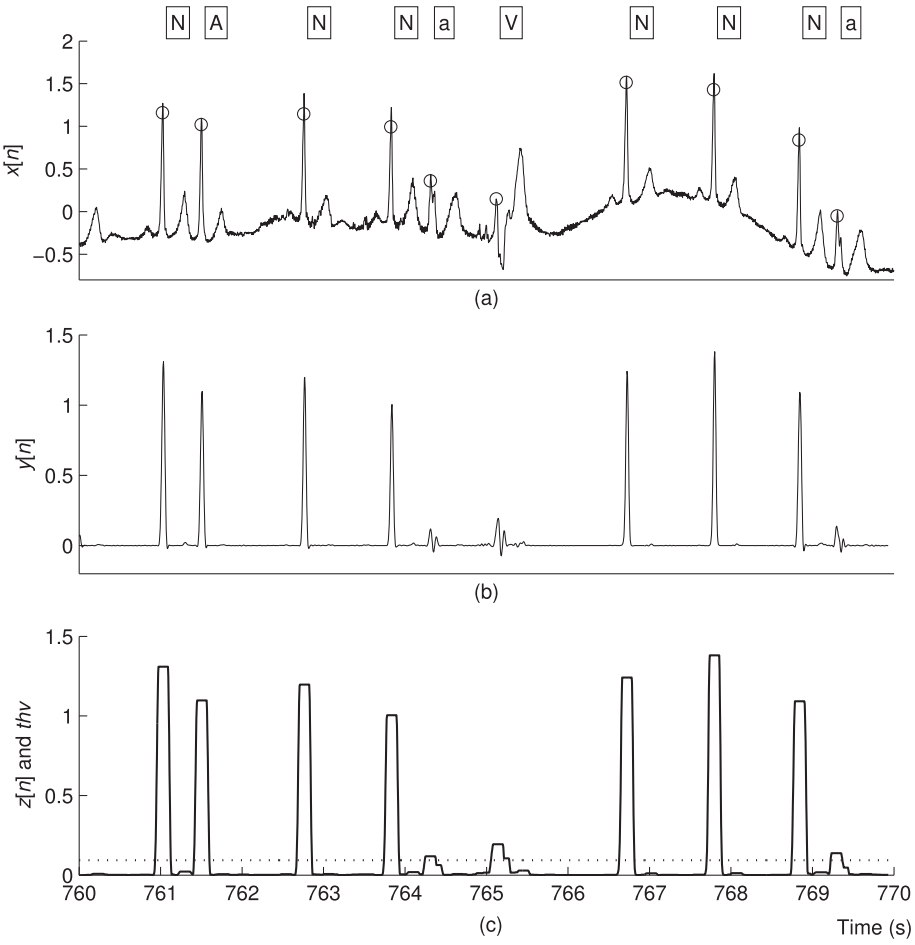

Fig. 8. Results of the proposed algorithm applied on the ECG signal record 202. (a) The ECG signal before noise removal $x[n]$ overlaid by the circle markers from the expert. "A" stands for an atrial premature beat, "a" for an aberrated atrial premature beat, and "V" for a premature ventricular contraction beat. (b) The ECG signal after noise removal $y[n]$. (c) The envelope signal $z[n]$ (solid line) and the threshold level thv (dotted line).

The rest of this paper is organized as follows. Section 2 presents the design method for the QF. Section 3 describes the proposed QRS detection algorithm as well as the measure and the ECG database used for performance evaluation. Results and discussion are given in Section 4. Finally, conclusions are drawn in Section 5.

2. Quadratic filter design

The application of the QF, which is derived from the second-order Volterra filter, in the ECG noise removal application has not been carefully studied. Unlike the linear filtering, the important advantage of the QF is that it has various degrees of freedom for optimization in removing noises contaminated in the ECG signal. Details of the QF derivation are given as follows.

The design of QF for removing noises in ECG signals is performed in frequency domain. Fig. 1 shows an example of 2D magnitude frequency response of the QF. The linear-phased QF is designed based on the sum of two 2D Gaussian filters, which is given by

$$G(\omega_{1k},\omega_{2l}) = \frac{G_1(\omega_{1k},\omega_{2l}) + G_2(\omega_{1k},\omega_{2l})}{\max\{G_1+G_2\}}, \tag{1}$$

where

$$G_i(\omega_{1k},\omega_{2l}) = \exp\{-[A(\omega_{1k}-\omega_{ai})^2 + B(\omega_{1k}-\omega_{ai})(\omega_{2l}-\omega_{bi}) + C(\omega_{2l}-\omega_{bi})^2]\}, \tag{2}$$

for $i = 1, 2$ with:

$$A = \left(\frac{\cos\theta}{\sigma_x}\right)^2 + \left(\frac{\sin\theta}{\sigma_y}\right)^2, \tag{3}$$

$$B = -\frac{\sin 2\theta}{\sigma_x^2} + \frac{\sin 2\theta}{\sigma_y^2}, \tag{4}$$

$$C = \left(\frac{\sin\theta}{\sigma_x}\right)^2 + \left(\frac{\cos\theta}{\sigma_y}\right)^2. \tag{5}$$

The coefficient $(\omega_{ai}, \omega_{bi})$ is the center of Gaussian filter, σ_x is a constant that defines the passband width along the cross-diagonal direction, σ_y is a constant that defines the passband width along the diagonal direction, and θ is the rotation angle.

Note that the passband frequencies should be approximately placed at the passband frequencies of the QRS response. To achieve the best filter for removing noise, parameters should be adjusted to maximize QRS signal to noise ratio. Fig. 2 shows a contour plot at −6 dB of the magnitude of 2D frequency responses of the QF from Fig. 1. The centers of Gaussian function are at $(\omega_{1k}, \omega_{2l})$ of (−15, 15) and (15, −15) Hz. Other parameters, i.e., $(\sigma_x, \sigma_y, \theta)$ for the QF are (1.1, 0.55, $-\pi/4$).

After the 2D magnitude frequency of the QF is formed, the frequency response can be given by

$$H(e^{j\omega_{1k}}, e^{j\omega_{2l}}) = G(\omega_{1k},\omega_{2l})e^{j\phi(\omega_{1k},\omega_{2l})}, \tag{6}$$

where $G(\omega_{1k}, \omega_{2l})$ represents the desired magnitude response based on the 2D Gaussian filters given in (1) and $\phi(\omega_{1k}, \omega_{2l})$ is the phase response, which can be expressed as

$$\phi(\omega_{1k}, \omega_{2l}) = -\frac{N_1 - 1}{2}\omega_{1k} - \frac{N_2 - 1}{2}\omega_{2l}, \quad (7)$$

where $\omega_{1k} = (2\pi k/M_1) - \pi, k = 0, 1, \ldots, M_1 - 1$ and $\omega_{2l} = (2\pi l/M_2) - \pi, l = 0, 1, \ldots, M_2 - 1$. We use the QF size $N_1 = N_2 = N$. As a result, the phase delay of the signal output is $(N - 1)/2$.

Subsequently, the filter coefficients $h[n_1, n_2]$ can be obtained by the inverse DFT of $H(e^{j\omega_{1k}}, e^{j\omega_{2l}})$. Please see Phukpattaranont and Limsakul (2009) for more details. Fig. 3 shows the coefficients of the QF corresponding the design parameters shown in Fig. 2. The ECG signal after noise removal $y[n]$ is produced by applying the QF coefficients to the ECG signal $x[n]$, which can be expressed as

$$y[n] = \sum_{k_1=0}^{P-1}\sum_{k_2=0}^{P-1} h[k_1, k_2]x[n - k_1]x[n - k_2]. \quad (8)$$

3. Materials and methods

3.1. Proposed algorithm

Fig. 4 shows a schematic diagram of the proposed QRS detection algorithm. The noises in the ECG signal $x[n]$ are removed in the preprocessing operation based on the QF designed using the method described in Section 2. Fig. 5(a) and (b) shows an example of 10-beat ECG signals before and after noise removal in the top and bottom panels, respectively.

Subsequently, to obtain the envelope signal $z[n], y[n]$ is processed with the envelope extraction algorithm. Fig. 6(a) shows an example of signals in beat detection algorithm. The signals $y[n]$ and $z[n]$ are shown with the thin and dotted lines, respectively. Then, the threshold value is defined as shown in Fig. 6(a) with a thick line to determine the time interval $[t_1\ t_2]$ where the QRS complex locates. Finally, the R peak in QRS complex is detected from the determination of the time t_R where the signal amplitude is maximum. Fig. 6(b) shows the ECG signal overlaid by the markers from the proposed algorithm (square) and the expert (asterisk). The details of proposed algorithm can be summarized as follows.

1. Determine the signal $y[n]$ from the ECG signal $x[n]$ by processing with the QF.
2. Determine the envelope signal $z[n]$ from $y[n]$ using the maximum filter with the length L = 120 ms as given by

$$z[n] = \max_{k\in[n-L+1,n]} y[k]. \quad (9)$$

3. Detect the R peak in QRS complex using the following steps.
   (a) Calculate a threshold value thv from $thv = \lambda y_m[n]$, where $y_m[n]$ is the maximum value of $y[n]$ and λ is a constant in the range of 0.10 to 0.17.

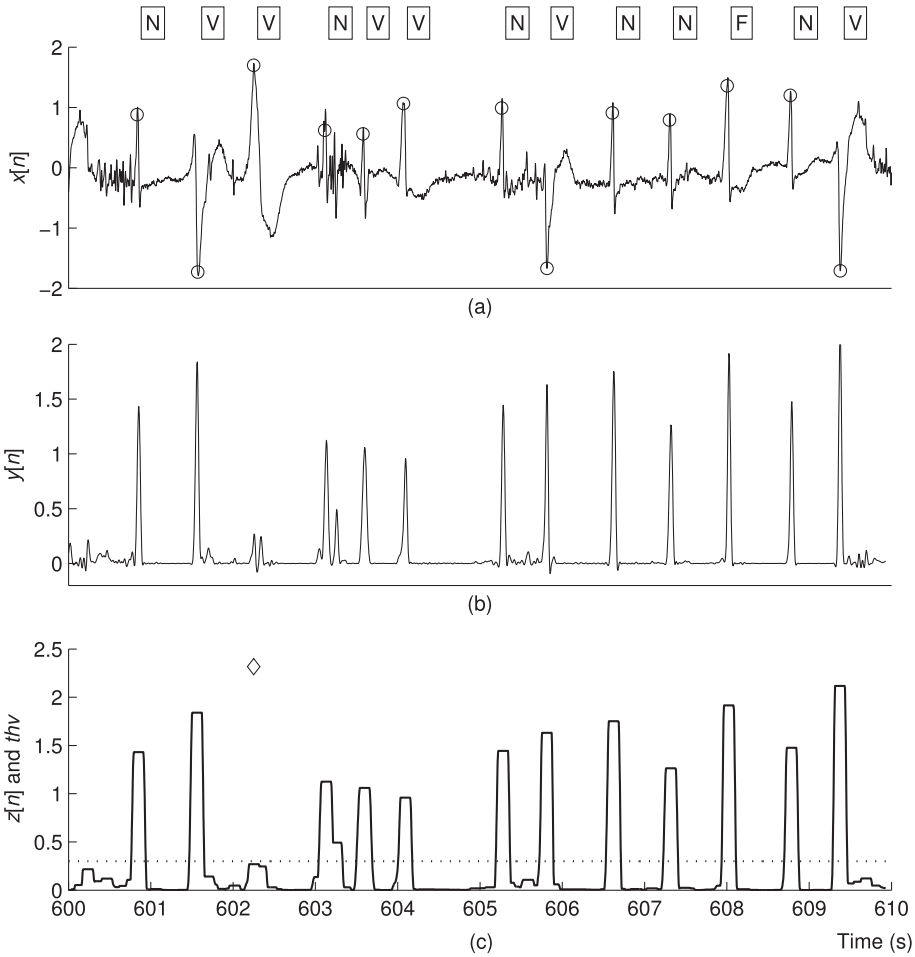

Fig. 9. Results of the proposed algorithm applied on the ECG signal record 200. (a) The ECG signal before noise removal $x[n]$ overlaid by the circle markers from the expert. "F" stands for a fusion of ventricular and normal beat. (b) The ECG signal after noise removal $y[n]$. (c) The envelope signal $z[n]$ (solid line) and the threshold level thv (dotted line). "◇" stands for an FN detection.

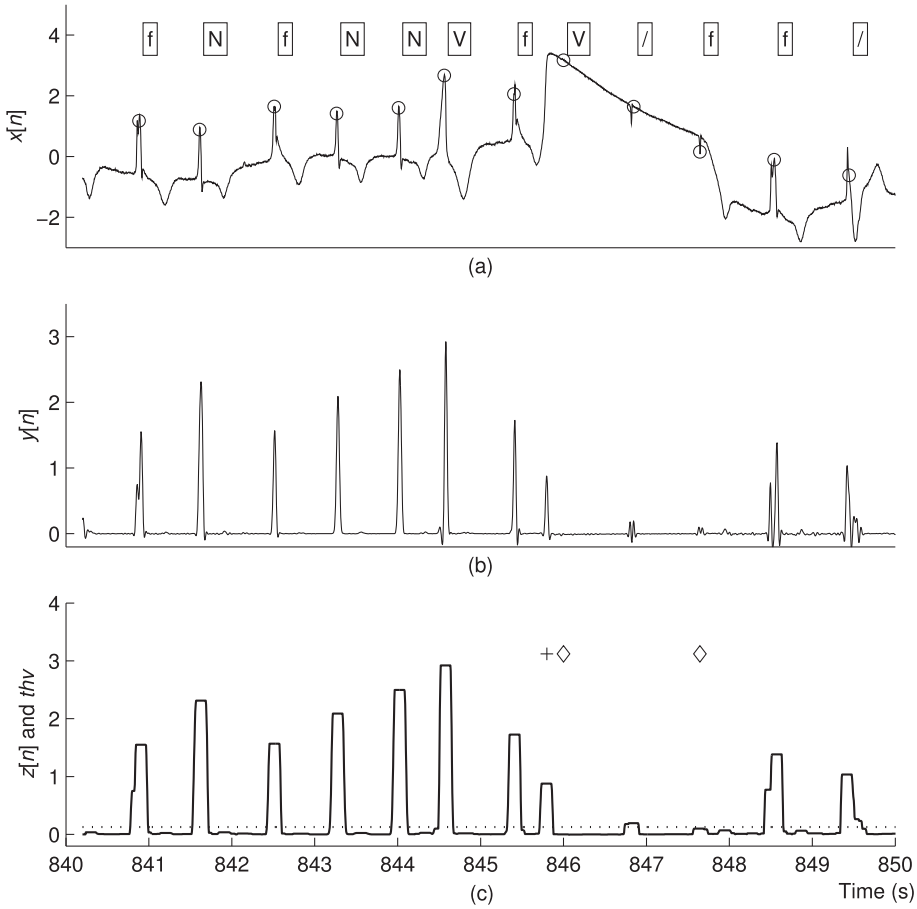

Fig. 10. Results of the proposed algorithm applied on the ECG signal record 217. (a) The ECG signal before noise removal $x[n]$ overlaid by the circle markers from the expert. "f" stands for a fusion of paced and normal beat and "/" for a paced beat. (b) The ECG signal after noise removal $y[n]$. (c) The envelope signal $z[n]$ (solid line) and the threshold level *thv* (dotted line). "+" stands for an FP detection.

(b) Find the time duration where $z[n]$ is greater than *thv* and determine the beginning time t_1, the half-duration time t_h, and the ending time t_2.
(c) Determine the amplitude of $y[n]$ at t_h. If the amplitude is greater than zero, which indicates that it is not a premature ventricular contraction beat, go to step (d), else go to step (e).
(d) Determine R peak location t_R from the time between $[t_1\ t_2]$ in $y[n]$ that gives the maximum amplitude.
(e) Determine R peak location t_R from the time between $[t_1\ t_h]$ in $y[n]$ that gives the maximum amplitude.

3.2. Performance measurement

The performance of QRS detection algorithm is evaluated with sensitivity (SEN), positive predictive rate (PPR), and detection error rate (DER). SEN is given by

$$\mathrm{SEN} = \frac{\mathrm{TP}}{\mathrm{TP}+\mathrm{FN}} \times 100, \tag{10}$$

where true positive (TP) is the number of correct QRS complex predictions. FN is the false negative prediction. In other words, the algorithm predicts that there is no QRS complex in the location where there is a real QRS complex. PPR can be expressed as

$$\mathrm{PPR} = \frac{\mathrm{TP}}{\mathrm{TP}+\mathrm{FP}} \times 100, \tag{11}$$

where FP is the false positive prediction. In other words, the algorithm predicts that there is a QRS complex in the location where there is no QRS complex. DER is used for evaluating the accuracy of algorithm including both FN and FP values, which can be given by

$$\mathrm{DER} = \frac{\mathrm{FN}+\mathrm{FP}}{\mathrm{TP}+\mathrm{FN}} \times 100. \tag{12}$$

3.3. ECG database

ECG data used in performance evaluation for the proposed algorithm are from MIT-BIH arrhythmia database (Goldberger et al., 2000; Moody & Mark, 2001). There are 48 records of ECG data. Each record consists of slightly over 30 min from two-channel of ECG data. Each channel was acquired at a sampling rate of 360 Hz. This database is considered as a class 1 database, which has been carefully scrutinized, thoroughly annotated, and used in many well-known publications. The ECG data from MIT-BIH have a variety of types including both normal and abnormal ECG data. In addition, there is a marker for each beat given by the expert demonstrating the QRS complex location and beat type. In this paper, the QRS complex is detected using the ECG signal from channel 1 or lead II only. In other words, the ECG signal from channel 1 was represented by $x[n]$.

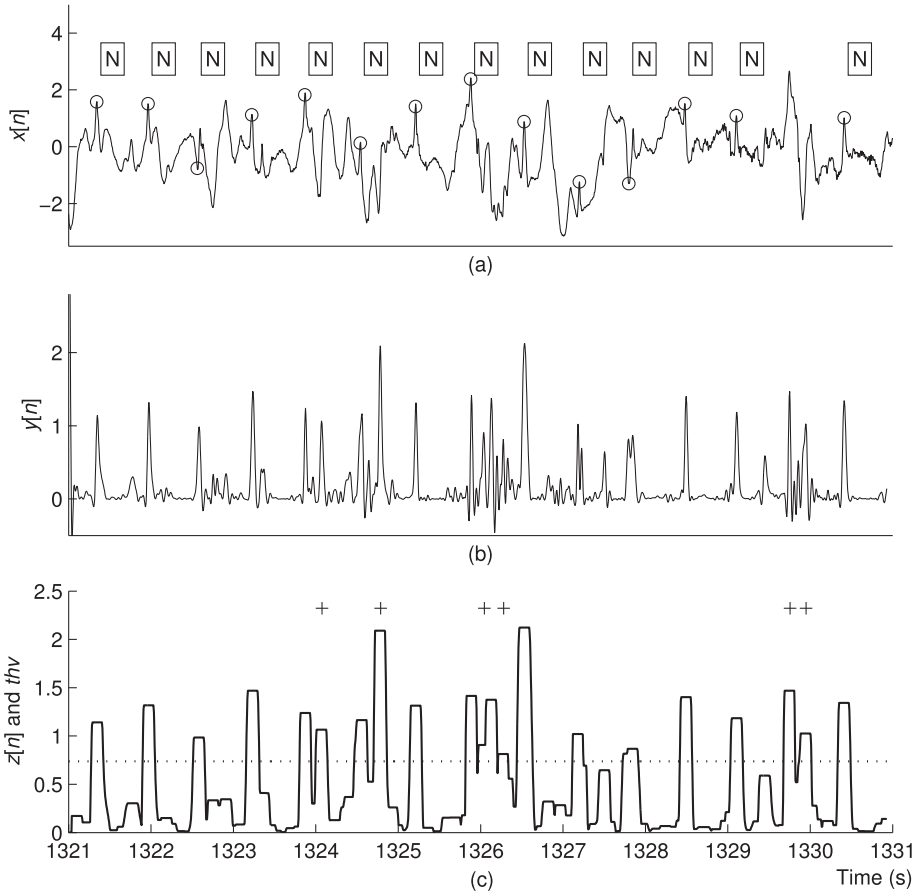

Fig. 11. Results of the proposed algorithm applied on the ECG signal record 105. (a) The ECG signal before noise removal $x[n]$ overlaid by the circle markers from the expert. (b) The ECG signal after noise removal $y[n]$. (c) The envelope signal $z[n]$ (solid line) and the threshold level *thv* (dotted line).

4. Results and discussion

4.1. Enhancement of QRS signal to noise ratio

To illustrate the capability of the QF in enhancing QRS signal to noise ratio, example results from ECG data of record 121, 202, 200, 217, 105, and 108 are demonstrated.

Fig. 7(a) shows the ECG data of record 121 from time 1650 s to time 1660 s. Although ECG data in this record are corrupted by baseline drift and some QRS complexes have very low amplitude, significant improvement in QRS signal to noise ratio of the ECG signal after noise removal $y[n]$ resulting from the QF can be obtained as shown in Fig. 7(b). Fig. 7(c) shows the envelope signal $z[n]$ and the threshold value *thv*, which allow us to correctly detect all QRS signals.

Fig. 8(a) shows the ECG data of record 202 from time 760 s to time 770 s. ECG data in this record consist of 6 normal beats, an atrial premature beat, two aberrated atrial premature beats, and a premature ventricular contraction beat. Fig. 8(b) shows that the QRS signal to noise ratio of $y[n]$ from the QF is good enough for all beats to be correctly detected using the envelope signal $z[n]$ and the threshold level *thv* shown in Fig. 8(c).

Fig. 9(a) shows the ECG data of record 200 from time 600 s to time 610 s. ECG data in this record consist of a fusion of ventricular and normal beat (“F”). In addition, we can see muscle noise in the segments [600–601 s] and [603–603.5 s]. Fig. 9(b) shows that the QF can efficiently remove noise and enhance QRS signal to noise ratio. There is an FN detection shown in Fig. 9(c) at time 602 s because the threshold level *thv* in this record is higher than the premature ventricular contraction beat after applying with the QF.

Fig. 10(a) shows the ECG data of record 217 from time 840 s to time 850 s. In addition to normal beats and a premature ventricular contraction, ECG data in this record is composed of fusion of paced and normal beats (“f”) and paced beats (“/”). Moreover, we can see abrupt baseline shift at time 846 s. Fig. 10(c) shows the envelope signal $z[n]$ resulting from the ECG signal after noise removal $y[n]$ in Fig. 10(b), two FN detections and an FP detection. While the 2 FN detections result from their inherent low amplitudes, the FP detection is caused by the high peak from the abrupt baseline shift after filtering.

Fig. 11(a) shows the ECG data of record 105 from time 1321 s to time 1331 s. ECG data in this record are contaminated with high-grade noise. Although the QRS complex can be emphasized by the QF as shown in Fig. 11(b), the high-grade noise is also amplified. The signal after filtering from high-grade noise causes 6 FP detections as shown in Fig. 11(c).

Fig. 12(a) shows the ECG data of record 108 from time 1655 s to time 1665 s. We can see that the QRS complexes in this record have low amplitude and are corrupted by muscle noise. The amplitude of noise after filtering from time 1662 s to time 1663 s is higher than that of QRS signals from time 1663 s to time 1665 s as shown in Fig. 12(b). As a result, the proposed algorithm gives 2 FP

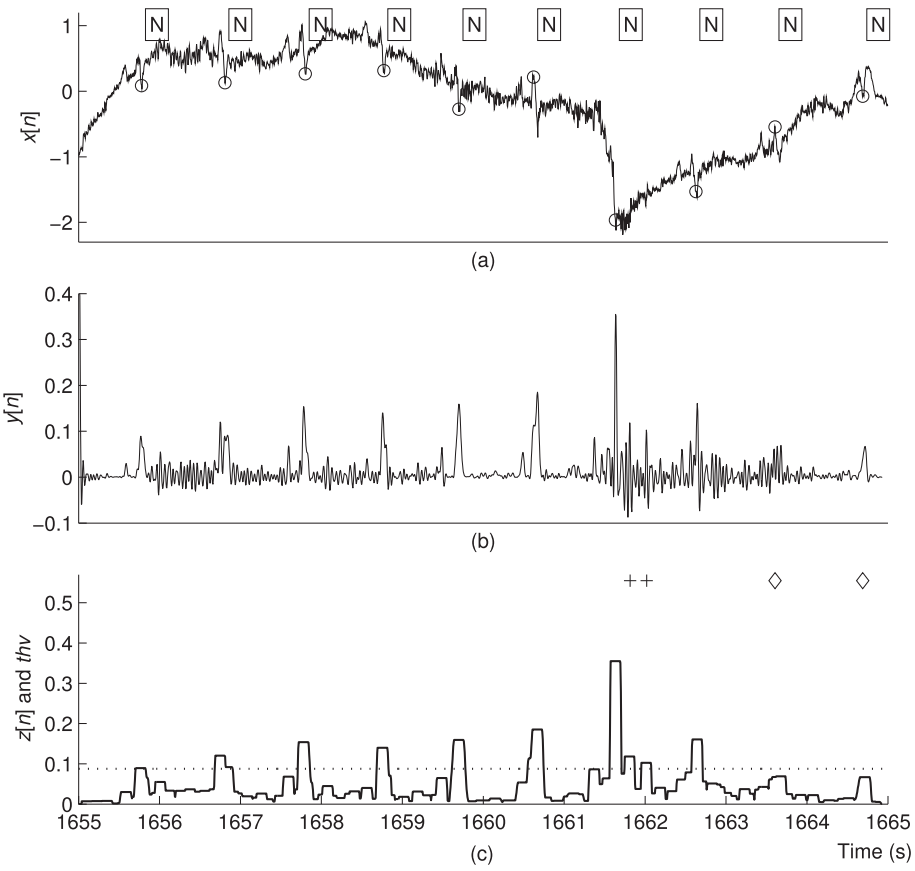

Fig. 12. Results of the proposed algorithm applied on the ECG signal record 108. (a) The ECG signal before noise removal $x[n]$ overlaid by the circle markers from the expert. (b) The ECG signal after noise removal $y[n]$. (c) The envelope signal $z[n]$ (solid line) and the threshold level *thv* (dotted line).

detections and 2 FN detections based on the threshold *thv* shown in Fig. 12(c).

4.2. Performance evaluation and comparison

Table 1 shows performance evaluation of the proposed algorithm applied on all 48 records of ECG data when the parameters $(\omega_{1k}, \omega_{2l}), \sigma_x, \sigma_y$, and θ of the QF are fixed at $(-15, 15)$, $(15, -15)$ Hz, 1.1, 0.70, and $-\pi/4$, respectively. The average DER value is 0.38%. The average values of TP, FN, FP, SEN, and PPR are 109,281 beats, 202 beats, 210 beats, 99.82%, and 99.81%, respectively. While the maximum DER value is 4.08% from the record 108, the minimum DER value is 0% from 21 records (record 100, 102, 103, 107, 112, 113, 115, 117, 118, 121–124, 202, 212, 213, 219–221, 230, and 231).

Table 2 shows the performance comparison of the proposed algorithm with that from other 7 state-of-the-art papers. The order of each method is sorted from the minimal average DER value to the maximal average DER value. The minimal and maximal average DER values are 0.17% (Zhu & Dong, 2013) and 0.54% (Choi et al., 2010), respectively. The average DER value from the proposed algorithm based on noise removal in ECG signals using the QF is 0.38%. This result shows that the QF can significantly increase the QRS signal to noise ratio. As a result, only the use of a single fixed threshold without additional post-processing techniques can yield low average DER value.

Table 3 shows comparison results of the DER values of ECG record 121, 202, 200, 217, 105, and 108 from the proposed method with that from other 7 papers. The minimum and maximum DER values for each record are shown using the boldface and italics fonts, respectively. The DER values of ECG record 121 and 202 from the proposed method are minimal at 0.00%. For other ECG records, the DER values from the proposed method are in the range between minimum and maximum DER values.

For ECG record 121 and 202, the proposed method performs better than the others because of its capability in enhancing QRS signal to noise ratio for challenging situations such as low amplitude ECG data corrupted with baseline drift and various types of abnormal morphologies. As a result, only a simple beat detection step based on a single fixed threshold with no additional post-processing techniques is enough for achieving the DER value of 0%. However, QRS signal to noise ratio from the QF is not high enough in some situations such as abrupt baseline shift (record 217), high-grade noise (record 105), and low amplitude QRS complex contaminated by muscle noise (record 108). Therefore, FP and FN detections are obtained from the proposed method. Other QRS algorithms overcome these problems using additional computations. On the one hand, the algorithms in some previous publications reduce FN detections using adaptive thresholding techniques (Arbateni & Bennia, 2014; Choi et al., 2010; Karimipour & Homaeinezhad, 2014; Zhang & Lian, 2009; Zidelmal et al., 2014) and false-noise detection algorithm (Zhu & Dong, 2013). On the other hand, some algorithms in previous publications decrease FP detections using the technique based on the refractory period of 200 ms (Bouaziz et al., 2014; Zhu & Dong, 2013; Zidelmal et al., 2014). In other words, two consecutive QRS complexes cannot be detected within 200 ms. Another example used to decrease FP detections is the check up for irregular beat-to-beat interval information algorithm (Choi et al., 2010).

Table 1
Performance evaluation of proposed algorithm.

Record	Total	TP	FN	FP	SEN (%)	PPR (%)	DER (%)
100	2272	2272	0	0	100.00	100.00	0.00
101	1865	1865	0	4	100.00	99.79	0.21
102	2187	2187	0	0	100.00	100.00	0.00
103	2084	2084	0	0	100.00	100.00	0.00
104	2228	2223	5	20	99.78	99.11	1.12
105	2572	2558	11	28	99.57	98.92	1.52
106	2027	2024	3	4	99.85	99.80	0.35
107	2136	2136	0	0	100.00	100.00	0.00
108	1763	1710	53	19	96.99	98.90	4.08
109	2532	2531	1	0	99.96	100.00	0.04
111	2124	2123	1	0	99.95	100.00	0.05
112	2539	2539	0	0	100.00	100.00	0.00
113	1794	1794	0	0	100.00	100.00	0.00
114	1879	1878	1	5	99.95	99.73	0.32
115	1953	1953	0	0	100.00	100.00	0.00
116	2412	2393	19	2	99.21	99.92	0.87
117	1535	1535	0	0	100.00	100.00	0.00
118	2278	2278	0	0	100.00	100.00	0.00
119	1987	1987	0	1	100.00	99.95	0.05
121	1863	1863	0	0	100.00	100.00	0.00
122	2476	2476	0	0	100.00	100.00	0.00
123	1518	1518	0	0	100.00	100.00	0.00
124	1619	1619	0	0	100.00	100.00	0.00
200	2601	2598	3	2	99.88	99.92	0.19
201	1963	1959	4	3	99.80	99.85	0.36
202	2136	2136	0	0	100.00	100.00	0.00
203	2980	2958	22	35	99.26	98.83	1.91
205	2656	2654	2	0	99.92	100.00	0.08
207	1860	1845	15	26	99.19	98.61	2.20
208	2955	2933	22	13	99.26	99.56	1.18
209	3005	3005	0	1	100.00	99.97	0.03
210	2650	2642	8	7	99.70	99.74	0.57
212	2748	2748	0	0	100.00	100.00	0.00
213	3250	3250	0	0	100.00	100.00	0.00
214	2262	2256	6	0	99.73	100.00	0.27
215	3363	3363	0	1	100.00	99.97	0.03
217	2208	2206	2	4	99.91	99.82	0.27
219	2154	2154	0	0	100.00	100.00	0.00
220	2047	2047	0	0	100.00	100.00	0.00
221	2427	2427	0	0	100.00	100.00	0.00
222	2483	2472	11	13	99.56	99.48	0.97
223	2605	2604	1	1	99.96	99.96	0.08
228	2053	2043	10	16	99.51	99.22	1.27
230	2256	2256	0	0	100.00	100.00	0.00
231	1571	1571	0	0	100.00	100.00	0.00
232	1780	1780	0	1	100.00	99.94	0.06
233	3079	3077	2	3	99.94	99.90	0.16
234	2753	2753	0	1	100.00	99.96	0.04
Total	109,483	109,281	202	210	99.82	99.81	0.38

Table 2
Performance comparison of the proposed algorithm with that from other 7 papers.

Method of noise removal	TP	FN	FP	SEN (%)	PPR (%)	DER (%)
Linear filtering (Zhu & Dong, 2013)	109,401	93	91	99.92	99.92	0.17
S-transform (Zidelmal et al., 2014)	108,323	171	97	99.84	99.91	0.25
Artificial neural network (Arbateni & Bennia, 2014)	109,273	210	109	99.82	99.91	0.28
Wavelet transform (Bouaziz et al., 2014)	109,354	140	232	99.87	99.79	0.34
Quadratic filtering (This work)	109,281	202	210	99.82	99.81	0.38
Mathematical morphology (Zhang & Lian, 2009)	109,297	213	204	99.80	99.81	0.38
Wavelet transform (Karimipour & Homaeinezhad, 2014)	115,945	192	308	99.81	99.70	0.49
Wavelet transform (Choi et al., 2010)	109,118	376	218	99.66	99.80	0.54

Table 3
Comparisons of the DER values in percent of ECG record 121, 202, 200, 217, 105, and 108 from the proposed method with that from other 7 papers.

Method of noise removal	121	202	200	217	105	108
Quadratic filtering (This work)	**0.00**	**0.00**	0.19	0.27	1.59	4.08
Wavelet transform (Bouaziz et al., 2014)	0.10	0.09	0.30	0.23	0.81	8.40
Linear filtering (Zhu & Dong, 2013)	0.11	0.09	**0.15**	**0.09**	1.25	0.57
S-transform (Zidelmal et al., 2014)	0.16	0.09	0.23	0.23	1.24	2.44
Artificial neural network (Arbateni & Bennia, 2014)	0.16	0.33	0.31	*0.64*	**0.23**	**0.51**
Wavelet transform (Choi et al., 2010)	0.16	*0.37*	*1.00*	0.32	2.02	4.71
Wavelet transform (Karimipour & Homaeinezhad, 2014)	0.32	**0.00**	0.19	0.27	*2.41*	*12.40*
Mathematical morphology (Zhang & Lian, 2009)	*0.70*	*0.37*	0.50	0.23	1.01	0.68

The minimum and maximum DER values for each record are shown in bold and italics, respectively.

5. Conclusions

This paper proposed the QRS detection algorithm, which employed the quadratic filter on enhancing QRS signal to noise ratio from ECG signals in preprocessing step. Results show that the quadratic filter achieves in improving QRS signal to noise ratio for some challenging situations such as low amplitude QRS complex corrupted by baseline drift and a variety of abnormal morphologies such as a fusion of ventricular and normal beat, an atrial premature beat, an aberrated atrial premature beat, a premature ventricular contraction beat, a fusion of paced and normal beat, and a paced beat. Subsequently, the QRS complex is obtained with a simple beat detection algorithm based on an envelope signal and a single fixed threshold without additional post-processing techniques. The proposed algorithm was validated with the MIT-BIH arrhythmia database. The average DER value from 48 records is at 0.38%.

To improve the accuracy of proposed QRS detection algorithm for abrupt baseline shift, high-grade noise, and low amplitude QRS complex contaminated by muscle noise, more computations in beat detection step can be added. The employment of more sophisticated thresholding techniques such as the multiple levels of fixed threshold, the single level of adaptive threshold, and the multiple levels of adaptive threshold can be used for decreasing FN detections. Moreover, FP detections can be reduced using the algorithm based on the refractory period of 200 ms.

Acknowledgment

The author thanks Ms. Saranya Chaiwisood for her help on the preliminary study of this research work. In addition, this research project was funded by a grant from the Thailand Research Fund and Faculty of Engineering, Prince of Songkla University through Contract No. RSA5680043.

References

Abibullaev, B., & Seo, H. D. (2011). A new QRS detection method using wavelets and artificial neural networks. *Journal of Medical Systems, 35*(4), 683–691.
Adnane, M., Jiang, Z., & Choi, S. (2009). Development of QRS detection algorithm designed for wearable cardiorespiratory system. *Computer Methods and Programs in Biomedicine, 93*(1), 20–31.
Afonso, V. X., Tompkins, W. J., Nguyen, T. Q., Michler, K., & Luo, S. (1999). ECG beat detection using filter banks. *IEEE Transactions on Biomedical Engineering, 46*(2), 192–202.
Arbateni, K., & Bennia, A. (2014). Sigmoidal radial basis function ANN for QRS complex detection. *Neurocomputing, 145*, 438–450.

Arzeno, N. M., Deng, Z. D., & Poon, C. S. (2008). Analysis of first-derivative based QRS detection algorithms. *IEEE Transactions on Biomedical Engineering, 55*(2), 478–484.

Babaeizadeh, S., White, D. P., Pittman, S. D., & Zhou, S. H. (2010). Automatic detection and quantification of sleep apnea using heart rate variability. *Journal of Electrocardiology, 43*(6), 535–541.

Bahoura, M., Hassani, M., & Hubin, M. (1997). DSP implementation of wavelet transform for real time ECG waveforms detection and heart rate analysis. *Computer Methods and Programs in Biomedicine, 52*(1), 35–44.

Benitez, D., Gaydecki, P. A., Zaidi, A., & Fitzpatrick, A. (2001). The use of the Hilbert transform in ECG signal analysis. *Computers in Biology and Medicine, 31*(5), 399–406.

Bouaziz, F., Boutana, D., & Benidir, M. (2014). Multiresolution wavelet-based QRS complex detection algorithm suited to several abnormal morphologies. *IET Signal Processing, 8*(7), 774–782.

Chen, S. W., Chen, H. C., & Chan, H. L. (2006). A real-time QRS detection method based on moving-averaging incorporating with wavelet denoising. *Computer Methods and Programs in Biomedicine, 82*(3), 187–195.

Choi, S., Adnane, M., Lee, G. J., Jang, H., Jiang, Z., & Park, H. K. (2010). Development of ECG beat segmentation method by combining lowpass filter and irregular RR interval checkup strategy. *Expert Systems with Applications, 37*(7), 5208–5218.

Chouakri, S. A., Reguig, F. B., & Ahmed, A. T. (2011). QRS complex detection based on multi wavelet packet decomposition. *Applied Mathematics and Computation, 217*(23), 9508–9525.

Dutta, S., Chatterjee, A., & Munshi, S. (2010). Correlation technique and least square support vector machine combine for frequency domain based ECG beat classification. *Medical Engineering and Physics, 32*(10), 1161–1169.

Goldberger, A. L., Amaral, L. A. N., Glass, L., Hausdorff, J. M., Ivanov, P. C., Mark, R. G., et al. (2000). PhysioBank, PhysioToolkit, and PhysioNet: Components of a new research resource for complex physiologic signals. *Circulation, 101*(23), e215–e220.

Hamilton, P. S., & Tompkins, W. J. (1986). Quantitative investigation of QRS detection rules using the MIT/BIH arrhythmia database. *IEEE Transactions on Biomedical Engineering, BME, 33*(12), 1157–1165.

Karimipour, A., & Homaeinezhad, M. R. (2014). Real-time electrocardiogram P-QRS-T detection-delineation algorithm based on quality-supported analysis of characteristic templates. *Computers in Biology and Medicine, 52*, 153–165.

Kohler, B. U., Hennig, C., & Orglmeister, R. (2003). QRS detection using zero crossing counts. *Progress in Biomedical Research, 8*(3), 138–145.

Korurek, M., & Dogan, B. (2010). ECG beat classification using particle swarm optimization and radial basis function neural network. *Expert Systems with Applications, 37*(12), 7563–7569.

Kutlu, Y., & Kuntalp, D. (2012). Feature extraction for ECG heartbeats using higher order statistics of WPD coefficients. *Computer Methods and Programs in Biomedicine, 105*(3), 257–267.

Lee, J. W., Kim, K. S., Lee, B. S., Lee, B. C., & Lee, M. H. (2002). A real time QRS detection using delay-coordinate mapping for the microcontroller implementation. *Annals of Biomedical Engineering, 30*(9), 1140–1151.

Li, C., Zheng, C. X., & Tai, C. F. (1995). Detection of ECG characteristic points using wavelet transforms. *IEEE Transactions on Biomedical Engineering, 42*(1), 21–28.

Madeiro, J. P. V., Cortez, P. C., Marques, J. A. L., Seisdedos, C. R. V., & Sobrinho, C. R. M. R. (2012). An innovative approach of QRS segmentation based on first-derivative, Hilbert and wavelet transforms. *Medical Engineering and Physics, 34*(9), 1236–1246.

Manikandan, M. S., & Soman, K. P. (2012). A novel method for detecting R-peaks in electrocardiogram (ECG) signal. *Biomedical Signal Processing and Control, 7*(2), 118–128.

Moody, G. B., & Mark, R. G. (2001). The impact of the MIT-BIH Arrhythmia database. *IEEE Engineering in Medicine and Biology, 20*(3), 45–50.

Pan, J., & Tompkins, W. J. (1985). A real-time QRS detection algorithm. *IEEE Transactions on Biomedical Engineering, BME, 32*(3), 230–236.

Phukpattaranont, P., & Limsakul, C. (2009). Optimum quadratic filters for nonlinear ultrasonic imaging. *Japanese Journal of Applied Physics, 48*(7), 1–7. 07GJ02.

Poli, R., Cagnoni, S., & Valli, G. (1995). Genetic design of optimum linear and nonlinear QRS detectors. *IEEE Transactions on Biomedical Engineering, 42*(11), 1137–1141.

Shih, D. H., Chiang, H. S., Lin, B., & Lin, S. B. (2010). An embedded mobile ECG reasoning system for elderly patients. *IEEE Transactions on Information Technology in Biomedicine, 14*(3), 854–865.

Slimane, Z. E. H., & Ali, A. N. (2010). QRS complex detection using empirical mode decomposition. *Digital Signal Processing, 20*(4), 1221–1228.

Yeh, Y. C., & Wang, W. J. (2008). QRS complexes detection for ECG signal: The difference operation method. *Computer Methods and Programs in Biomedicine, 91*(3), 245–254.

Yildiz, A., Akin, M., & Poyraz, M. (2011). An expert system for automated recognition of patients with obstructive sleep apnea using electrocardiogram recordings. *Expert Systems with Applications, 38*(10), 12880–12890.

Yu, S. N., & Lee, M. Y. (2012a). Bispectral analysis and genetic algorithm for congestive heart failure recognition based on heart rate variability. *Computers in Biology and Medicine, 42*(8), 816–825.

Yu, S. N., & Lee, M. Y. (2012b). Conditional mutual information-based feature selection for congestive heart failure recognition using heart rate variability. *Computer Methods and Programs in Biomedicine, 108*(1), 299–309.

Zhang, C. F., & Bae, T. W. (2012). VLSI friendly ECG QRS complex detector for body sensor networks. *IEEE Journal on Emerging and Selected Topics on Circuits and Systems, 2*(1), 52–59.

Zhang, F., & Lian, Y. (2009). QRS detection based on multi-scale mathematical morphology for wearable ECG device in body area networks. *IEEE Transaction on Biomedical Circuits and Systems, 3*(4), 220–228.

Zhang, F., & Lian, Y. (2011). QRS detection based on morphological filter and energy envelope for applications in body sensor networks. *Journal of Signal Processing Systems, 64*(2), 187–194.

Zhu, H., & Dong, J. (2013). An R-peak detection method based on peaks of Shannon energy envelope. *Biomedical Signal Processing and Control, 8*, 466–474.

Zidelmala, Z., Amiroua, A., Adnaneb, M., & Belouchranib, A. (2012). QRS detection based on wavelet coefficients. *Computer Methods and Programs in Biomedicine, 107*(3), 490–496.

Zidelmal, Z., Amirou, A., Ould-Abdeslamb, D., Moukadem, A., & Dieterlen, A. (2014). QRS detection using S-Transform and Shannon energy. *Computer Methods and Programs in Biomedicine, 116*, 1–9.

Pornchai Phukpattaranont, “Improvement of signal to noise ratio (SNR) in ECG signals based on dual-band continuous wavelet transform,” in *Proceedings of Asia-Pacific Signal and Information Processing Association Annual Summit and Conference* (*APSIPA ASC 2014*), Siem Reap, Cambodia, Dec. 10-12, 2014.

APSIPA ASC 2014

Asia-Pacific Signal and Information Processing Association Annual Summit and Conference 2014

December 9-12, 2014
Siem Reap,
city of Angkor Wat
Cambodia

Technical Co-Sponsor
IEEE Signal Processing Society

Improvement of signal to noise ratio (SNR) in ECG signals based on dual-band continuous wavelet transform

Pornchai Phukpattaranont*
*Department of Electrical Engineering, Prince of Songkla University, Songkhla, Thailand
E-mail: pornchai.p@psu.ac.th Tel: +66-74-558831

***Abstract*—For ECG signal analysis, a QRS detection algorithm is very important. The QRS detection algorithm consists of two steps, i.e., ECG preprocessing and ECG beat detection. In preprocessing step, noises in ECG signals are removed. The higher signal to noise ratio (SNR) after noise removal in preprocessing step leads to the less complicated algorithm in beat detection step and the increase in accuracy. However, ECG signals have various types in the real situation such as normal beat and premature ventricular contraction (PVC) beat. Each type of beat has its own frequency response. Therefore, we propose the dual-band continuous wavelet transform to maximize the SNR of ECG signals after noise removal in this paper. The proposed algorithm was evaluated with the ECG signals from MIT-BIH arrhythmia database. Results demonstrate the feasibility of the method.**

I. Introduction

World Health Organization (WHO) reported that 17.5 million people died of cardiovascular disease in 2005. It has been the first cause of death for people around the world. This disease tends to increase steadily. It is expected that 20 million people will die from this disease in 2015 [1],[2]. In Thailand, the death rate from cardiovascular disease is found to be the top three. In other words, there are 35050 Thai people die from this disease in 2009 or the average death rate from this disease is four people per hour [3].

The early detection of the heart disease is very important. One of the measurement used for checking the condition of the heart is the electrocardiogram (ECG) signal. The components of each ECG beat consist of the P wave, the QSR complex, and the S wave. The detection of the R peak in the QRS complex is a preliminary step to other ECG signal analysis such as arrhythmia analysis [4] and heart rate variability (HRV) analysis [5].

Generally, the algorithm of R peak detection in the QRS complex is composed of two main steps, i.e. ECG pre-processing and ECG beat detection. The objective of the ECG pre-processing step is to remove a variety of noises in the ECG signal, such as the muscle noise, the power line noise, and the baseline drift noise. Examples of the methods used for noise removal in the ECG signal include the linear filtering technique [6], the wavelet transform technique [7], and mathematical morphology technique [8]. In ECG beat detection step, the envelope signal is obtained from the ECG signal after noise removal and the threshold is defined to determine the time period where the QRS complex locates. The R peak can be detected from the time position where the amplitude of the ECG signal after noise removal is maximum.

The ECG pre-processing step is very important because if noises in the ECG signal can be effectively removed in this step, the computational complexity of the algorithm in the ECG beat detection step can be reduced. Therefore, we proposed the noise removal algorithm based on the dual-band continuous wavelet transform (CWT) in this paper to effectively remove noises in the ECG signal.

II. Continuous wavelet transform

The CWT have been gained popular uses for decomposing signals in many applications including ECG noise removal. Given the input signal $x(t)$, which is the ECG signal in this paper, the CWT of $x(t)$ can be expressed as

$$T_{a,b} = \int_{-\infty}^{\infty} x(t) \frac{1}{\sqrt{a}} \psi^* \left(\frac{t-b}{a} \right) dt \qquad (1)$$

where $T_{a,b}$ is the CWT of $x(t)$, a is the dilation parameter, b is the location parameter, and $\psi^*(t)$ is the complex conjugate of the wavelet function. There are a variety types of the wavelet function. However, the Maxican-hat wavelet function is selected in this paper for removing noises because its similarity to the shape of the QRS complex from the normal ECG beat [9]. The Maxican-hat wavelet function, which is the second derivative of a Gaussian function, is given by

$$\psi(t) = \frac{1}{\sqrt{2\pi}} (1 - t^2) \exp\left(\frac{-t^2}{2} \right). \qquad (2)$$

III. Materials and Methods

A. Proposed Algorithm

Fig. 1 shows a block diagram of the proposed QRS detection algorithm. The ECG signal $x[n]$ is determined from the ECG signal $x(t)$ at a sampling rate of 200 Hz. Fig. 2(b) shows an example of two beats of the ECG signal $x[n]$. While the beat in the left hand side is a normal ECG beat, the beat in the right hand side is a premature ventricular contraction (PVC) beat. Then, the noises in the ECG signal $x[n]$ are removed based on the CWT to obtain $y[n]$. Three types of the CWT processing method are explored and compared as follows:

- A: $T_{3,b}^2 + T_{3,b}^2$
- B: $T_{6,b}^2 + T_{6,b}^2$

978-616-361-823-8

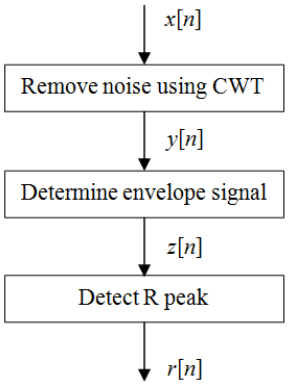

Fig. 1. Block diagram of the proposed QRS detection algorithm.

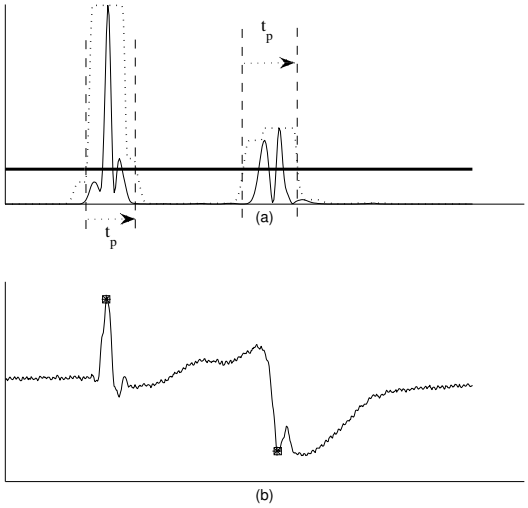

Fig. 2. ECG beat detection algorithm. (a) Thin line: ECG signal after noise removal $y[n]$. Dotted line: Envelope signal $z[n]$. Thick line: Threshold value line. (b) ECG signal overlaid by the markers from the proposed algorithm (square) and the expert (asterisk). While the signal in the left hand side is a normal ECG beat, the signal in the right hand side is a PVC beat.

- C: $T_{3,b}^2 + T_{6,b}^2$.

While case A and case B are the representative of a single-band CWT processing method, case C is the representative of a dual-band CWT processing method. Fig. 2(a) shows an example of the ECG signal after noise removal $y[n]$ with the CWT method of case C using a thin line. While the normal beat has a single peak after noise removal, the PVC beat has double peaks. Subsequently, the envelope signal $z[n]$ is calculated from $y[n]$ as shown in Fig. 2(a) using a dotted line. Then, the threshold value is defined as shown in Fig. 2(a) using a thick line. Finally, the R peak in the QRS complex $r[n]$ is determined from the time where the maximum peak occurs within the time period defined by $z[n]$ and the threshold

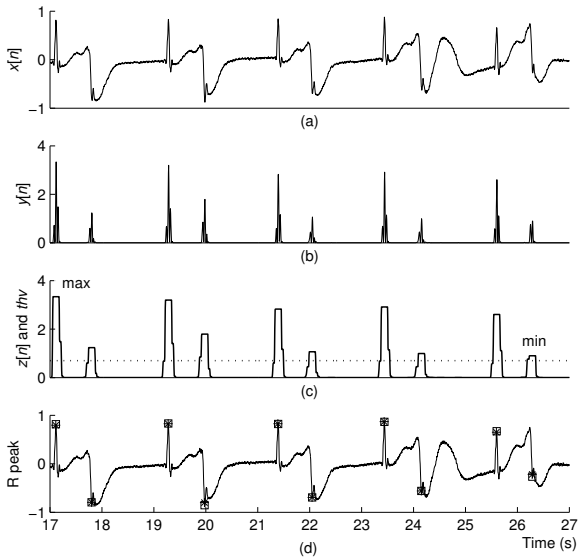

Fig. 3. Results of the proposed algorithm case A applied on the ECG signal record 207. (a) The ECG signal before noise removal $x[n]$. (b) The ECG signal after noise removal $y[n]$. (c) The envelope signal $z[n]$ shown in a solid line and the threshold level thv shown in a dotted line. (d) The ECG signal overlaid by the markers from the proposed algorithm (square) and the expert (asterisk).

value. Fig. 2(a) shows an example the time period t_p where the maximum peak locates. In addition, the ECG signal overlaid by the markers from the proposed algorithm (square) and the expert (asterisk) is shown in Fig. 2(b).

B. Performance Evaluation

Two parameters were used in the performance evaluation of the proposed method. The first parameter is the ratio of the maximum $z[n]$ to the minimum $z[n]$ (RMM), which can be expressed as

$$\text{RMM} = z_{max}/z_{min}. \tag{3}$$

If the value of RMM is closed to 1, the maximum amplitude of all beats in the envelope signal $z[n]$ is almost equal. In other words, the signal to noise ratio (SNR) of the z_{min} beat is maximized. As a result, the fixed threshold technique can be used instead of the adaptive threshold technique. This is important because it can reduce the computational complexity of QRS detection algorithm without compromising of accuracy. The second parameter is the time period indicating false detection (FD), which is the average of absolute of time error in the unit of ms. The best value of FD is 0, which means that all R peaks in the QRS complex are correctly detected by the proposed algorithm.

IV. Results and Discussion

A. Scale adjustment

Fig. 3 shows results of the proposed algorithm case A applied on the ECG signal record 207. Fig. 3(a) shows the ECG signal before noise removal $x[n]$ from time 17 s to 27 s.

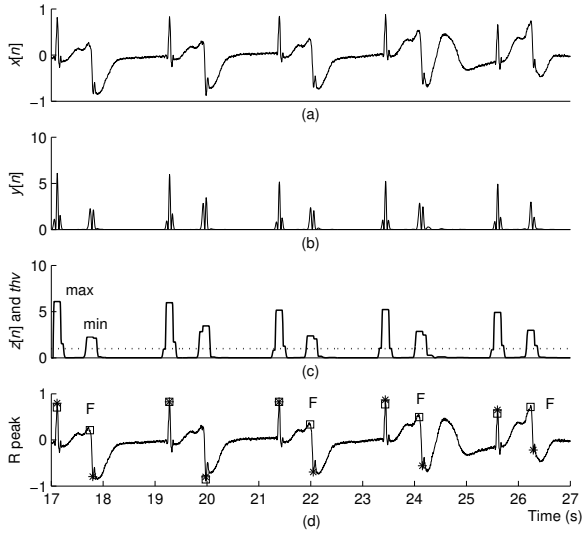

Fig. 4. Results of the proposed algorithm case B applied on the ECG signal record 207. (a) The ECG signal before noise removal $x[n]$. (b) The ECG signal after noise removal $y[n]$. (c) The envelope signal $z[n]$ shown in a solid line and the threshold level thv shown in a dotted line. (d) The ECG signal overlaid by the markers from the proposed algorithm (square) and the expert (asterisk).

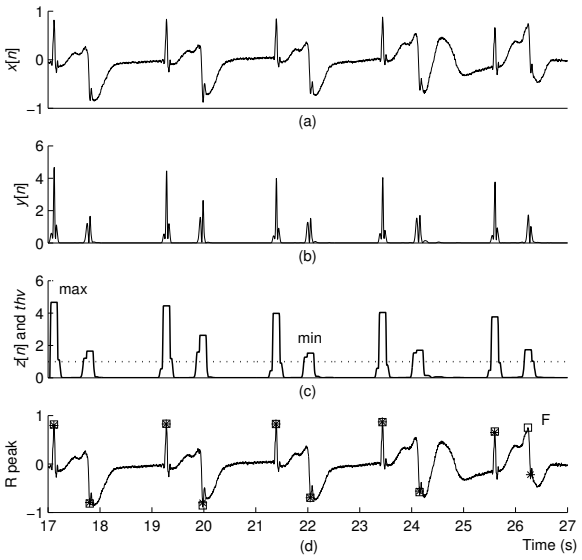

Fig. 5. Results of the proposed algorithm case C applied on the ECG signal record 207. (a) The ECG signal before noise removal $x[n]$. (b) The ECG signal after noise removal $y[n]$. (c) The envelope signal $z[n]$ shown in a solid line and the threshold level thv shown in a dotted line. (d) The ECG signal overlaid by the markers from the proposed algorithm (square) and the expert (asterisk).

The ECG signal $x[n]$ consists of 5 normal beats and 5 PVC beats. Fig. 3(b) shows the ECG signal after noise removal $y[n]$. While the normal beat has a single peak amplitude, the PVC beat comprises double peak amplitudes. Fig. 3(c) shows the envelope signal $z[n]$ using a solid line and the threshold level thv using a dotted line. While the first beat has maximum amplitude, the last beat has minimum amplitude. Fig. 3(d) shows the ECG signal overlaid by the markers from the proposed algorithm (square) and the expert (asterisk). In this case, all R peaks in QRS complex are correctly detected.

Fig. 4 shows results of the proposed algorithm case B applied on the ECG signal record 207. Fig. 4(b) shows the ECG signal after noise removal $y[n]$. Similar to case A, the normal beat has a single peak amplitude and the PVC beat comprises double peak amplitudes. However, the position of maximum peak in each PVC beat is different from that in case A except the second beat. Fig. 4(c) shows that the maximum beat and the minimum beat locate at the first beat and the second beat, respectively. Fig. 4(d) shows that there are four wrong beat detections.

Fig. 5 shows results of the proposed algorithm case C applied on the ECG signal record 207. The ECG signal after noise removal $y[n]$ and the envelope signal $z[n]$ shown in Fig. 5(b) and (c) are slightly different from those in case A and case B in terms of both the position of the maximum peak in $y[n]$ and the maximum beat and the minimum beat in $z[n]$. In addition, there is a single false detection in the last beat shown in Fig. 5(d). As more quantitative details on performance comparisons, Table I shows the values of z_{max}, z_{min}, RMM, and FD from all cases. Case A gives the best FD among all cases at an expense of the worst RMM. In contrast, case B gives the best RMM among all cases at an expense of the worst FD. However, with the use of the dual-band CWT processing technique (case C), the improvement in terms of both the RMM and the FD is possible as shown in the third row of Table I. In other words, while the RMM of case C decreases from 3.65 to 3.05 compared to case A, the FD of case C decreases from 23.9 to 6.9 compared to case B.

TABLE I
PERFORMANCE COMPARISON OF THE PROPOSED ALGORITHM.

Method	z_{max}	z_{min}	RMM	FD
A	3.32	0.91	3.65	2.5
B	6.05	2.25	2.69	23.9
C	4.69	1.54	3.05	6.9

Fig. 6(a) shows the results of RMM as a function of the second scale from 1 to 8 applied on the ECG signal record 207. In other words, the CWT processing method is $T^2_{3,b}+T^2_{a,b}$ when the first scale is fixed at 3 and the second scale is varied from 1 to 8. The maximum RMM is 3.91 at the second scale 4 and the minimum RMM is 2.16 at the second scale 8. Fig. 6(b) shows the results of FD as a function of the second scale from 1 to 8. The maximum FD is 26.9 at the second scale 8 and the minimum FD is 2.5 at the second scale 3. These results show that the second scale 6 is the optimized selection because it can achieve both RMM and FD.

B. Wavelet function

In addition to the scale and scale combination, the type of wavelet function is another important parameter affecting the

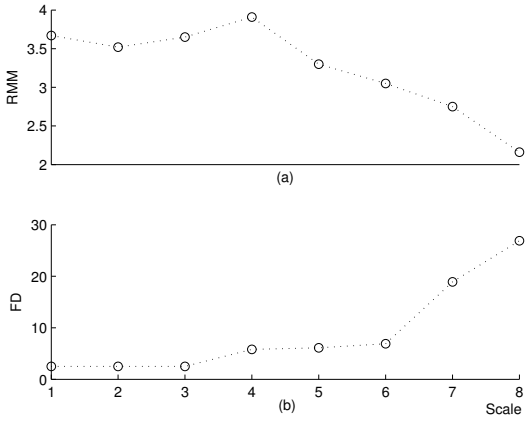

Fig. 6. (a) RMM as a function of the second scale from 1 to 8. (b) FD as a function of the second scale from 1 to 8.

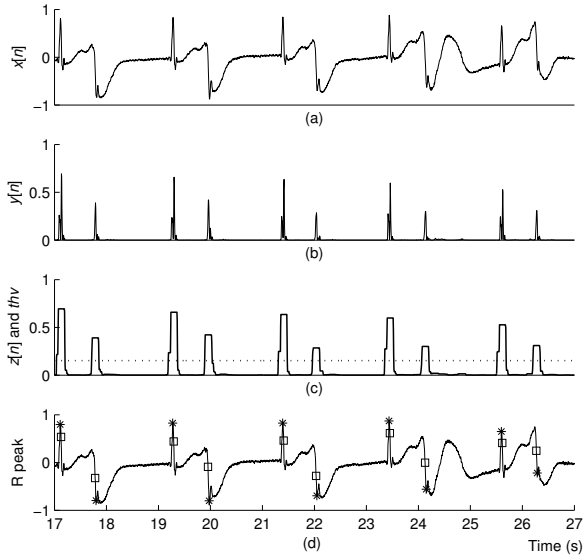

Fig. 7. Results of the proposed algorithm with the Haar wavelet function.

SNR. Fig. 7 shows the results from the Haar wavelet function. The RMM and FD are 2.38 and 18.1, respectively. Fig. 8 shows the results from the 2.2 reverse biorthogonal wavelet function with the RMM and FD of 3.72 and 2.5, respectively. These results confirm the importance of the wavelet function selection.

V. Conclusions

We present the improvement of signal to noise ratio (SNR) in ECG signals based on dual-band continuous wavelet transform (CWT). The ECG signal after noise removal using the dual-band CWT at dilation parameter combination of 3 and 6 shows the feasibility of the method in maximizing the SNR without the loss of accuracy compared to the single-band CWT at the dilation parameter of 3 and the dilation parameter of 6. However, more studies on other combinations of dilation

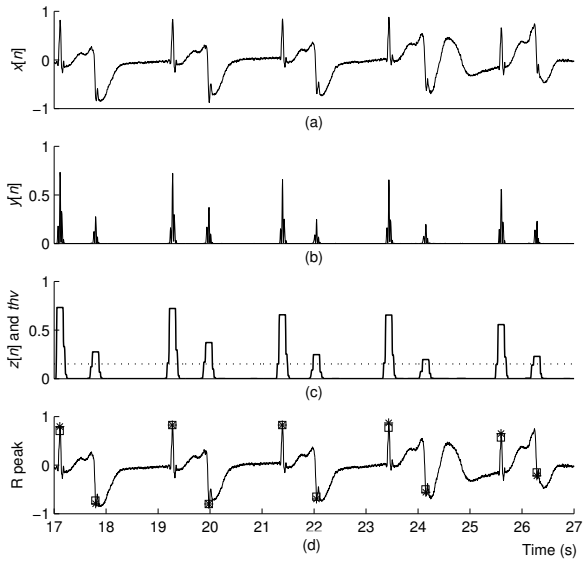

Fig. 8. Results of the proposed algorithm with the 2.2 reverse biorthogonal wavelet function.

parameters should be performed and performance evaluation to all records of ECG data in MIT-BIH arrhythmia database should be investigated. In addition, others wavelet functions should be carefully considered. The results will be reported soon in the near future.

Acknowledgment

The author thanks Ms. Saranya Chaiwisood for her help on the preliminary study of this research work. In addition, this research project was funded by a grant from the Thailand Research Fund and Faculty of Engineering, Prince of Songkla University through Contract No. RSA5680043.

References

[1] Cardiovascular diseases. 2010 June 31 [online]. Available:URL:http://www.who.int/cardiovascular_diseases/en/index.html.

[2] World Health Organization. Cardiovascular diseases (CVDs). 2010 June 31[online]. Available:http://www.who.int/mediacentre/factsheets/fs317/en/index.html.Book

[3] Ministry of Public Health. Bureau of Non Communicable Disease. Annual Report in 2009. Bangkok.

[4] Y. Kutlu, D. Kuntalp, "Feature extraction for ECG heartbeats using higher order statistics of WPD coefficients," *Comput. Meth. Prog. Bio.,* vol. 105, no. 3, pp. 257-267, 2012.

[5] S.-N. Yu, M.-Y. Lee, "Conditional mutual information-based feature selec- tion for congestive heart failure recognition using heart rate variability," *Comput. Meth. Prog. Bio.,* vol. 108, no. 1, pp. 299-309, 2012.

[6] J. Pan, W. J. Tompkins, "A real-time QRS detection algorithm," *IEEE Trans. Biomed. Eng.,* vol. BME-32, no. 3, pp. 230-236, 1985.

[7] Z. Zidelmala, A. Amiroua, M. Adnaneb, A. Belouchranib, "QRS detection based on wavelet coefficients," *Comput. Meth. Prog. Bio.,* vol. 107, no. 3, pp. 490-496, 2012.

[8] F. Zhang, Y. Lian, "QRS detection based on morphological filter and energy envelope for applications in body sensor networks," *J. Sign. Process. Syst.,* vol. 64, no. 2, pp. 187-194, 2011.

[9] I. R. Legarreta, P. S. Addison, N. R. Grubb, G. R. Clegg, C. E. Roberson, and J. N. Watson, "A comparison of continuous waveket transforms modulus maxima analysis of characteristic ECG features," *Computer in Cardiology,* vol. 32, pp. 755-758, 2005.